

## REVIEW

View Article Online  
View Journal | View IssueCite this: *Mater. Chem. Front.*,  
2023, 7, 5693Received 23rd April 2023,  
Accepted 21st August 2023

DOI: 10.1039/d3qm00430a

rsc.li/frontiers-materials

# Recent progress in metal–organic frameworks for the separation of gaseous hydrocarbons

Jing-Hong Li, Jun-Xian Chen, Rui-Biao Lin \* and Xiao-Ming Chen \*

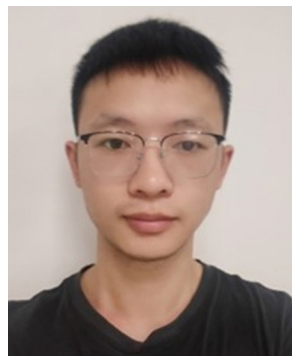
The separation of gaseous hydrocarbons is involved in many important industrial processes for manufacturing chemicals, polymers, plastics, and fuels, and is performed through cryogenic distillation, which is heavily energy-intensive. Adsorption-based gas separation technology by using adsorbent materials can potentially fulfill a much energy-efficient gas separation. As a new generation of adsorbent materials, metal–organic frameworks (MOFs) have been demonstrated to have great potential in addressing important gas separations of hydrocarbons. In this review, we outline the uniqueness of MOF adsorbents for their separation application for gaseous hydrocarbons. A variety of microporous MOFs have been developed for separating gaseous hydrocarbons, which have been achieved by fine-tuning their pore sizes for high molecular sieving effects and/or immobilizing binding sites on their pore surfaces for their specific recognition of small molecules. Herein, we highlight recent important progress in this very important topic, focusing on the purification of ethylene, propylene, and butadiene.

## 1. Introduction

Gaseous hydrocarbons involve not only essential fuels for modern society but also are applied as important feedstocks in the chemical industry. Hydrocarbons usually are volatile, invisible, and flammable, and tend to be highly dispersed, easily contain mixtures of low concentration, and thus are difficult to handle. The separation and purification of hydrocarbons are critical industrial chemical processes to produce bulk commodities for fuels, polymers, and plastics. Some of these separation processes are carried out on a very large

industrial scale. For example, olefin/paraffin separation produces light olefins of over 200 million tonnes.<sup>1</sup> The huge markets of hydrocarbon products make a large contribution (thousands of billions of US dollars) to the annual revenues of the oil and gas industry. Most of the industrial separations of hydrocarbons traditionally rely on thermal-driven technologies, mainly fractional distillation involving numerous evaporation–condensation cycles, which are a high energy-intensity process. In particular, to separate mixed hydrocarbons of similar volatilities for high purity, relevant industrial processes are operated in complicated facilities and under harsh conditions. For the separation and purification of industrial commodities, it is believed that energy-intensive processes, such as distillation consume 10–15% of the world's energy production. Adsorptive separation based on porous adsorbents is a promising technology to lower relevant separation

Key Laboratory of Bioinorganic and Synthetic Chemistry of Ministry of Education, School of Chemistry, IGCME, Sun Yat-Sen University, Guangzhou 510275, China. E-mail: linruibiao@mail.sysu.edu.cn, cxm@mail.sysu.edu.cn

**Jing-Hong Li**

Jing-Hong Li obtained his BS degree from Gannan Normal University in 2017, and MS from Shantou University in 2020. Currently, he is a PhD scholar in Sun Yat-sen University. His main interests include the design and fabrication of porous coordination polymers (PCPs), hydrogen-bonded organic frameworks (HOFs), and their functions.

**Jun-Xian Chen**

Jun-Xian Chen obtained her BS degree in Chemical Engineering and Technology from Sun Yat-sen University in 2021. She is currently a PhD scholar in Chemistry in Sun Yat-sen University under the supervision of Prof. Xiao-Ming Chen. Her current research interest includes the design and fabrication of functional porous coordination polymers for gas separation.

energy use. For example, alternative technologies, such as adsorptive separation and/or membrane-based technologies, can be up to 10 times more energy-efficient than the traditional distillation methods, which have not been fully realized.<sup>1</sup> These nonthermal technologies can separate hydrocarbon molecules according to their chemical affinities or sizes rather than differences in boiling points, and thus can be carried out under mild conditions, hence greatly reducing the energy inputs.<sup>2</sup> The core of these candidate technologies is the separation performance of solid porous media or permeable membranes, which are often made of porous materials with nanosized voids and desired internal pore features.

Metal-organic frameworks (MOFs, also known as porous coordination polymers) are an emerging type of crystalline porous solids, which are assembled by metal-containing nodes and organic linkers or struts through coordination bonds to have pore space. MOFs are unique owing to their exceptional porosity, diverse structures, tunable pore size, and ease of functionality.<sup>3-6</sup> After two decades of intensive practices, MOF materials are well demonstrated for their exceptional capability for pore adjustment and interior modification. Today, about 100 000 of MOFs have been synthesized. MOFs can show ultrahigh porosity with the largest pore surface area of over 7000 m<sup>2</sup> g<sup>-1</sup>, or with pore sizes ranging from 3 to 100 Å, the highest thermal stability of over 600 °C, or exceptional chemical stability in concentrated acidic/basic solutions.<sup>3,7,8</sup> The high modularity of MOFs enables us to construct their isostructural analogues of different pore sizes/shapes and surfaces (such as functional organic groups, metal open sites, *etc.*) with the same coordination networks. The key design element for MOFs is thus to functionalize their pore surface with binding sites and/or adjust their pore size/shape for molecular separation. In this context, MOFs have shown great promise that is superior to conventional porous materials (activated carbon and zeolites) in addressing important separations of gaseous hydrocarbons.<sup>9-19</sup>

For separation processes in physical adsorbents, their separation mechanism can be roughly categorized into either equilibrium or non-equilibrium adsorption. Equilibrium adsorption processes are thermodynamic and are mainly driven by binding affinity differences dominated by those functional sites (*i.e.*, binding sites) through supramolecular interactions. Pore functionalization with strong binding sites can significantly boost such type of separation performance. For non-equilibrium adsorption processes,<sup>20</sup> including kinetic separation and molecular sieving, the separation is achieved by differing the diffusivity, which is highly affected by the pore sizes and flexibility of adsorbents. The kinetic separation can be amplified after narrowing the pores of adsorbents. There are also cases that the separation is achieved by a combination of both thermodynamic and kinetic processes. In addition, there are gas separation processes that are usually performed with the collaboration of framework flexibility and structural transformation, namely, gate-opening or pore opening. Considering all aspects, it is very important to systematically control the pore size, pore surface and even the flexibility of adsorbents.

On the other hand, hydrocarbons are composed of the same elements with different carbon bonds and carbon/hydrogen ratios. Their physical properties and even chemical properties can be very similar (Table 1). The adsorptive separation by differing their molecular shapes or adsorption affinities in physical adsorbents is thus required to perform with high accuracy, which can be achieved by MOFs.<sup>13</sup> For example, compared with the mixture counterpart propane, propylene, as one major petrochemical product, differs by just two hydrogen atoms, and there is around a 5 K difference in their boiling points. It has been demonstrated that MOFs with embedded binding sites (ranging from open metal sites to polar functional groups, such as anionic fluoride, hydroxyl and amino) can effectively separate olefins/paraffins owing to the difference in thermodynamic affinity. Another applicable approach is to adjust the pore sizes of MOFs



**Rui-Biao Lin**

*Rui-Biao Lin obtained his BSc in Chemistry from Sun Yat-Sen University (SYSU) in 2009. He obtained his PhD in 2014 (SYSU). During 2016–2020, he worked at the University of Texas at San Antonio as a postdoctoral fellow. Since 2021, he has been working as a full professor in SYSU, where he is working on multifunctional porous materials, including metal-organic frameworks and hydrogen-bonded organic frameworks.*



**Xiao-Ming Chen**

*Xiao-Ming Chen received his BS (1983) and MS (1986) degrees from Sun Yat-Sen University and PhD from the Chinese University of Hong Kong in 1992. He is an Academician of the Chinese Academy of Sciences, and Academician of The World Academy of Sciences for the advancement of science in developing countries (TWAS). He is a professor in the School of Chemistry at Sun Yat-Sen University and director of the Institute of Green Chemistry and Molecular Engineering. His current research interest includes the design, synthesis, and crystal engineering of functional metal-organic/hybrid materials, including coordination polymers, metal-organic frameworks, and their applications (such as adsorption/separation, catalysis, and electric/magnetic properties).*

Table 1 Physical parameters of selected gas and vapor hydrocarbons<sup>12</sup>

Adsorbate	Normal boiling point/K	Density/g L <sup>-1</sup> (101.325 kPa, 273.15 K)	Kinetic diameter/Å	Polarizability × 10 <sup>25</sup> /cm <sup>3</sup>	Dipole moment × 10 <sup>18</sup> /esu cm	Quadruple moment × 10 <sup>26</sup> /esu cm <sup>2</sup>
CH <sub>4</sub>	111.66	0.717	3.758	25.93	0	0
C <sub>2</sub> H <sub>4</sub>	169.42	1.261	4.163	42.52	0	1.50
C <sub>2</sub> H <sub>6</sub>	184.55	1.355	4.443	44.3–44.7	0	0.65
C <sub>2</sub> H <sub>2</sub>	188.40	—	3.3	33.3–39.3	0	—
C <sub>3</sub> H <sub>6</sub>	225.46	1.914	4.678	62.6	0.366	—
C <sub>3</sub> H <sub>8</sub>	231.02	2.011	4.3–5.118	62.9–63.7	0.084	—
<i>c</i> -C <sub>3</sub> H <sub>6</sub>	240.34	1.920	4.23–4.807	56.6	0	—
<i>i</i> -C <sub>4</sub> H <sub>10</sub>	261.34	2.689	5.278	81.4–82.9	0.132	—
<i>i</i> -Butene	266.25	—	4.84	8.14–8.29	—	—
1-Butene	266.92	—	4.5	79.7–85.2	0.359–0.438	—
1,3-Butadiene	268.62	—	5.2	86.4	0	—
<i>n</i> -C <sub>4</sub> H <sub>10</sub>	272.66	2.704	4.687	82.0	0.05	—
<i>trans</i> -2-Butene	274.03	—	—	84.9	0	—
<i>cis</i> -2-Butene	276.87	—	4.23	—	0.253	—
<i>neo</i> -C <sub>5</sub> H <sub>12</sub> (2,2-dimethylpropane)	282.65	2.334 (70.922 kPa)	6.2–6.464	102.0	0	—
<i>i</i> -C <sub>5</sub> H <sub>12</sub>	300.99	1.120 (34.543 kPa)	5.0	—	0.13	—
<i>n</i> -C <sub>5</sub> H <sub>12</sub>	309.22	0.789 (24.455 kPa)	4.5	99.9	0	—
<i>neo</i> -C <sub>6</sub> H <sub>14</sub> (2,2-dimethylbutane)	322.87	—	6.2	—	—	—
<i>i</i> -C <sub>6</sub> H <sub>14</sub> (2-methylpentane)	333.40	0.343 (8.960 kPa)	5.5	—	0.1	—
3-Methylpentane	336.40	—	5.5	—	—	—
<i>n</i> -C <sub>6</sub> H <sub>14</sub>	341.88	0.231 (6.041 kPa)	4.3	119	0	—
C <sub>6</sub> H <sub>6</sub>	353.24	0.403 <sup>a</sup> (12.695 kPa)	5.349–5.85	100–107.4	0	—
<i>c</i> -C <sub>6</sub> H <sub>12</sub> (cyclohexane)	353.93	0.446 <sup>a</sup> (13.019 kPa)	6.0–6.182	108.7–110	0	—
<i>n</i> -C <sub>7</sub> H <sub>16</sub>	371.57	0.067 (15.250 kPa)	4.3	136.1	0	—
<i>i</i> -C <sub>8</sub> H <sub>18</sub> (2,2,4-trimethylpentane)	372.39	—	6.2	154.4	0	—
Toluene	383.79	0.037 (0.906 kPa)	5.25	118–123	0.375	—
Ethylbenzene	409.36	—	5.8	142	0.59	—
<i>p</i> -Xylene	411.53	—	5.8	137–149	0.1	—
<i>m</i> -Xylene	412.34	—	6.8	142	0.37	—
<i>o</i> -Xylene	417.59	—	6.8	141–149	0.640	—

<sup>a</sup> Density at 298.15 K.

for size-matching of gas molecules, which is expected to enhance kinetic separation or sieving effect and finally achieve high selectivity. If the pore aperture size of adsorbents is right between the molecular sizes of different gas components, an adsorption cut-off happens along with the inaccessibility of internal pore space to certain gas components, thus leading to molecular sieving. For some MOFs, the adjustment of pore size in MOFs can be done up to a precision level of 0.1 Å.<sup>13</sup> Given that most hydrocarbon gases have their molecular sizes or kinetic diameters between 3 and 5 Å, microporous MOFs with comparable pore sizes have been intensively investigated for separating hydrocarbon mixtures. Usually, MOFs with large pores can show high sorption capacity but low separation selectivity for gas, whereas the ultramicroporous ones can exhibit high selectivity but low sorption capacity (termed sorption capacity *versus* selectivity trade off). By simultaneously tuning the pore size and incorporating binding sites, the internal pore space of MOFs can integrate molecular shape matching and preferential binding toward the targeted gas molecules, which is expected to address the trade-off for exceptional separation performance. The complicated effects of MOF flexibility for separation of hydrocarbons have also been noted.<sup>21</sup>

By virtue of pore structural and chemical control of MOF materials, namely, tuning pore size, incorporating functional sites, or their combination, significant progress has been made

for gaseous hydrocarbon separation. This review focuses on the research progress of MOF materials for separation of gaseous hydrocarbons in about recent five years. In particular, we summarize representative MOF materials with unique pores and functional sites for C<sub>2</sub>H<sub>2</sub> and CO<sub>2</sub> separation, C<sub>2</sub>H<sub>2</sub>/C<sub>2</sub>H<sub>4</sub> separation, C<sub>2</sub>H<sub>4</sub> and C<sub>2</sub>H<sub>6</sub> separation, C<sub>3</sub>H<sub>4</sub>/C<sub>3</sub>H<sub>6</sub> separation, C<sub>3</sub>H<sub>6</sub>/C<sub>3</sub>H<sub>8</sub> separation, and purification of butadiene, xylenes and other volatile gaseous hydrocarbons.

## 2. Pore structure control of MOFs for separating gaseous hydrocarbons

The separation performance of adsorbents towards target molecules can be affected by various factors, mainly dominated by the adsorbent–adsorbate and adsorbate–adsorbate interactions in the pore space. The adsorbent–adsorbate interactions for specific gases can be adjusted by controlling the pore chemistry and pore size of porous materials for optimal binding affinity, whereas adsorbate–adsorbate interactions are dependent on the physical properties of gas molecules including molecular polarity or polarizability, sizes and shapes. Therefore, rationally tuning the pore sizes of MOFs and/or functionalizing their pore surface have been demonstrated as efficient approaches to boost the separation performance for gases. Both adsorbent–adsorbate and

adsorbate-adsorbate intermolecular interactions for larger or heavier molecules with high polarizability are usually superior to those for small, light and non-polar ones, due to more supramolecular interactions (ranging from hydrogen bonding to electrostatic interactions and van der Waals forces). In this section, representative examples of MOFs for hydrocarbon separation were presented according to the sequence of the polarizability and boiling points of various gases (Table 2).

### 2.1. Methane purification

Natural gas is a cleanest fossil fuel and has been widely used due to its natural abundance and high energy intensity, and is usually contaminated with gas impurities such as carbon dioxide (CO<sub>2</sub>) and nitrogen (N<sub>2</sub>). The upgrading of natural gas involves the purification of methane (CH<sub>4</sub>). Coal-bed methane (CBM) is an excellent complement to conventional natural gas; the recovery of CH<sub>4</sub> from it can also reduce the emission of the greenhouse gas CH<sub>4</sub> from CBM as well as enhance the safety of coal mineral.<sup>22</sup>

Ma *et al.* used an alkyl MOF, Cu<sub>2</sub>(ATC) (ATC-Cu, H<sub>2</sub>ATC = 1,3,5,7-adamantane tetracarboxylic acid), as a methane nanopore that features oppositely adjacent open metal sites (OMSS) and dense alkyl groups for capturing methane molecules.<sup>23</sup> At 1 bar and 298 K, this MOF exhibits the highest methane uptake capacity (2.90 mmol g<sup>-1</sup>) among reported MOFs, showing a high CH<sub>4</sub>/N<sub>2</sub> selectivity of 9.7 for an equimolar mixture under ambient conditions. ATC-Cu thus shows promising potential for capturing methane from CBM with low content of methane (<30%). Structural and computational modelling indicated that pairs of open Cu sites with a Cu...Cu distance of 4.43 Å between two neighboring Cu paddlewheels afford considerable dual Coulombic interactions and act as strong binding sites for methane molecules. Also, there are cavities with an aliphatic surface that can serve as the second binding sites for CH<sub>4</sub>, with an average interaction distance of *ca.* 3.5 Å.

Yang *et al.* studied four nickel-based coordination networks with functional sites (-NH<sub>2</sub>) or varied pore sizes for the separation of CH<sub>4</sub>/N<sub>2</sub>, which supports that the pore size and chemical environment of adsorbents play an important role during methane purification.<sup>24</sup> Among those four MOFs, Ni(ina)<sub>2</sub> showed the highest CH<sub>4</sub>/N<sub>2</sub> selectivity (15.8) with an adsorption capacity of 1.82 mmol g<sup>-1</sup> under ambient conditions. Ni(ina)<sub>2</sub> shows good thermal and moisture stability as well, which can be easily scaled up at a low cost.

The influence of humidity on the separation performances of MOFs for CH<sub>4</sub> separation has been noticed. Li *et al.* investigated a series of isostructural MOFs, [Zn<sub>2</sub>(1,4-NDC)<sub>2</sub>(DABCO)], [Zn<sub>2</sub>(ADC)<sub>2</sub>(DABCO)], [Ni<sub>2</sub>(ADC)<sub>2</sub>(DABCO)], and [Cu<sub>2</sub>(ADC)<sub>2</sub>(-DABCO)] (namely, DMOF-N, DMOF-A<sub>1</sub>, DMOF-A<sub>2</sub>, DMOF-A<sub>3</sub>, respectively, H<sub>2</sub>1,4-NDC = 1,4-naphthalenedicarboxylic acid, H<sub>2</sub>ADC = 9,10-anthracene dicarboxylic acid, and DABCO = 1,4-diazabicyclo[2.2.2]octane), for CH<sub>4</sub> purification.<sup>25</sup> Altering their aromatic moieties and/or metal centers results in varied pore sizes, hydrophobicity and stability. The hydrophobic pore space suppressed the water sorption and enhanced the moisture resistance of those MOFs, which show high CH<sub>4</sub> uptakes and CH<sub>4</sub>/N<sub>2</sub>

selectivity. Breakthrough experiments for the CH<sub>4</sub>/N<sub>2</sub> mixture under humid conditions indicated that their CH<sub>4</sub>/N<sub>2</sub> separation performance can be retained even under high humidity (40% RH).<sup>26</sup>

Zhang *et al.* reported two isostructural flexible metal-azolate frameworks (abbreviated as MAFs, a subclass of MOFs with azolate ligands<sup>19</sup>) [Zn<sub>3</sub>(OH)<sub>2</sub>(pzdc)(tz)]·DMA and [Zn<sub>3</sub>(OH)<sub>2</sub>(pzdc)(atz)]·DMA (MAF-91·DMA and MAF-92·DMA, respectively, H<sub>3</sub>pzdc = 3,5-pyrazoledicarboxylic acid, Htz = 1,2,4-triazole, and Hatz = 3-amino-1,2,4-triazole), which possess quasi-discrete pores with analogous sizes (MAF-91·DMA: 3.6 × 2.4 and 4.0 × 2.1 Å<sup>2</sup>, and MAF-92·DMA: 3.7 × 1.3 and 4.0 × 2.1 Å<sup>2</sup>).<sup>27</sup> Due to the stronger intra-framework hydrogen-bonding interaction in MAF-92, there is a higher gating energy than MAF-91. Thus, MAF-92 showed tremendous shrinkage of apertures (1.0 × 0.8 and 2.5 × 1.0 Å<sup>2</sup>) after guest removal, while those in MAF-91 (3.5 × 2.2 and 4.4 × 2.0 Å<sup>2</sup>) showed negligible changes (Fig. 1). Single-component gas adsorption revealed that MAF-92 can adsorb a large amount of CO<sub>2</sub> (2.1 mmol g<sup>-1</sup> at 273 K and 1 bar), but completely excludes N<sub>2</sub> and CH<sub>4</sub>. The molecular sieving performance was further confirmed by breakthrough experiments for CO<sub>2</sub>/N<sub>2</sub> and CO<sub>2</sub>/CH<sub>4</sub>, giving selectivities of >1500. This work revealed that the controlled gated barrier can be expected to achieve definite and ideal molecular sieve effect. In contrast, the very commonly encountered framework flexibility of MOFs could be an important drawback to size-dependent molecular sieving for separation of similar molecules.

### 2.2. C<sub>2</sub>H<sub>4</sub> and C<sub>2</sub>H<sub>6</sub> separation

Ethylene (C<sub>2</sub>H<sub>4</sub>) is one of the most important chemical raw materials, which is widely used in the production of plastics, rubber, coatings, and other chemical products. It is mainly produced by cracking ethane (C<sub>2</sub>H<sub>6</sub>) or naphtha; thus, C<sub>2</sub>H<sub>6</sub> is a major impurity in the raw mixture. However, the separation of C<sub>2</sub>H<sub>4</sub> from the C<sub>2</sub>H<sub>4</sub>/C<sub>2</sub>H<sub>6</sub> mixture is highly challenging due to their small molecular size difference (<0.5 Å) and boiling point difference (*ca.* 15 K). MOFs have been reported to exhibit significant progress in the separation of C<sub>2</sub>H<sub>4</sub>/C<sub>2</sub>H<sub>6</sub>.<sup>28-41</sup>

Usually, the introduction of OMSS on the pore surface of MOFs enables preferential adsorption of C<sub>2</sub>H<sub>4</sub> over C<sub>2</sub>H<sub>6</sub>.<sup>28-33,38,41-44</sup> For example, HKUST-1<sup>28</sup> and M<sub>2</sub>(dobdc)<sup>29-31</sup> (M-MOF-74; M = Mg, Mn, Fe, Co, Ni, and Zn) exhibit stronger binding enthalpies for olefins than alkanes due to the metal-π interactions. Altering the charge density of the metal centers can improve the olefin adsorption and selectivity as revealed by M<sub>2</sub>(dobdc) isomers.<sup>33</sup> The appropriate aperture combined with OMSS of high density can also significantly improve the bonding affinity for olefins. In 2020, Qian *et al.* reported two microporous MOFs functionalized with different amounts of carboxylate groups, in which the carboxylate groups not only can adjust the aperture size, but also chelate with copper(I) ions *via* post-synthetic modification.<sup>41</sup> Therefore, Cu<sup>I</sup>@UiO-66-(COOH)<sub>2</sub> exhibits optimal apertures and exposed Cu(I) centers to form a strong binding affinity for C<sub>2</sub>H<sub>4</sub>, while suppressing the adsorption of C<sub>2</sub>H<sub>6</sub>. Compared with other UiO-66 materials, Cu<sup>I</sup>@UiO-66-(COOH)<sub>2</sub> showed the highest ideal adsorbed solution

Table 2 Summary of representative MOFs for adsorptive separation of important gases

Materials	Gas separation	Strategies	Uptake <sup>d</sup> (mmol g <sup>-1</sup> )	Selectivity <sup>b</sup>	Ref.
ATC-Cu	CH <sub>4</sub> /N <sub>2</sub>	Incorporating adjacent open copper sites	2.9/0.75	9.7	23
Ni(ina) <sub>2</sub>		Optimizing pore sizes (5.0 × 4.8 Å <sup>2</sup> )	1.82/0.53	15.8	24
DMOF-A <sub>2</sub>		Optimizing pore sizes (5.3 Å) and incorporating parallel aromatic rings	1.65/0.39	7.2	25
MAF-92	CO <sub>2</sub> /CH <sub>4</sub>	Optimizing pore sizes (5.0 × 4.8 Å <sup>2</sup> )	2.06/0.06	1.3 × 10 <sup>7</sup>	27
Cu <sup>+</sup> @UiO-66-(COOH) <sub>2</sub>	C <sub>2</sub> H <sub>4</sub> /C <sub>2</sub> H <sub>6</sub>	Optimizing pore sizes (4.1 Å) and incorporating copper(i) ions onto the pore surfaces	1.9/0.9	80.8	41
UTSA-280		Optimizing pore rigidity and pore size (3.8 Å)	2.5/0.098	>10000	35
Co-gallate		Optimizing pore size (5.2 Å)	3.37/0.31	52	36
ZnAl <sub>2</sub> PO <sub>4</sub>		Optimizing pore structure (3.8 Å) and incorporating electronegative functional groups	1.92/1.04	36.6 <sup>c</sup> /12.4 <sup>d</sup>	39
ZU-901		Optimizing pore size (3.4 × 4.2 Å <sup>2</sup> )	1.55/0.26	—	40
MAF-49	C <sub>2</sub> H <sub>6</sub> /C <sub>2</sub> H <sub>4</sub>	Incorporating multiple hydrogen-bonding acceptors and dipole repulsion groups	1.7/1.69	2.7	59
Cu(Oc) <sub>b</sub>		Optimizing pore size (3.3 Å)	1.85/0.78	3.4	60
[Fe <sub>2</sub> (O <sub>2</sub> )(dobdc)]		Incorporating Fe-peroxo sites	3.29/2.6	4.4	61
SIFSIX-2-Cu-i	C <sub>2</sub> H <sub>2</sub> /C <sub>2</sub> H <sub>4</sub>	Optimizing pore size (4.4 Å) and incorporating SiF <sub>6</sub> <sup>2-</sup> sites	4.02/2.19	44.8	70
UTSA-200a		Optimizing pore size (3.4 Å) and incorporating SiF <sub>6</sub> <sup>2-</sup> sites	3.65/0.63	6320	71
UTSA-300a		Optimizing pore size (1.3 × 2.8 Å <sup>2</sup> ) and incorporating SiF <sub>6</sub> <sup>2-</sup> sites	3.08/0.04	27	72
NCU-100a		Optimizing pore size (1.4 × 3.0 Å <sup>2</sup> ) and incorporating SiF <sub>6</sub> <sup>2-</sup> sites	4.57/0.32	7291	76
UTSA-74	C <sub>2</sub> H <sub>2</sub> /CO <sub>2</sub>	Incorporating open Zn sites	4.82/3.03	9	101
Cu <sup>+</sup> @UiO-66-(COOH) <sub>2</sub>		Incorporating copper(i) ions onto the pore surfaces	2.44/0.85	185	107
JNU-4		Incorporating open Cu sites	9.82/7.1	8.2	108
CPL-1-NH <sub>2</sub>		Incorporating amine sites	1.84/0.21	119	114
CAU-10-H		Suitable pore sizes (4.7 Å)	4.01/2.68	4	115
CAU-10-NH <sub>2</sub>		Suitable pore sizes (3.8 Å) and incorporating amine sites	3.57/2.08	10.8	116
FJU-90		Pore space partition	8.04/4.6	4.3	122
UTSA-300a		Optimizing pore size (1.3 × 2.8 Å <sup>2</sup> ) and incorporating SiF <sub>6</sub> <sup>2-</sup> sites	3.08/0.18	860	72
NCU-100a		Optimizing pore size (1.4 × 3.0 Å <sup>2</sup> ) and incorporating SiF <sub>6</sub> <sup>2-</sup> sites	4.57/0.49	1787	125
FJI-H36		Suitable pore sizes (12.9 × 12.9 Å <sup>2</sup> and 8.4 × 10.2 Å <sup>2</sup> ), flexible pore structure, incorporating Ni and free N atoms sites	6.46/4.20	3.5	127
SOFOR-TEPE-Zn		Incorporating electronegative pore surfaces	3.98/0.63	16 833	97
ZUL-330		Optimizing pore size (3.3 × 3.7 Å <sup>2</sup> ) and incorporating SiF <sub>6</sub> <sup>2-</sup> sites	7.33/1.1	10 086	98
Cu-F-pymo	CO <sub>2</sub> /C <sub>2</sub> H <sub>2</sub>	Incorporating residual guest molecules blocking the priority site for C <sub>2</sub> H <sub>2</sub>	2.09/0.1	>10 <sup>5</sup>	143
Cd-NP		Suitable pore space (6.1 × 4.5 × 4.5 Å <sup>3</sup> ), window size (3.2 Å) and incorporating complementary electrostatic potentials on the pore surface	2.59/0.43	85	144
Y-bptic		Incorporating large pore cage space (pore diameter: 9.46 Å), suitable pore window (4.2 Å) and μ <sub>3</sub> -OH <sup>-</sup> anions sites	2.48/1.17	4.1/114 <sup>c</sup>	136
MUF-4		Suitable pore window size (2.2 Å)	3.17/—	3363 <sup>c</sup>	139
ALF		Incorporating electropositive surface and the hydrogen-confined pore cavities with appropriate dimensional size (4.1 × 5.3 Å <sup>2</sup> )	3.85/0.15	6.5 × 10 <sup>5</sup>	148
MAF-23-O		Incorporating carbonyl oxygen atoms sites	1.34/1	8.8/71 <sup>c</sup>	149
UTSA-400	C <sub>3</sub> H <sub>6</sub> /C <sub>3</sub> H <sub>8</sub>	Optimizing pore sizes (3.0 Å) and incorporating WO <sub>2</sub> F <sub>4</sub> <sup>2-</sup> sites	1.84/0.05	>10 <sup>7</sup>	151
Y-abtc		Optimizing pore sizes (4.7 Å)	2/0.07	—	152
HIAM-301		Optimizing pore sizes (4.6 Å)	3.16/0.27	150	153
Co-gallate		Optimizing pore sizes (4.2 × 5.1 Å <sup>2</sup> )	1.79/0.14	333	154
JNU-3a		Incorporating orthogonally arrayed dynamic apertures	2.62/2.14	513	155
NTU-85		Optimizing pore sizes (4.5 Å)	0.45/0.003	1570	156
ZJU-75a		Suitable pore sizes (4.1 × 4.4 Å <sup>2</sup> ) and incorporating high-density open Ni sites	3.31/2.33	54.2	157
PCP-IPA	C <sub>3</sub> H <sub>8</sub> /C <sub>3</sub> H <sub>6</sub>	Suitable pore sizes (4.7 × 5.6 Å <sup>2</sup> ) and incorporating parallel-aligned aromatic-based units	2.23/2.25	2.48	169
FDMOF-2		Optimizing pore sizes (3.0 Å) and incorporating -CF <sub>3</sub> groups	5.04/4.15	2.18	170
ELM-12	C <sub>3</sub> H <sub>4</sub> /C <sub>3</sub> H <sub>6</sub>	Suitable pore cavities (6.1 × 4.3 × 4.3 Å <sup>3</sup> and 6.8 × 4.0 × 4.2 Å <sup>3</sup> ) and incorporating dynamic dangling OTF <sup>-</sup> groups	2.79/1.45	83	181
UTSA-200		Optimizing pore size (3.4 Å) and incorporating SiF <sub>6</sub> <sup>2-</sup> sites	3.58/1.20	>20 000	182
sql-NbOFFIVE-bpe-Cu-AB		Optimizing pore size (3.96 × 5.56 Å <sup>2</sup> ) and incorporating NbOF <sub>5</sub> <sup>2-</sup> sites	3.04/2.10	220	189
ZU-52	C <sub>3</sub> H <sub>6</sub> /n-C <sub>4</sub> H <sub>10</sub> /i-C <sub>4</sub> H <sub>10</sub>	Optimizing pore size (4.31 Å) and incorporating fluoroniobate sites	2.64/2.26/0.48	—	192

Table 2 (continued)

Materials	Gas separation	Strategies	Uptake <sup>d</sup> (mmol g <sup>-1</sup> )	Selectivity <sup>b</sup>	Ref.
ZU-33	i-C <sub>4</sub> H <sub>8</sub> /n-C <sub>4</sub> H <sub>10</sub> /C <sub>4</sub> H <sub>6</sub>	Optimizing pore size (4.20 Å) and incorporating GeF <sub>6</sub> <sup>2-</sup> sites	2.67/0.57/0.42	—	193
MAF-23	n-C <sub>4</sub> H <sub>10</sub> /i-C <sub>4</sub> H <sub>10</sub>	Incorporating flexible quasi-discrete pores	2/2/2/2	—	195
Zn-bzc-2CH <sub>3</sub>	nHEX/3MP/23DMB	Optimizing pore size (4.13 Å)	2.42/0.03	—	197
Zr-abtc	nHEX/3MP/22DMB	Suitable pore window size (4.5 Å)	1.28/1.02/0.58	—	198
HIAM-203	nHEX/3MP/22DMB	Suitable pore window size (4.8 Å)	1.7/1.43/0.07	—	199
CopzNi	nHEX/2MP/22DMB	Incorporating open Ni sites	2.17/1.46/0.08	—	206
Mn-dhbc	pX/mX/oX	Incorporating multiple open Mn sites, rich π-electrons, and structural flexibility	1.74/1.48/0.22 <sup>e</sup> 1.33/0.16/0.21 <sup>f</sup>	—	207
ZU-61	pX/mX/oX/EB	Incorporating adaptable pore structure and NbOF <sub>5</sub> <sup>2-</sup> sites	3.44/3.37/3.2 <sup>g</sup>	—	208
ZUL-C3	EB/ST/ToI/Bz	Incorporating nonaromatic low-polar pore environment	3.25/5.35/3.41/3.27	—	209
MAF-41		Incorporating structural flexibility	2.31/0.3	—	209

<sup>a</sup> Uptake amount at 1 bar and room temperature. <sup>b</sup> Calculated by IAST at ambient temperature and 1 bar. <sup>c</sup> Kinetic selectivity at ambient temperature. <sup>d</sup> Equilibrium-kinetic combined selectivity at ambient temperature. <sup>e</sup> Uptake amount at 1.05 bar and 333 K. <sup>f</sup> Uptake amount at 1.05 bar and 393 K. <sup>g</sup> Uptake amount at 7.1 mbar and 333 K.

theory (IAST) selectivity of 80.8 for an equimolar C<sub>2</sub>H<sub>4</sub>/C<sub>2</sub>H<sub>6</sub> mixture at 298 K and 1 bar.

Molecular sieves can show the maximum C<sub>2</sub>H<sub>4</sub>/C<sub>2</sub>H<sub>6</sub> selectivity *via* molecular size exclusion, though it is quite challenging due to their similar molecular sizes. In 2018, Chen *et al.* reported a rigid ultramicroporous MOF [Ca(C<sub>4</sub>O<sub>4</sub>)(H<sub>2</sub>O)] (UTSA-280, H<sub>2</sub>C<sub>4</sub>O<sub>4</sub> = squaric acid) with one-dimensional (1D) pore channels for molecular sieving separation of C<sub>2</sub>H<sub>4</sub>/C<sub>2</sub>H<sub>6</sub>. UTSA-280, being assembled by calcium oxide chains and squarate linkers, shows 1D pores with the minimum cross-sectional area of 14.4 Å<sup>2</sup>, which falls precisely between the sizes of C<sub>2</sub>H<sub>4</sub> and C<sub>2</sub>H<sub>6</sub> (13.7 Å<sup>2</sup> and 15.5 Å<sup>2</sup>, respectively). Therefore, UTSA-280 can adsorb C<sub>2</sub>H<sub>4</sub> with an adsorption capacity of 2.5 mmol g<sup>-1</sup> at 298 K and 1 bar while blocking the diffusion of the relatively large C<sub>2</sub>H<sub>6</sub> molecules (Fig. 2).<sup>35</sup> The C<sub>2</sub>H<sub>4</sub>/C<sub>2</sub>H<sub>6</sub> selectivity of UTSA-280 was estimated to be over 10 000. The adsorption heat (*Q*<sub>st</sub>) of UTSA-280 for C<sub>2</sub>H<sub>4</sub> ranges from 20.5 to 35.0 kJ mol<sup>-1</sup>, which is lower than those of MOFs with OMSs (40–85 kJ mol<sup>-1</sup>).<sup>30,45</sup> Breakthrough experiments confirmed that high purity (>99.2%) of C<sub>2</sub>H<sub>4</sub> can be obtained from an equimolar C<sub>2</sub>H<sub>4</sub>/C<sub>2</sub>H<sub>6</sub> mixture with a productivity of 1.86 mmol g<sup>-1</sup>. It is worth noting that UTSA-280 is capable of efficiently capturing C<sub>2</sub>H<sub>4</sub> from a quaternary CH<sub>4</sub>/C<sub>2</sub>H<sub>4</sub>/C<sub>2</sub>H<sub>6</sub>/C<sub>3</sub>H<sub>8</sub> mixture (45/25/25/5). Dispersion-corrected density functional theory (DFT-D) calculations and single-crystal X-ray diffraction experiments revealed that C<sub>2</sub>H<sub>4</sub> molecules are adsorbed by UTSA-280 in a linear array with weak C–H···O hydrogen bonding, π···π stacking and van der Waals (vdW) interactions.

In 2018, Ren *et al.* reported a series of gallate-based MOFs, [M(C<sub>7</sub>O<sub>5</sub>H<sub>4</sub>)·2H<sub>2</sub>O] (termed M-gallates, M = Mg, Ni, and Co), for C<sub>2</sub>H<sub>4</sub>/C<sub>2</sub>H<sub>6</sub> separation with high sieving effect.<sup>36</sup> These MOFs contain 3D interconnected zigzag channels and have Brunauer–Emmett–Teller (BET) surfaces of *ca.* 424 (Ni), 559 (Mg), and 475 (Co) m<sup>2</sup> g<sup>-1</sup>. The pore sizes (3.47–3.69 Å) of these MOFs are close to the molecular sizes of C<sub>2</sub>H<sub>4</sub> (3.28 × 4.18 × 4.84 Å<sup>3</sup>) and C<sub>2</sub>H<sub>6</sub> (3.28 × 4.18 × 4.84 Å<sup>3</sup>). Therefore, M-gallates could highly selectively adsorb C<sub>2</sub>H<sub>4</sub> over C<sub>2</sub>H<sub>6</sub>. Among them, Co-gallate displays the highest performance for separation of C<sub>2</sub>H<sub>4</sub>/C<sub>2</sub>H<sub>6</sub>. The C<sub>2</sub>H<sub>4</sub> uptake capacity of Co-gallate is much higher than that for C<sub>2</sub>H<sub>6</sub> (3.37 mmol g<sup>-1</sup> vs. 0.31 mmol g<sup>-1</sup>), resulting in a high IAST selectivity of 52 at 298 K and 1 bar for an equimolar C<sub>2</sub>H<sub>4</sub>/C<sub>2</sub>H<sub>6</sub> mixture. The IAST selectivity of Mg-gallate is about 37.3 for an equimolar C<sub>2</sub>H<sub>4</sub>/C<sub>2</sub>H<sub>6</sub> mixture at 298 K and 1 bar. Breakthrough experiments for a 50/50 C<sub>2</sub>H<sub>4</sub>/C<sub>2</sub>H<sub>6</sub> mixture further demonstrated the excellent C<sub>2</sub>H<sub>4</sub>/C<sub>2</sub>H<sub>6</sub> separation performances of these low-cost M-gallates.

In 2020, Xing *et al.* reported a phosphate-pillared MOF, [Zn<sub>3</sub>(atz)<sub>3</sub>(PO<sub>4</sub>)<sub>n</sub>] (ZnAtzPO<sub>4</sub>, Hatz = 3-amino-1,2,4-triazole), for C<sub>2</sub>H<sub>4</sub>/C<sub>2</sub>H<sub>6</sub> separation with high selectivity (12.4 at 298 K and 32.4 at 273 K).<sup>39</sup> Single-component gas adsorption and kinetic studies revealed that ZnAtzPO<sub>4</sub> has a higher C<sub>2</sub>H<sub>4</sub> adsorption capacity (1.92 mmol g<sup>-1</sup>) than for C<sub>2</sub>H<sub>6</sub> (1.04 mmol g<sup>-1</sup>) at 298 K and 1 bar, as well as a faster adsorption rate for C<sub>2</sub>H<sub>4</sub> compared with C<sub>2</sub>H<sub>6</sub>, giving a kinetic selectivity of 36.6. DFT calculations demonstrated that electronegative groups decorated on the narrow pore apertures of ZnAtzPO<sub>4</sub> can effectively capture C<sub>2</sub>H<sub>4</sub> and inhibit the diffusion of C<sub>2</sub>H<sub>6</sub>, resulting in an

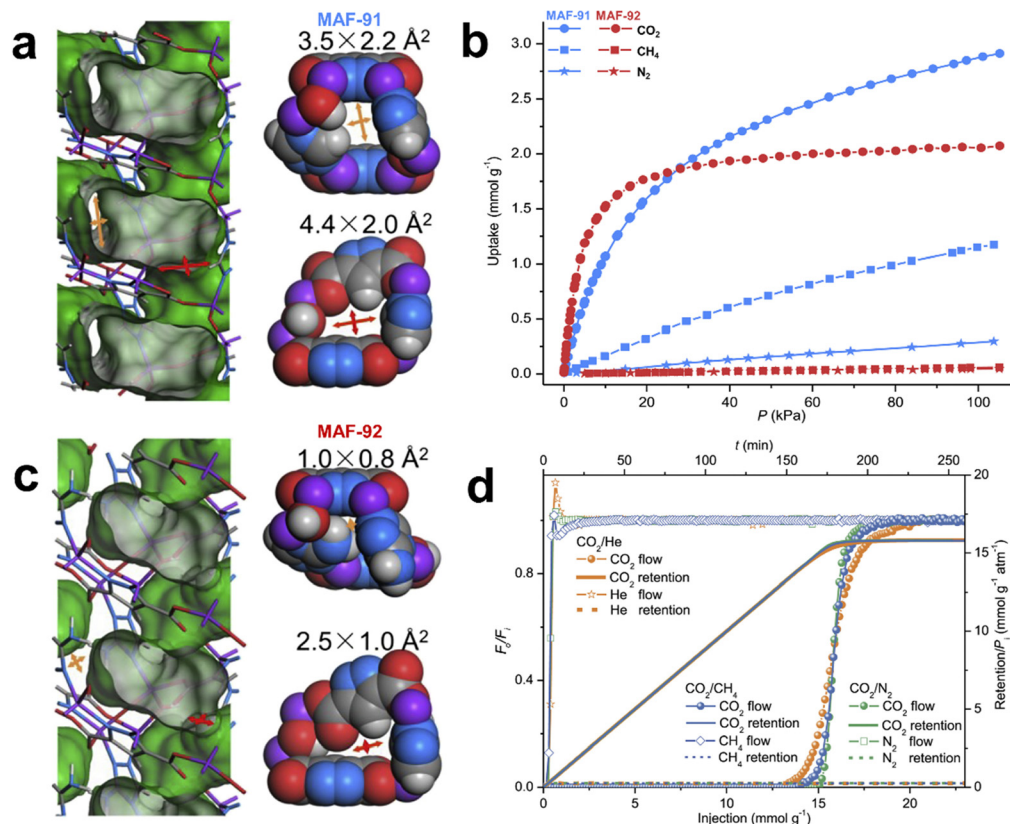


Fig. 1 (a) and (c) Crystal structures of MAF-91 and MAF-92. (b)  $\text{CO}_2$ ,  $\text{CH}_4$ , and  $\text{N}_2$  adsorption isotherms of MAF-91 and MAF-92 at 298 K. (d) Column breakthrough behaviors of MAF-92 for 10:90  $\text{CO}_2/\text{N}_2$ , 10:90  $\text{CO}_2/\text{CH}_4$  and 10:90  $\text{CO}_2/\text{He}$  mixtures. Reprinted with permission from ref. 27. Copyright 2021 Cell Press.

efficient equilibrium-kinetic  $\text{C}_2\text{H}_4/\text{C}_2\text{H}_6$  separation. A flexible ultramicroporous MOF,  $[\text{Cu}_2(\text{pyz-CH}_3)(\text{pzdc})_2]$  (ZU-901,  $\text{pyz-CH}_3 = 2$ -methylpyrazine, and  $\text{H}_2\text{pzdc} = 2,3$ -pyrazinedicarboxylic acid), with a pore size of  $3.4 \times 4.2 \text{ \AA}^2$  was recently reported to show a  $\text{C}_2\text{H}_4$  adsorption-desorption curve in an S shape with high  $\text{C}_2\text{H}_4$  working capacity and facile regeneration.<sup>40</sup> Single-component sorption experiments showed that ZU-901 can adsorb  $1.55 \text{ mmol g}^{-1} \text{ C}_2\text{H}_4$  and much less  $\text{C}_2\text{H}_6$  ( $0.26 \text{ mmol g}^{-1}$ ) at 298 K and 1 bar. The adsorption selectivity of ZU-901 calculated for the pressure swing adsorption (PSA) process is 65. The  $Q_{\text{st}}$  of ZU-901 for  $\text{C}_2\text{H}_4$  was calculated to be  $\sim 25 \text{ kJ mol}^{-1}$ , which indicates that ZU-901 can be mildly regenerated. The simulated two-bed PSA process revealed that polymer-grade ethylene (ca. 99.5%) can be obtained by ZU-901 with only 1/10 of the energy consumption compared to simulating cryogenic distillation ( $2.03 \text{ kJ mol}^{-1}$  vs.  $21.84 \text{ kJ mol}^{-1}$ ).

For  $\text{C}_2\text{H}_4$ -selective MOF materials, multiple adsorption and desorption cycles are typically required to achieve high-purity ethylene. In contrast,  $\text{C}_2\text{H}_6$ -selective adsorbents can directly give pure ethylene by one single separation operation, making it simple to operate and more energy efficient. Compared to the  $\text{C}_2\text{H}_4$  molecule, the  $\text{C}_2\text{H}_6$  molecule has a slightly larger polarizability and two additional hydrogen atoms. MOFs with OMSs usually interact strongly with  $\text{C}_2\text{H}_4$  molecules *via*  $\pi$  complexation, whereas MOFs with relatively less polar sites, usually, can preferentially adsorb  $\text{C}_2\text{H}_6$  over  $\text{C}_2\text{H}_4$ .<sup>46–66</sup>

In an earlier study, Gascon *et al.* firstly reported preferential capture of  $\text{C}_2\text{H}_6$  over  $\text{C}_2\text{H}_4$  by utilizing the gate-opening effect of ZIF-7 (also known as MAF-3).<sup>58</sup> However, the separation efficiency was low due to the lack of active binding sites. In 2015, Zhang *et al.* reported a porous MAF  $[\text{Zn}(\text{batz})]$  (MAF-49,  $\text{H}_2\text{batz} = \text{bis}(5\text{-amino-1H-1,2,4-triazol-3-yl)methane}$ ), which shows a high  $\text{C}_2\text{H}_6/\text{C}_2\text{H}_4$  selectivity of 9 at 316 K.<sup>59</sup> In MAF-49, there are quasi-discrete cages functionalized with a high density of electronegative nitrogen atoms on the surface, which are further interconnected by smaller paths into 1D channels (Fig. 3). DFT calculations and crystallographic study indicated that a  $\text{C}_2\text{H}_6$  molecule confined in the cage can form stronger and more non-classical C–H $\cdots$ N hydrogen bonds or electrostatic interactions through better structural matching with the cage surface of MAF-49 as compared to the  $\text{C}_2\text{H}_4$  molecule, which is beneficial for capture, or stronger binding of  $\text{C}_2\text{H}_6$  compared with  $\text{C}_2\text{H}_4$ . MAF-49 showed, for the first time, an exceptional reversed selectivity compared with porous materials including MOFs, which conventionally bind more strongly with  $\text{C}_2\text{H}_4$  vs.  $\text{C}_2\text{H}_6$ . Breakthrough experiments for the  $\text{C}_2\text{H}_4/\text{C}_2\text{H}_6$  (15:1) mixture showed that MAF-49 can give highly pure  $\text{C}_2\text{H}_4$  (99.95%+) within a single breakthrough operation under ambient conditions.

An appropriate combination of pore sites and pore surface can maximize the weak host-guest interactions, thus highly enhancing the performance of MOFs for  $\text{C}_2\text{H}_6/\text{C}_2\text{H}_4$  separation.

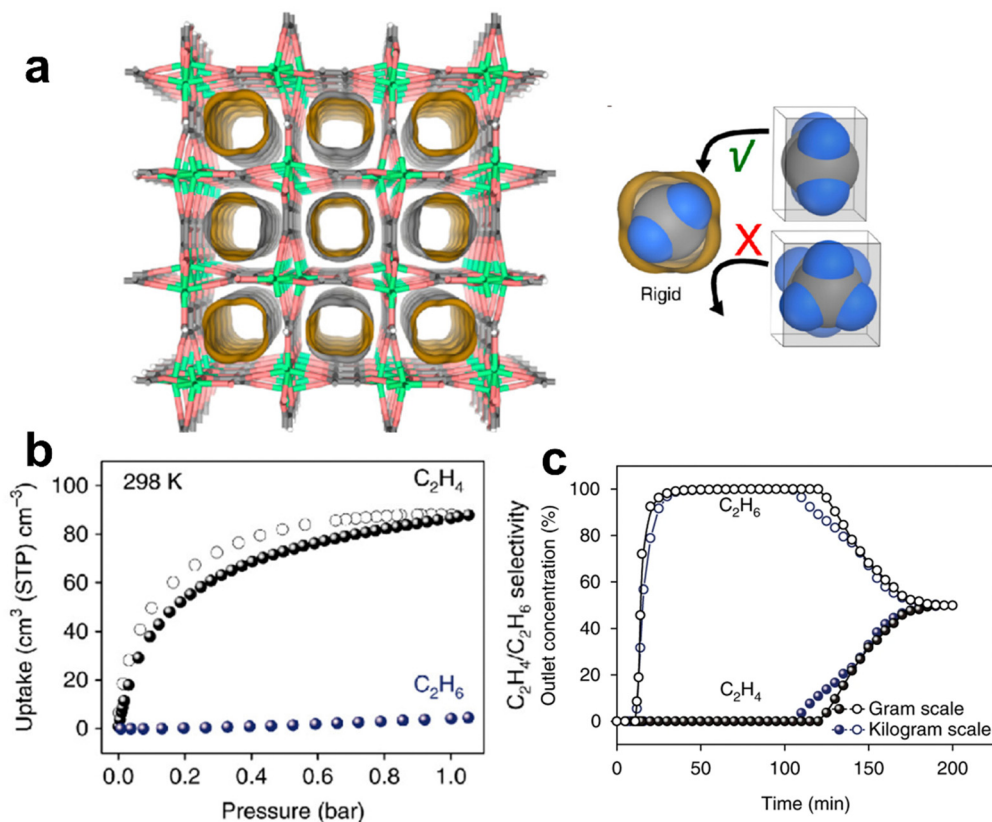


Fig. 2 (a) Structure of UTSA-280. (b) Sorption isotherms of UTSA-280 for  $C_2H_4$  and  $C_2H_6$  at 298 K. (c) Breakthrough curves for UTSA-280 from different scales for an equimolar mixture of  $C_2H_4/C_2H_6$  at 298 K and 1 bar. Reprinted with permission from ref. 35. Copyright 2018 Nature Publishing Group.

In 2018, Chen *et al.* reported two isorecticular MOFs,  $[Cu(Qc)_2]$  (HQc = quinoline-5-carboxylic acid) and  $[Cu(ina)_2]$  (Hina = isonicotinic acid), featuring 1D channels with pore sizes of  $\sim 4.1$  and  $\sim 3.3$  Å, respectively, and an array of low-polarity aromatic surfaces with different contact areas on the channels (Fig. 4).<sup>60</sup> Single-component sorption results demonstrated that  $[Cu(Qc)_2]$  shows a higher  $C_2H_6$  uptake than  $C_2H_4$  ( $60.0$   $cm^3$   $cm^{-3}$  vs.  $25.3$   $cm^3$   $cm^{-3}$ , *i.e.*,  $1.85$   $mmol$   $g^{-1}$  vs.  $0.78$   $mmol$   $g^{-1}$ ) at 298 K and 1 bar, thus giving a high  $C_2H_6/C_2H_4$  selectivity of 3.4 for an equimolar  $C_2H_6/C_2H_4$  mixture at 298 K and 1 bar. In contrast,  $[Cu(ina)_2]$  shows comparable adsorption capacity for both gases ( $C_2H_4$ :  $67.4$   $cm^3$   $cm^{-3}$ , and  $C_2H_6$ :  $64.3$   $cm^3$   $cm^{-3}$ , *i.e.*,  $1.99$   $mmol$   $g^{-1}$  vs.  $1.90$   $mmol$   $g^{-1}$ ) due to the smaller polar surface. Neutron powder diffraction and DFT-D calculations showed that the high  $C_2H_6$  selectivity in  $[Cu(Qc)_2]$  can be attributed to the more C–H $\cdots\pi$  interactions formed between  $C_2H_6$  and  $[Cu(Qc)_2]$ . Breakthrough experiments demonstrated that high purity of  $C_2H_4$  ( $> 99.9\%$ ) can be directly collected from a 50/50  $C_2H_6/C_2H_4$  mixture by a packed column bed of  $[Cu(Qc)_2]$ , with a separation productivity of  $587$   $mmol$   $L^{-1}$ .

The incorporation of the peroxo sites into MOFs can improve the affinity for  $C_2H_6$ . In 2018, Chen *et al.* reported a microporous MOF  $[Fe_2(O_2)(dobdc)]$  ( $dobdc^{4-} = 2,5$ -dioxido-1,4-benzenedicarboxylate) decorated with Fe–peroxo sites that exhibits a high  $C_2H_6$  affinity with a large  $Q_{st}$  of  $66.8$   $kJ$   $mol^{-1}$  (Fig. 5).<sup>61</sup> Single-component sorption isotherms showed that

$[Fe_2(O_2)(dobdc)]$  can adsorb a large amount of  $C_2H_6$  ( $74.3$   $cm^3$   $g^{-1}$ ,  $3.32$   $mmol$   $g^{-1}$ ) at 1 bar and 298 K and the IAST selectivity for 50/50  $C_2H_6/C_2H_4$  was calculated to be 4.4 under the same conditions. High-resolution neutron powder diffraction showed that  $C_2D_6$  molecules can form strong non-classical C–D $\cdots$ O hydrogen bonds with very short D $\cdots$ O distances ( $\sim 2.17$  to  $2.22$  Å). Therefore,  $[Fe_2(O_2)(dobdc)]$  exhibits excellent separation performance, yielding polymer-grade  $C_2H_4$  ( $\geq 99.99\%$ ) from 50/50  $C_2H_4/C_2H_6$  mixtures in a single breakthrough operation and a productivity of  $0.79$   $mmol$   $g^{-1}$ . This result further confirms the unique and important role of non-classical C–H $\cdots$ O hydrogen bonds in the molecular recognition and selective adsorption of ethane by MOFs.

### 2.3. $C_2H_2/C_2H_4$ separation

In the petrochemical industry, the production of  $C_2H_4$  involves trace amounts of acetylene ( $C_2H_2$ ) impurities ( $\sim 1\%$ ). The removal of these impurities is crucial as even small amounts of acetylene during ethylene polymerization can cause catalyst poisoning and highly affect the production of polyethylene. Extensive research has been conducted on the adsorptive separation of MOFs for  $C_2H_2/C_2H_4$  mixtures.<sup>67–78</sup> Chen *et al.* first reported a series of M'MOFs for separation of  $C_2H_4$  from  $C_2H_2/C_2H_4$ .<sup>67</sup> However, these M'MOFs show modest selectivity for  $C_2H_2$  over  $C_2H_4$ . In 2015, they further reported an amino-functionalized microporous MOF (UTSA-100) with 1D channels ( $4.3$  Å) and small cages ( $4.0$  Å), showing a moderately high  $C_2H_2$  uptake of

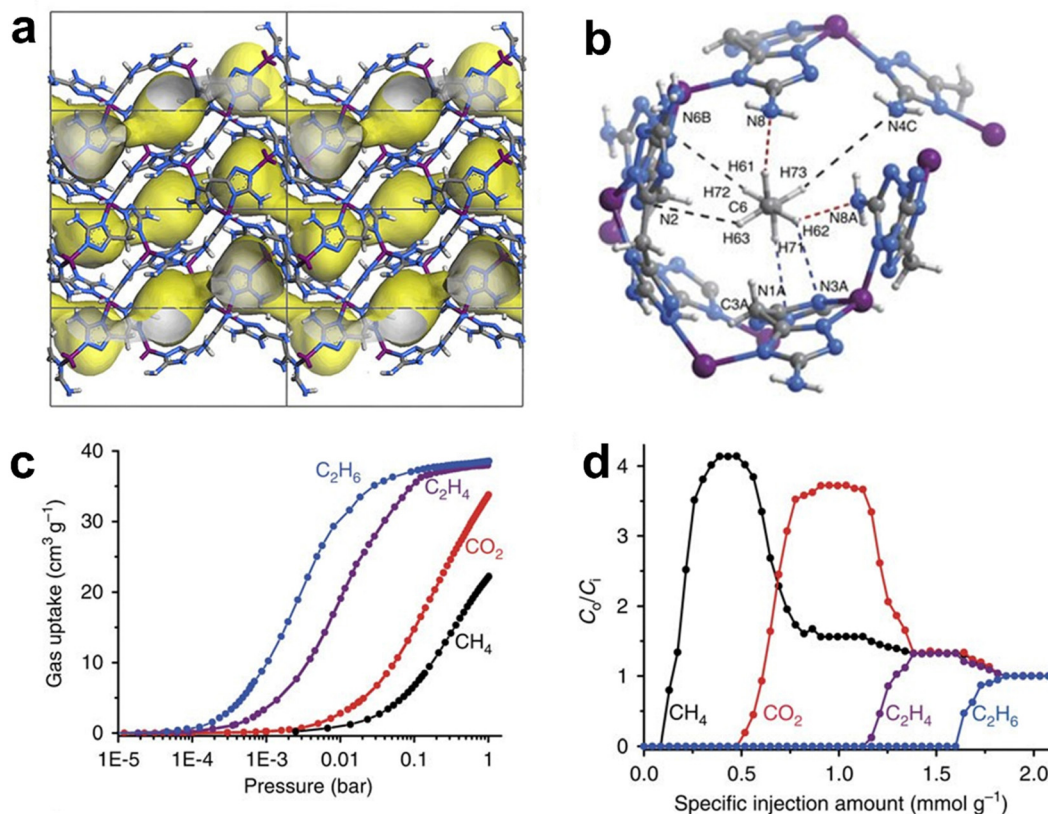


Fig. 3 (a) Crystal structure of MAF-49. (b) Preferential adsorption sites for  $C_2H_6$  in MAF-49 revealed by DFT calculations. (c) Gas adsorption isotherms for  $C_2H_6$ ,  $C_2H_4$ ,  $CO_2$  and  $CH_4$  in MAF-49 at 316 K. (d) Breakthrough curves of the  $CH_4/CO_2/C_2H_4/C_2H_6$  mixture (1 : 1 : 1 : 1 (vol)) for MAF-49 measured at 313 K and 1 bar. Reprinted with permission from ref. 59. Copyright 2018 Nature Publishing Group.

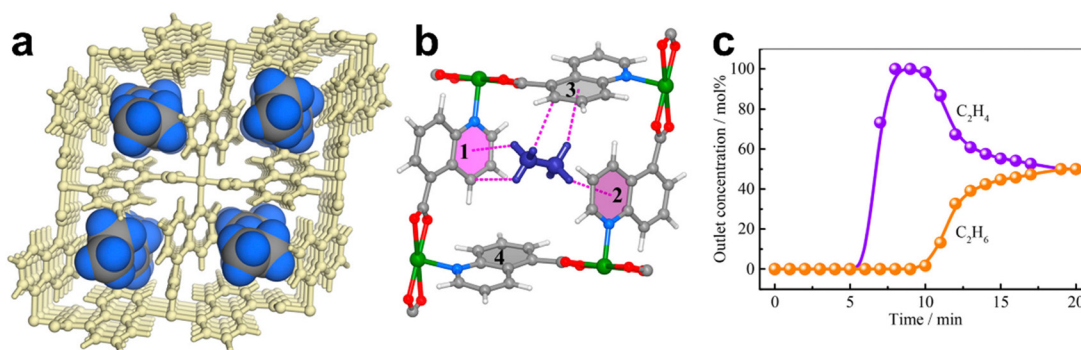


Fig. 4 (a) Neutron diffraction crystal structure of  $[Cu(Qc)_2] \cdot 0.41C_2D_6$ . (b) Preferential binding sites for the  $C_2D_6$  molecule and the close vdW contacts within the rhombic cavity of aromatic rings, highlighting  $C-H \cdots \pi$  interactions in pink dashed bonds. (c) Experimental column breakthrough curves for an equimolar  $C_2H_6/C_2H_4$  mixture (298 K, 1 bar) in an adsorber bed packed with  $Cu(Qc)_2$ . Reprinted with permission from ref. 60. Copyright 2018 American Chemical Society.

$95.6 \text{ cm}^3 \text{ g}^{-1}$  ( $4.27 \text{ mmol g}^{-1}$ ) at 296 K but with a much lower  $C_2H_4$  uptake ( $37.2 \text{ cm}^3 \text{ g}^{-1}$ ,  $1.66 \text{ mmol g}^{-1}$ ). The calculated IAST selectivity of UTSA-100 for a 1/99  $C_2H_2/C_2H_4$  mixture is 10.7. This work well demonstrates that suitable pore sizes and binding sites can highly improve the separation performance of MOFs for removing trace  $C_2H_2$  from  $C_2H_4$ .<sup>68</sup>

To obtain materials with high  $C_2H_2$  adsorption capacity and high selectivity, in 2016, Chen *et al.* reported a series of SIFSIX

MOFs, namely, SIFSIX-1-Cu, SIFSIX-2-Cu, SIFSIX-2-Cu-i, SIFSIX-3-Ni, and SIFSIX-3-Zn, which allow preferential capture of  $C_2H_2$  from the  $C_2H_2/C_2H_4$  mixture with high selectivity and adsorption capacity.<sup>70</sup> These materials possess different pore sizes, which can be systematically fine-tuned by replacing ligands, metal nodes, inorganic anions or framework interpenetration. Among them, SIFSIX-2-Cu-i with a two-fold interpenetrated framework and pore size of  $5.2 \times 5.2 \text{ \AA}^2$  (BET surface area

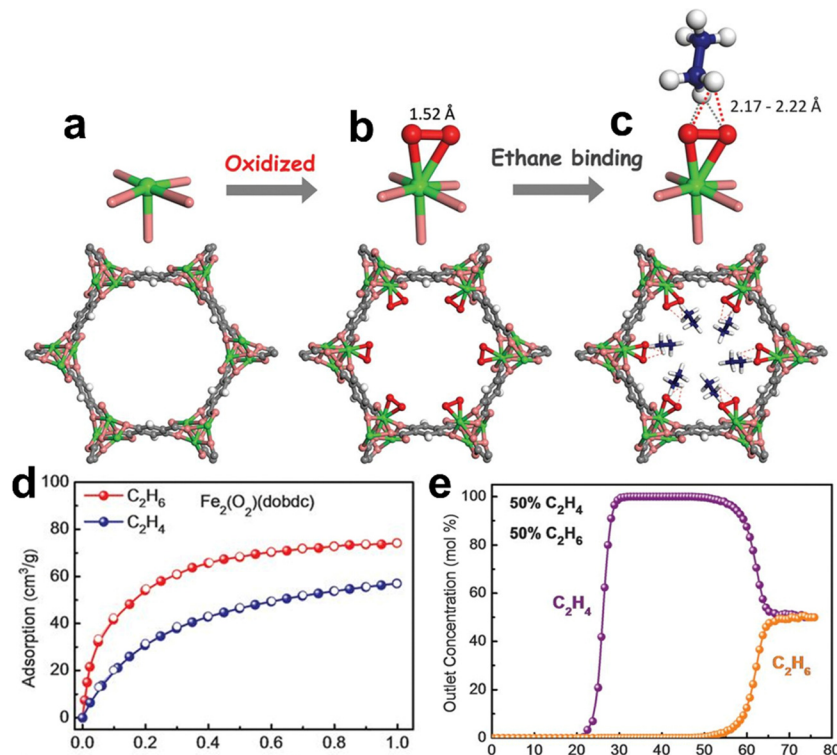


Fig. 5 Crystal structures of (a) pristine [Fe<sub>2</sub>(dobdc)] and [Fe<sub>2</sub>(O<sub>2</sub>)(dobdc)] (b) after oxidation and (c) after final C<sub>2</sub>D<sub>6</sub>-loading. (d) Sorption isotherms of [Fe<sub>2</sub>(O<sub>2</sub>)(dobdc)] for C<sub>2</sub>H<sub>6</sub> and C<sub>2</sub>H<sub>4</sub> under ambient conditions. (e) Breakthrough curves of [Fe<sub>2</sub>(O<sub>2</sub>)(dobdc)] for an equimolar C<sub>2</sub>H<sub>6</sub>/C<sub>2</sub>H<sub>4</sub> mixture under ambient conditions. Reprinted with permission from ref. 61. Copyright 2018 the American Association for the Advancement of Science.

503 m<sup>2</sup> g<sup>-1</sup>) exhibits a high uptake for C<sub>2</sub>H<sub>2</sub> (2.1 mmol g<sup>-1</sup>, *i.e.*, 47 cm<sup>3</sup> g<sup>-1</sup>) at a low pressure of 0.025 bar, indicating its strong binding affinity for C<sub>2</sub>H<sub>2</sub> (Fig. 6). The IAST selectivity of SIFSIX-2-Cu-i for C<sub>2</sub>H<sub>2</sub>/C<sub>2</sub>H<sub>4</sub> (1/99) is up to 44.54. SIFSIX-2-Cu with a pore size of 8.0 × 8.0 Å<sup>2</sup> (BET surface area: 1178 m<sup>2</sup> g<sup>-1</sup>) shows the highest C<sub>2</sub>H<sub>2</sub> uptake of 8.5 mmol g<sup>-1</sup> and a moderate IAST selectivity for C<sub>2</sub>H<sub>2</sub>/C<sub>2</sub>H<sub>4</sub> (1/99) of 10.6. Breakthrough experiments demonstrated that all these SIFSIX MOFs can produce polymer-grade C<sub>2</sub>H<sub>4</sub> from C<sub>2</sub>H<sub>2</sub>/C<sub>2</sub>H<sub>4</sub> (1/99 or 50/50 mixtures). DFT-D calculations and high-resolution neutron powder diffraction studies revealed that SiF<sub>6</sub><sup>2-</sup> pillars in the framework can form strong hydrogen-bonding interactions with C<sub>2</sub>H<sub>2</sub>, resulting in the high selectivity and adsorption capacity for C<sub>2</sub>H<sub>2</sub>. This work revealed that the combination of optimal pore size and multiple active sites can greatly improve the selectivity and adsorption capacity of the MOFs.

In 2017, Chen *et al.* reported a 2-fold interpenetrated MOF SIFSIX-14-Cu-i (UTSA-200) with a smaller pore size (3.4 Å) than SIFSIX-2-Cu-i (4.4 Å) and also functional as SiF<sub>6</sub><sup>2-</sup> sites that can enhance the binding affinity for C<sub>2</sub>H<sub>2</sub> (Fig. 7).<sup>71</sup> The pore size of the activated structure (UTSA-200a) ideally falls between the kinetic diameter of C<sub>2</sub>H<sub>4</sub> (4.2 Å) and C<sub>2</sub>H<sub>2</sub> (3.3 Å), endowing UTSA-200a with a high performance of molecular sieving separation of C<sub>2</sub>H<sub>2</sub>/C<sub>2</sub>H<sub>4</sub>. Single component equilibrium adsorption isotherms showed that UTSA-200a exhibits a high low-pressure uptake (58 cm<sup>3</sup> cm<sup>-3</sup>) for C<sub>2</sub>H<sub>2</sub> at 0.01 bar but a negligible uptake (~0.25 mmol g<sup>-1</sup>) for C<sub>2</sub>H<sub>4</sub> below 0.2 bar, which is significantly lower than the absorption of SIFSIX-2-Cu-i

(2.28 mmol g<sup>-1</sup>). The IAST selectivity for a 1/99 C<sub>2</sub>H<sub>2</sub>/C<sub>2</sub>H<sub>4</sub> mixture of UTSA-200a was calculated to be 6000 at 298 K and 1 bar. High-resolution neutron powder diffraction further revealed that the strong binding affinity of UTSA-200a for the C<sub>2</sub>D<sub>2</sub> molecule was achieved by short C–D···F hydrogen-bonding interactions (1.921 Å). Breakthrough experiments revealed that UTSA-200a can efficiently separate C<sub>2</sub>H<sub>2</sub> from a 1/99 C<sub>2</sub>H<sub>2</sub>/C<sub>2</sub>H<sub>4</sub> mixture to give an extremely high purity C<sub>2</sub>H<sub>4</sub> (99.9999%) with a productivity of 87.5 mmol g<sup>-1</sup>.

In 2017, Chen *et al.* reported an ultramicroporous SIFSIX-MOF [Zn(dps)<sub>2</sub>(SiF<sub>6</sub>)] (UTSA-300, dps = 4,4'-dipyridylsulfide) with small apertures (2.4 × 3.3 Å<sup>2</sup>) for specific recognition of C<sub>2</sub>H<sub>2</sub> from C<sub>2</sub>H<sub>4</sub>.<sup>72</sup> The desolvated structure UTSA-300a (aperture size: 3.3 Å) exhibits large affinity toward C<sub>2</sub>H<sub>2</sub> with a *Q<sub>st</sub>* of up to 57.6 kJ mol<sup>-1</sup> and thus can be selectively gate opened by C<sub>2</sub>H<sub>2</sub>. It should be noted that UTSA-300 shows complete size exclusion of C<sub>2</sub>H<sub>4</sub>, giving IAST selectivity for the equimolar C<sub>2</sub>H<sub>2</sub>/C<sub>2</sub>H<sub>4</sub> mixture up to >10<sup>4</sup> at 298 K. Breakthrough experiments confirmed its good separation performance for an equimolar C<sub>2</sub>H<sub>2</sub>/C<sub>2</sub>H<sub>4</sub> mixture. Subsequently, an isostructural framework of UTSA-300 [Cu(dps)<sub>2</sub>(SiF<sub>6</sub>)] (NCU-100 or UTSA-300-Cu) was reported.<sup>76</sup> In contrast to UTSA-300, NCU-100 possesses elongated Cu(II)–F bonds, showing a larger cavity size (3.6 × 4.3 × 4.2 Å<sup>3</sup> vs. 3.5 × 3.9 × 4.1 Å<sup>3</sup>) in the closed-pore phase. Single-component sorption experiments revealed that NCU-100a shows not only higher low-pressure uptake (0.73 mmol g<sup>-1</sup> vs. 0.04 mmol g<sup>-1</sup>) for C<sub>2</sub>H<sub>2</sub> at 0.01 bar and 298 K but also a higher total uptake capacity (4.57 mmol g<sup>-1</sup> vs. 3.08 mmol g<sup>-1</sup>) at 298 K and 1 bar, resulting

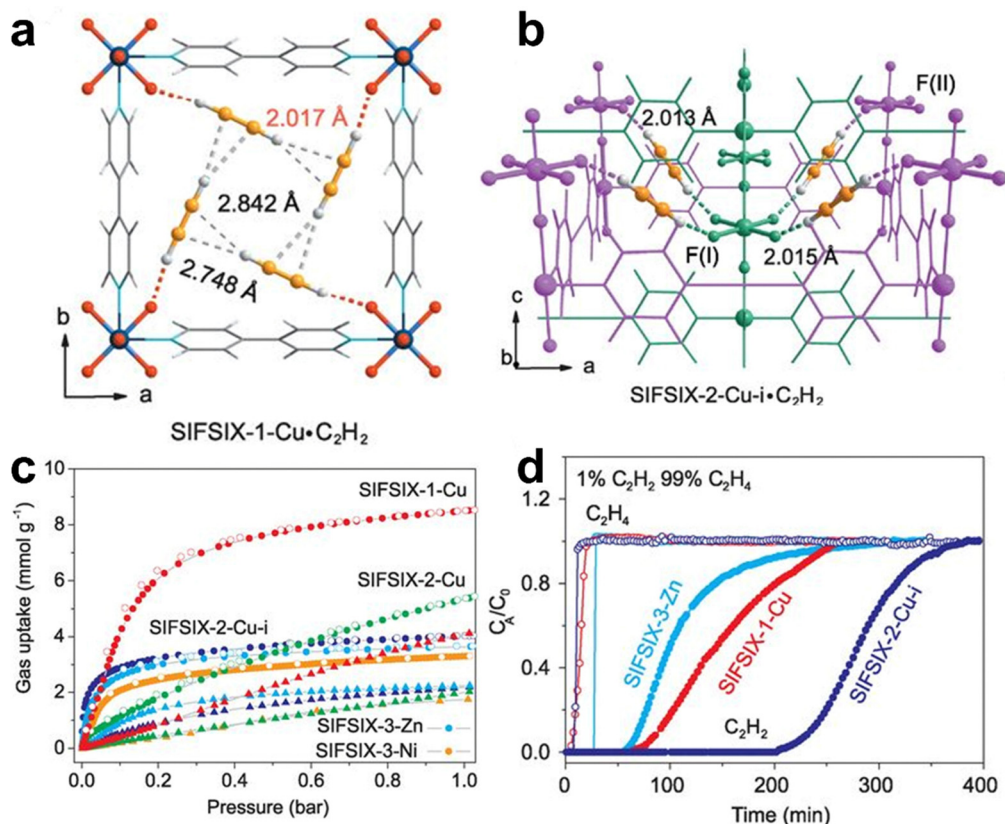


Fig. 6 (a) Crystal structure of SIFSIX-1-Cu·C<sub>2</sub>H<sub>2</sub>. (b) DFT-D simulated structure of C<sub>2</sub>H<sub>2</sub>-loaded SIFSIX-2-Cu-i. (c) Single-component sorption isotherms of SIFSIX-1-Cu, SIFSIX-2-Cu, SIFSIX-2-Cu-i, SIFSIX-3-Zn, and SIFSIX-3-Ni for C<sub>2</sub>H<sub>2</sub> and C<sub>2</sub>H<sub>4</sub> under ambient conditions. (d) Breakthrough curves of SIFSIX-1-Cu, SIFSIX-2-Cu, and SIFSIX-3-Zn for a 1/99 C<sub>2</sub>H<sub>2</sub>/C<sub>2</sub>H<sub>4</sub> mixture. Reprinted with permission from ref. 70. Copyright 2016 the American Association for the Advancement of Science.

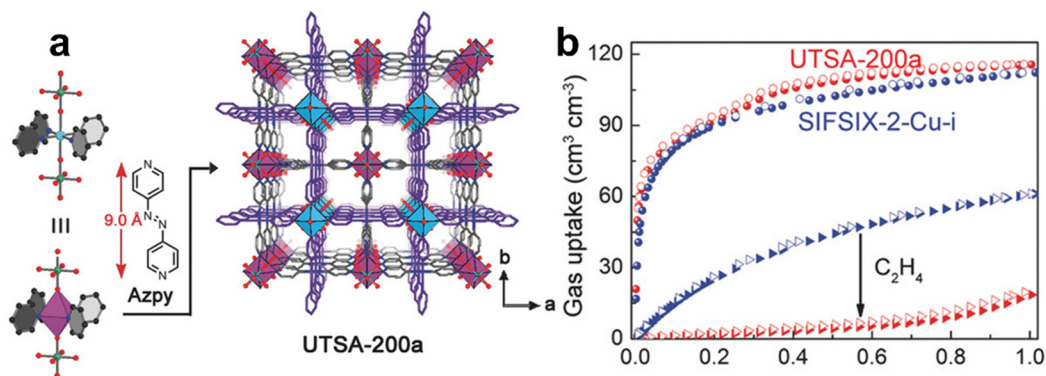


Fig. 7 (a) Crystal structure of UTSA-200. (b) C<sub>2</sub>H<sub>2</sub> and C<sub>2</sub>H<sub>4</sub> adsorption isotherms of UTSA-200a at 298 K. Adapted from ref. 71 with permission from Wiley-VCH, Copyright 2018.

in an IAST selectivity for 1/99 C<sub>2</sub>H<sub>2</sub>/C<sub>2</sub>H<sub>4</sub> up to 7291 (298 K and 1 bar). This excellent performance for C<sub>2</sub>H<sub>2</sub>/C<sub>2</sub>H<sub>4</sub> separation can also be attributed to the combination of optimal pore size and strong binding sites, as confirmed by DFT calculations and crystallographic studies. Breakthrough experiments confirmed that high purity C<sub>2</sub>H<sub>4</sub> (> 99.99%) can be obtained from a 1/99 C<sub>2</sub>H<sub>2</sub>/C<sub>2</sub>H<sub>4</sub> mixture with a productivity of 14.9 mmol g<sup>-1</sup>.

Recently, Zhai *et al.* synthesized a series of cluster-based MOFs, [M<sub>9</sub>(μ<sub>4</sub>-TAZ)<sub>6</sub>(μ<sub>3</sub>-HTAZ)<sub>x</sub>(μ<sub>3</sub>-TAZ)<sub>12-x</sub>(A)<sub>y</sub>] solvent (SNNU-98-M, M = Mn, Co, Ni, and Zn), for the purification of C<sub>2</sub>H<sub>2</sub>, in which the tetrazolate (TAZ) ligands coordinate with metal centers in tridentate (μ<sub>3</sub>-TAZ) and tetradentate (μ<sub>4</sub>-TAZ) bridging modes.<sup>78</sup> These MOFs of *acs* topology show high framework densities and high stabilities, as well as small pore sizes of

5.2 Å (Mn), 4.8 Å (Co), 4.8 Å (Ni), and 4.2 Å (Zn), respectively, which are expected to increase the separation selectivity and volumetric storage capacity. Single-component gas adsorption revealed that SNNU-98-Mn exhibits the highest volumetric  $C_2H_2$  uptake ( $222.9 \text{ cm}^3 \text{ cm}^{-3}$ ) at 298 K and 1 bar, and a high uptake for  $C_2H_2$  ( $175.3 \text{ cm}^3 \text{ cm}^{-3}$ ) at 298 K and 0.1 bar, whereas SNNU-98-Co shows the highest  $C_2H_2/C_2H_4$  IAST selectivity (2405.7) under room temperature and 1 bar. Column breakthrough experiments revealed that all these materials show good  $C_2H_2/C_2H_4$  separation performance, with SNNU-98-Mn displaying a higher  $C_2H_4$  productivity of  $64.6 \text{ mmol g}^{-1}$  from a 1/99  $C_2H_2/C_2H_4$  mixture and a longer breakthrough retention time ( $1362 \text{ min g}^{-1}$  and  $701 \text{ min g}^{-1}$  at 273 K and 298 K, respectively, with a gas flow rate of  $2 \text{ mL min}^{-1}$ ).

The separation of  $C_2H_4$  from multicomponent mixtures in one step is significant for obtaining polymer-grade  $C_2H_4$  due to the presence of multiple impurities in the cracking gas. Recently, more MOFs have been revealed to be capable of such multicomponent separation.<sup>79–94</sup> In 2018, Lu *et al.* reported the highly selective adsorption of  $C_2H_4$  from a  $C_2H_2/C_2H_4/C_2H_6$  mixture by a stable MOF,  $(Me_2NH_2)[Co_3(DCPN)_2(\mu_3-OH)(H_2O)] \cdot 11H_2O$  (TJT-100, DCPN = 5-(3',5'-dicarboxylphenyl)nicotinate).<sup>79</sup> TJT-100 exhibits a 1D channel (pore size:  $\sim 8.0 \text{ Å}$ ) decorated with a high density of carboxylate oxygen atoms. Single-component adsorption showed that the adsorption capacities of TJT-100 for  $C_2H_2$ ,  $C_2H_4$ , and  $C_2H_6$  were  $127.7 \text{ cm}^3 \text{ g}^{-1}$ ,  $98.1 \text{ cm}^3 \text{ g}^{-1}$ , and  $105.4 \text{ cm}^3 \text{ g}^{-1}$ , respectively. The breakthrough experimental results of TJT-100 for

the  $C_2H_2/C_2H_4/C_2H_6$  mixture (0.5:99:0.5) confirmed the preferential capture of  $C_2H_2$  and  $C_2H_6$ , giving  $C_2H_4$  with an excellent purity of 99.997%. DFT calculations revealed that  $C_2H_2$  and  $C_2H_6$  have multiple electrostatic interactions with the framework, which facilitates preferential adsorption of  $C_2H_2$  and  $C_2H_6$  by TJT-100.

In 2019, Zaworotko *et al.* reported a synergistic sorbent separation technique (SSST), which enables the one-step production of polymer-grade  $C_2H_4$  from a ternary ( $C_2H_2/C_2H_4/C_2H_6$ ) gas mixture, and even a quaternary ( $CO_2/C_2H_2/C_2H_4/C_2H_6$ ) gas mixture (Fig. 8).<sup>80</sup> Three microporous MOFs, TIFSIX-2-Cu-I, SIFSIX-3-Ni, and Zn-atz-ipa, were placed in tandem on the sorbent bed, offering selective adsorption of  $C_2H_2$ ,  $CO_2$ , and  $C_2H_6$ , respectively. Notably, Zn-atz-ipa shows a rare, higher uptake of  $C_2H_6$  than  $CO_2$ ,  $C_2H_2$  and  $C_2H_4$  at 0 to 0.4 bar. Breakthrough experiments showed that the packing order of the three MOFs in the sorbent bed has a significant impact on the separation performance, whereas the particle size and amount of the adsorbent have a minor effect. When the packing order is SIFSIX-3-Ni@Znatz-ipa@TIFSIX-2-Cu-i, high purity  $C_2H_4$  can be gained from a 1/49.5/49.5  $C_2H_2/C_2H_4/C_2H_6$  or 1/33/33/33  $C_2H_2/C_2H_4/C_2H_6/CO_2$  mixture and the working capacities are 0.32 and 0.10  $\text{mmol g}^{-1}$ , respectively. This work provides a new path for selective separation of a specific component molecule from a multicomponent gas mixture.

#### 2.4. $C_2H_2$ and $CO_2$ separation

Acetylene ( $C_2H_2$ ) is an important chemical raw material that is mainly produced by thermal cracking of hydrocarbons or the

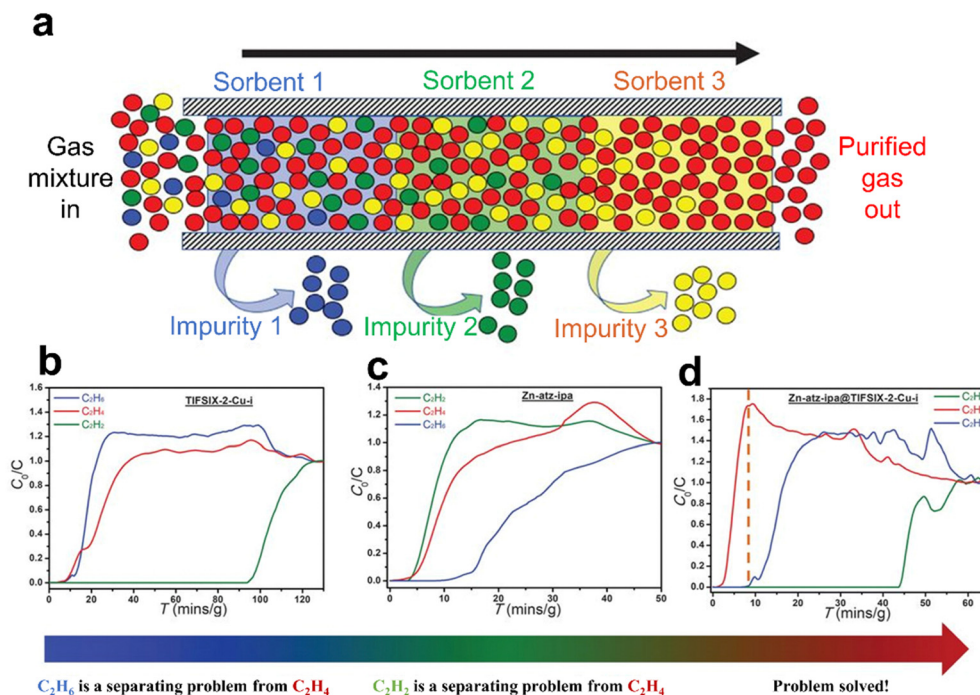


**Fig. 8** (a) SSST involves an adsorption bed with three task-specific physisorbents to purify the commodity (red) with specific binding sites for each trace impurity (blue, green, and yellow). (b) and (c) Experimental column breakthrough curves for  $C_2H_2/C_2H_4/C_2H_6$  separation (1:1:1 mixture) on TIFSIX-2-Cu-i and Zn-atz-ipa at 298 K and 1 bar. Breakthrough experiments were conducted in a column (inner diameter, 8 mm) at a flow rate of  $2.1 \text{ mL min}^{-1}$ . (d) Experimental column breakthrough curves for  $C_2H_2/C_2H_4/C_2H_6$  separation (1:1:1 mixture) on a tandem-packed column of TIFSIX-2-Cu-i ( $\sim 250 \text{ mg}$ ) and Zn-atz-ipa ( $\sim 600 \text{ mg}$ ) at 298 K and 1 bar. Reprinted with permission from ref. 80. Copyright 2019 the American Association for the Advancement of Science.

partial combustion of methane. The resulting gas stream contains various impurities, with carbon dioxide (CO<sub>2</sub>) being the major one. Thus, the separation of C<sub>2</sub>H<sub>2</sub> from CO<sub>2</sub>/C<sub>2</sub>H<sub>2</sub> mixtures is important in industry. Although CO<sub>2</sub> and C<sub>2</sub>H<sub>2</sub> have similar sizes (CO<sub>2</sub>: 3.18 × 3.33 × 5.36 Å<sup>3</sup>, and C<sub>2</sub>H<sub>2</sub>: 3.32 × 3.34 × 5.7 Å<sup>3</sup>) and physical properties (boiling point of CO<sub>2</sub> = 194.7 K and of C<sub>2</sub>H<sub>2</sub> = 189.3 K), the opposite quadrupole moments and slightly discrepant polarizabilities between C<sub>2</sub>H<sub>2</sub> and CO<sub>2</sub>, as well as the stronger  $\pi$ -bonding ability with metal sites and hydrogen-bonding donor ability of C<sub>2</sub>H<sub>2</sub>, allow the realization of their separation by means of rational design of pore surfaces and flexible framework amplification.<sup>72,95–98</sup>

In the early studies, Kitagawa *et al.* reported that a microporous MOF material, Cu<sub>2</sub>(pzdC)<sub>2</sub>(pyz), with non-coordinated oxygen atoms on the pore surface forms strong hydrogen-bonding interactions with C<sub>2</sub>H<sub>2</sub>, showing high C<sub>2</sub>H<sub>2</sub>/CO<sub>2</sub> separation potential.<sup>99</sup> This study firstly demonstrates the effective role of Lewis base sites in enhancing the affinity of a MOF for C<sub>2</sub>H<sub>2</sub>. In addition, MOFs with high density of OMSs can facilitate the recognition of acetylene.<sup>100–108</sup> In 2016, Chen *et al.* reported a MOF-74 isomer, namely, UTSA-74, which has two different (octahedral and tetrahedral) metal coordination geometries along the 1D channel.<sup>101</sup> Each octahedrally coordinated metal ion provides two OMSs upon removal of the coordinated water molecules, leading to enhanced C<sub>2</sub>H<sub>2</sub>/CO<sub>2</sub> separation. The single-component adsorption isotherms showed that UTSA-74 has a comparable C<sub>2</sub>H<sub>2</sub> uptake capacity (145 cm<sup>3</sup> cm<sup>-3</sup>) to Zn-MOF-74 but a smaller CO<sub>2</sub> uptake capacity (90 cm<sup>3</sup> cm<sup>-3</sup> vs. 146 cm<sup>3</sup> cm<sup>-3</sup>), resulting in UTSA-74 with a good C<sub>2</sub>H<sub>2</sub>/CO<sub>2</sub> separation performance. This result can be attributed to that each open Zn site can bind with two C<sub>2</sub>H<sub>2</sub> molecules, whereas two oxygen atoms of a CO<sub>2</sub> molecule occupy two adjacent OMSs, as demonstrated by the single-crystal X-ray structures and molecular modeling studies. Breakthrough experiments for a 50/50 C<sub>2</sub>H<sub>2</sub>/CO<sub>2</sub> mixture further demonstrate its good practical separation performance. This is also the first example of using breakthrough experiments to demonstrate the separation performance of MOFs for the C<sub>2</sub>H<sub>2</sub>/CO<sub>2</sub> mixture.

Based on copper(I)-alkynyl chemistry, anchoring Cu(I) on the surface of a MOF can significantly improve its specific recognition for C<sub>2</sub>H<sub>2</sub>. Qian *et al.* reported a Cu(I)-modified porous MOF, Cu(I)@UiO-66-(COOH)<sub>2</sub>, which exhibits significantly enhanced C<sub>2</sub>H<sub>2</sub>/CO<sub>2</sub> separation performance with a high C<sub>2</sub>H<sub>2</sub>/CO<sub>2</sub> IAST selectivity of 185, compared to the prototype UiO-66-(COOH)<sub>2</sub>.<sup>107</sup> The strong  $\pi$ -complexation between the  $\pi$  electrons on C<sub>2</sub>H<sub>2</sub> and Cu ions enables Cu(I)@UiO-66-(COOH)<sub>2</sub> to adsorb a large amount of C<sub>2</sub>H<sub>2</sub> (0.9 mmol g<sup>-1</sup>) at low pressure (0.01 bar) and exhibit a high Q<sub>st</sub> of 74.5 kJ mol<sup>-1</sup>. Breakthrough experiments demonstrated its highly efficient separation performance for C<sub>2</sub>H<sub>2</sub>/CO<sub>2</sub>. In addition, optimal distribution of OMSs on the pore surface of MOFs can achieve the maximum utilization of these sites. Recently, Li *et al.* reported a microporous MOF (JNU-4) with high-density OMSs.<sup>108</sup> These sites consist of square-planar copper centers separated by organic ligands, allowing each metal center to effectively bind with C<sub>2</sub>H<sub>2</sub>; thus, JNU-4 achieves a high C<sub>2</sub>H<sub>2</sub> adsorption capacity (222 cm<sup>3</sup> g<sup>-1</sup>, 9.91 mmol g<sup>-1</sup>) and a moderate IAST selectivity of 8.2 for an equimolar C<sub>2</sub>H<sub>2</sub>/CO<sub>2</sub>

mixture. Notably, this material absorbs C<sub>2</sub>H<sub>2</sub> up to 200 cm<sup>3</sup> g<sup>-1</sup> (8.93 mmol g<sup>-1</sup>) at 298 K and 0.5 bar, but demonstrates a low Q<sub>st</sub> of 26.8 kJ mol<sup>-1</sup>. Grand Canonical Monte Carlo (GCMC) simulations demonstrated that C<sub>2</sub>H<sub>2</sub> molecules can bind on both sides of OMSs, while CO<sub>2</sub> molecules can only bind on one side. Breakthrough experiments revealed that it has a high C<sub>2</sub>H<sub>2</sub> absorption capacity (160 cm<sup>3</sup> g<sup>-1</sup>, 7.14 mmol g<sup>-1</sup>) from an equimolar C<sub>2</sub>H<sub>2</sub>/CO<sub>2</sub> mixture and can provide fuel-grade C<sub>2</sub>H<sub>2</sub> gas.

Although a high density of OMSs can improve the selectivity for C<sub>2</sub>H<sub>2</sub>, electrostatic interactions between CO<sub>2</sub> and metal also exist simultaneously.<sup>109–111</sup> This requires a rational distribution of metal sites or the combination of multiple functions such as the pore size and shape to achieve a better C<sub>2</sub>H<sub>2</sub> selectivity.<sup>100,105,112</sup> However, OMSs of high density may result in a high Q<sub>st</sub>, thus leading to an increase of the energy consumption for adsorbent regeneration. In addition to OMSs, the introduction of functional groups (-NH<sub>2</sub>, -F, -Cl, -Br, -CF<sub>3</sub>, *etc.*) on organic ligands is also an effective strategy to promote selective adsorption of C<sub>2</sub>H<sub>2</sub>.<sup>113–116</sup> In 2021, Zhao *et al.* reported that an amine-functionalized flexible MOF (CPL-1-NH<sub>2</sub>) with a 1D channel (3.8 × 4.4 Å<sup>2</sup>) exhibits a high IAST selectivity of 119 for a 50/50 C<sub>2</sub>H<sub>2</sub>/CO<sub>2</sub> mixture at 298 K and 1 bar.<sup>114</sup> Theoretical calculations showed that the high selectivity of CPL-1-NH<sub>2</sub> for C<sub>2</sub>H<sub>2</sub> can be attributed to the NH<sub>2</sub> functionalization that enhances C<sub>2</sub>H<sub>2</sub> interaction with the framework, but blocks the stronger interaction between the non-coordinated oxygen atoms and CO<sub>2</sub> molecules by occupying the adsorption site of CO<sub>2</sub>. In the same year, Qian *et al.* reported an Al-MOF (CAU-10-H) with a pore size of 4.7 Å, exhibiting a high C<sub>2</sub>H<sub>2</sub> storage density (392 g L<sup>-1</sup>) and a separation factor (3.4).<sup>115</sup> GCMC simulations showed that the suitable pore size not only enhances the interaction of C<sub>2</sub>H<sub>2</sub> with high density oxygen atoms and aromatic rings on the pore surface, but also enables synergistic interaction between adjacent C<sub>2</sub>H<sub>2</sub> molecules. Subsequently, CAU-10-H was functionalized with amine to furnish a new MOF (CAU-10-NH<sub>2</sub>).<sup>116</sup> The later study showed that the amine groups can improve the uptake capacity of C<sub>2</sub>H<sub>2</sub> at low pressure, and significantly enhance the stacking density (0.46 cm<sup>3</sup> g<sup>-1</sup>) and C<sub>2</sub>H<sub>2</sub>/CO<sub>2</sub> selectivity (10.8) compared with the prototype MOF. In addition, these materials have the advantages of high stability, low Q<sub>st</sub>, easy scale-up, and low cost.

It is well known that pore size and shape play an important role in the separation process, as an appropriate pore size can enhance the strength of interactions between the pore surface and adsorbate, as well as among adsorbates themselves.<sup>97,100,112,117–123</sup> MOFs can be designed and modified to alter the pore sizes, even at the sub-nanometer scale, through substitutions of metal ions, organic ligands, or inorganic anions. Strategies such as building self-interpenetrated networks and pore space partition (PSP) can also be used for the pore size or space modulation.<sup>13,124</sup> In 2019, Chen *et al.* reported a PSP approach for highly efficient C<sub>2</sub>H<sub>2</sub>/CO<sub>2</sub> separation. The new porous MOF (FJU-90) was synthesized by inserting a triangular ligand (2,4,6-tris(4-pyridyl)pyridine) into the cylindrical channel of prototype FJU-88.<sup>122</sup> The 1D channel of FJU-88 was separated into a number of aperture cavities with the aperture size decreasing from 12.0 × 9.4 to 5.4 × 5.1 Å<sup>2</sup>.

Thus, the combination of optimized pore space and oxygen atom sites endows FJU-90a with a high  $C_2H_2$  adsorption capacity ( $180 \text{ cm}^3 \text{ g}^{-1}$ ,  $8.04 \text{ mmol g}^{-1}$ ). The separation performance of the activated MOF (FJU-90a) for a 50/50  $C_2H_2/CO_2$  mixture was further confirmed by breakthrough experiments with a productivity of  $1.87 \text{ mol kg}^{-1}$ .

In 2017, Chen *et al.* reported a SIFSIX-MOF UTSA-300 that exhibits not only efficient separation of  $C_2H_2/C_2H_4$  but also a high selective uptake for  $C_2H_2$  from the  $C_2H_2/CO_2$  mixture.<sup>72</sup> Single-component adsorption isotherms revealed that the activated MOF (UTSA-300a) shows a high capacity for  $C_2H_2$  adsorption ( $68.9 \text{ cm}^3 \text{ g}^{-1}$ ,  $3.08 \text{ mmol g}^{-1}$ ) but adsorbs negligible  $CO_2$  ( $3.25 \text{ cm}^3 \text{ g}^{-1}$ ,  $0.14 \text{ mmol g}^{-1}$ ) at 298 K and 1 bar, resulting in a high IAST  $C_2H_2/CO_2$  selectivity of 743 (298 K and 1 bar) (Fig. 9). Due to the strong  $C-H \cdots F$  interactions formed between  $C_2H_2$  molecules and  $SiF_6^{2-}$ ,  $C_2H_2$  can easily diffuse into UTSA-300a, while  $CO_2$  is restricted because of electrostatic repulsion, as confirmed by DFT calculations and neutron powder diffraction studies. The separation performance of UTSA-300a for a 50/50  $C_2H_2/CO_2$  mixture was further demonstrated by breakthrough experiment in a packed column bed of UTSA-300a. Subsequently, systematic fine-tuning of the pore size of UTSA-300 was performed by replacing the fluoride anionic linkers and metal ions.<sup>125</sup> Three new SIFSIX-type MOFs, namely SIFSIX-dps-Cu (NCU-100), GeFSIX-dps-Cu, and NbOFFIVE-dps-Cu, were

reported to exhibit different pore sizes ( $1.4 \times 3.0 \text{ \AA}^2$ ,  $1.5 \times 3.0 \text{ \AA}^2$ , and  $2.2 \times 2.7 \text{ \AA}^2$ , respectively) and interlayer distances ( $4.10 \text{ \AA}$ ,  $4.06 \text{ \AA}$ , and  $3.69 \text{ \AA}$ , respectively). Single-component adsorption isotherms indicated that SIFSIX-dps-Cu shows the highest  $C_2H_2$  uptake ( $4.57 \text{ mmol g}^{-1}$ ) with a high IAST  $C_2H_2/CO_2$  selectivity up to 1787 at 298 K and 1 bar. In addition, the gate-opening pressure of SIFSIX-dps-Cu for  $C_2H_2$  is 0.035 bar, which is lower than those of GeFSIX-dps-Cu (0.05 bar), NbOFFIVE-dps-Cu (0.3 bar), and UTSA-300 (0.06 bar), probably because of its larger interlayer distance. DFT and grand canonical Monte Carlo simulations further revealed that  $C_2H_2$  molecules have multiple host-guest interactions ( $H \cdots F$  hydrogen-bonding interactions) in both inter- and intra-layer cavities. Breakthrough experiments confirmed that high purity  $C_2H_2$  ( $\geq 99.9\%$ ) can be obtained from  $C_2H_2/CO_2$  (50/50) with a high productivity of  $2.48 \text{ mmol g}^{-1}$ .

A suitable pore size combined with active sites and a flexible structure can greatly improve the adsorption capacity of a material for  $C_2H_2$ .<sup>95,106,114,125-127</sup> Recently, Hong *et al.* reported that a flexible MOF, namely,  $[Ni(DTBDA)(MeOH)_2(DMA)(H_2O)_2]$  (FJI-H36, DTBDA = 3',5'-di(1H-1,2,4-triazol-1-yl)-[1,1'-biphenyl]-3,5-dicarboxylic acid), with adaptive channels shows efficient adsorption of  $C_2H_2$ .<sup>127</sup> FJI-H36 contains two types of cavities with the size of  $12.9 \times 12.9 \text{ \AA}^2$  and  $8.4 \times 10.2 \text{ \AA}^2$ , respectively, as well as high-density active sites of open  $Ni^{II}$  ( $4.52 \text{ mol L}^{-1}$ ) and

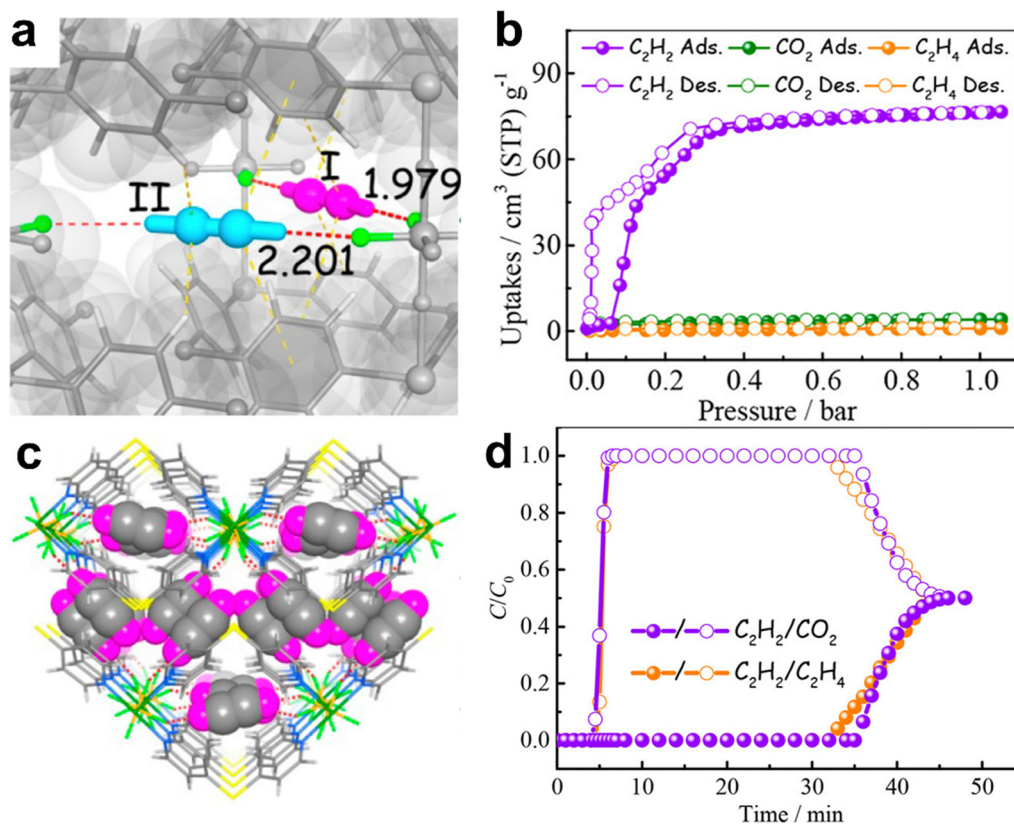


Fig. 9 (a) and (c) Neutron diffraction crystal structure of  $UTSA-300 \supset C_2D_2$  and (b)  $C_2H_2$ ,  $CO_2$ , and  $C_2H_4$  sorption isotherms for UTSA-300a at 273 K. (d) Experimental column breakthrough curves for equimolar  $C_2H_2/CO_2$  (purple) and  $C_2H_2/C_2H_4$  (orange) mixtures (298 K, 1 bar) in a fixed-bed packed with UTSA-300a. Reprinted with permission from ref. 72. Copyright 2017 American Chemical Society.

free N atoms ( $9.04 \text{ mol L}^{-1}$ ). Single-component sorption experiments confirmed that FJI-H36 shows a high  $\text{C}_2\text{H}_2$  uptake of  $159.9 \text{ cm}^3 \text{ cm}^{-3}$  at 298 K and 1 bar, and an ultra-high  $\text{C}_2\text{H}_2$  storage density of  $561 \text{ g L}^{-1}$ . Breakthrough experiments for a 50/50  $\text{C}_2\text{H}_2/\text{CO}_2$  mixture further demonstrated its high adsorption capacity for  $\text{C}_2\text{H}_2$  ( $3.82 \text{ mmol g}^{-1}$ ). The structure of FJI-H36 adaptively changes with the adsorption of  $\text{C}_2\text{H}_2$ , leading to a dense packing of  $\text{C}_2\text{H}_2$  in it, as demonstrated by the X-ray crystal structure of  $\text{C}_2\text{H}_2@ \text{FJI-H36}$ .

Recently, Wang *et al.* reported a sulfate-pillared MOF [ $\text{Zn}(\text{tepb})(\text{SO}_4)$ ] (SOFOUR-TEPE-Zn, TEPE = tetra(4-pyridyl)-benzene), which possesses dense electronegative pore surfaces to highly promote the separation of  $\text{C}_2\text{H}_2/\text{CO}_2$  (Fig. 10).<sup>97</sup> SOFOUR-TEPE-Zn is an isostructural framework with SOFOUR-1-Zn,<sup>128</sup> but with more electron-rich pore surfaces due to the higher electronegative ethylene groups in the TEPE ligand in contrast to the phenyl ring in the TEPB ligand. Single-component sorption results of SOFOUR-TEPE-Zn revealed a higher  $\text{C}_2\text{H}_2$  uptake ( $89.1 \text{ cm}^3 \text{ g}^{-1}$ ,  $3.98 \text{ mmol g}^{-1}$ ) than SOFOUR-1-Zn ( $69.4 \text{ cm}^3 \text{ g}^{-1}$ ,  $3.10 \text{ mmol g}^{-1}$ ) at 1 bar and 298 K, but a much lower  $\text{CO}_2$  uptake ( $14.1 \text{ cm}^3 \text{ g}^{-1}$ ,  $0.63 \text{ mmol g}^{-1}$ ), resulting in a very high IAST selectivity of 16833 for 50/50  $\text{C}_2\text{H}_2/\text{CO}_2$ . Breakthrough experiments for 50/50  $\text{C}_2\text{H}_2/\text{CO}_2$  of SOFOUR-TEPE-Zn give a productivity of  $60.1 \text{ cm}^3 \text{ g}^{-1}$  ( $2.68 \text{ mmol g}^{-1}$ ) of 99.5% purity or  $33.2 \text{ cm}^3 \text{ g}^{-1}$  ( $1.48 \text{ mmol g}^{-1}$ ) of 99.99% purity in its desorption process by stepped helium purging and mild heating. Moreover, SOFOUR-TEPE-Zn also maintains a

high  $\text{C}_2\text{H}_2$  productivity of  $75.5 \text{ cm}^3 \text{ g}^{-1}$  ( $3.37 \text{ mmol g}^{-1}$ ) of 99.5% purity with 99.82%  $\text{C}_2\text{H}_2$  recovery in the simulated pressure swing adsorption processes. DFT-D and GCMC simulation studies revealed that the preferential binding of  $\text{C}_2\text{H}_2$  in SOFOUR-TEPE-Zn can be mainly attributed to electron-rich pore surfaces, providing multiple optimal adsorption sites for  $\text{C}_2\text{H}_2$ .

$\text{CO}_2$ -selective adsorbents can yield high purity  $\text{C}_2\text{H}_2$  in one step rather than multiple adsorption-desorption steps, making the operation simple and more energy efficient. Currently, only a limited number of  $\text{CO}_2$ -selective MOF materials have been reported, manifesting the challenge in the design of  $\text{CO}_2$ -selective materials.<sup>129-148</sup> Fortunately, several strategies have been reported to promote the selective adsorption of  $\text{CO}_2$  in MOFs. For example, Chen *et al.* introduced hydroxyl functional groups into MOF frameworks, enabling selective capture of  $\text{CO}_2$  from  $\text{C}_2\text{H}_2$ , with a high IAST selectivity of 118.7 for  $\text{CO}_2/\text{C}_2\text{H}_2$  (1:2, v:v) at 0.1 bar and ambient temperature.<sup>137</sup> In 2021, Chen *et al.* reported an ultramicroporous MOF [ $\text{Cu}(\text{F-pymo})_2$ ] $\cdot 1.25\text{H}_2\text{O}$  (Cu-F-pymo, F-pymo = 5-fluoropyrimidin-2-olate) with zeolitic gismondine (GIS) topology exhibiting a high selective adsorption of  $\text{CO}_2$  over  $\text{C}_2\text{H}_2$ , which depends on activation temperature (Fig. 11).<sup>143</sup> Cu-F-pymo contains two distinct pore environments, namely, spherical cavities and 1D helical channels, both of which are occupied by removable water molecules. Single-component adsorption isotherms revealed that partially dehydrated Cu-F-pymo can adsorb  $1.19 \text{ mmol g}^{-1}$   $\text{C}_3\text{H}_6$

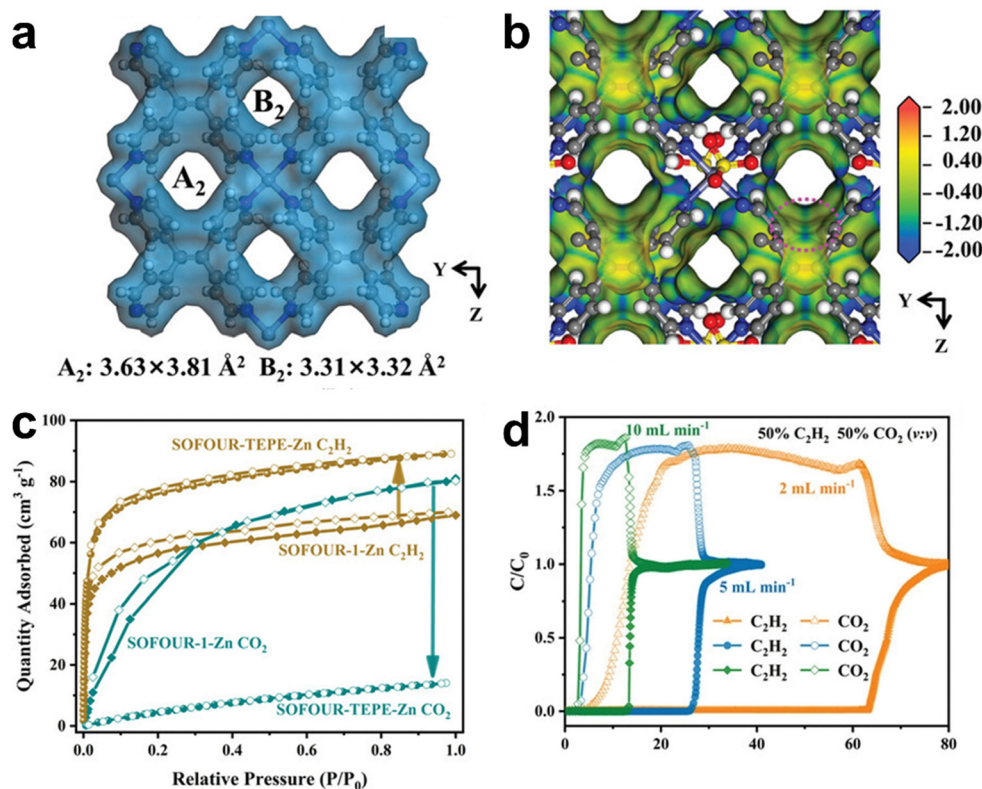


Fig. 10 (a) and (b) The building blocks of SOFOUR-TEPE-Zn and electrostatic surface potential. (c)  $\text{C}_2\text{H}_2$  and  $\text{CO}_2$  adsorption isotherms for SOFOUR-1-Zn and SOFOUR-TEPE-Zn at 298 K. (d) Breakthrough curves of SOFOUR-TEPE-Zn for  $\text{C}_2\text{H}_2/\text{CO}_2$  (50/50, v/v) at different flow rates at 298 K. Reprinted with permission from ref. 97. Copyright 2023 Wiley-VCH.

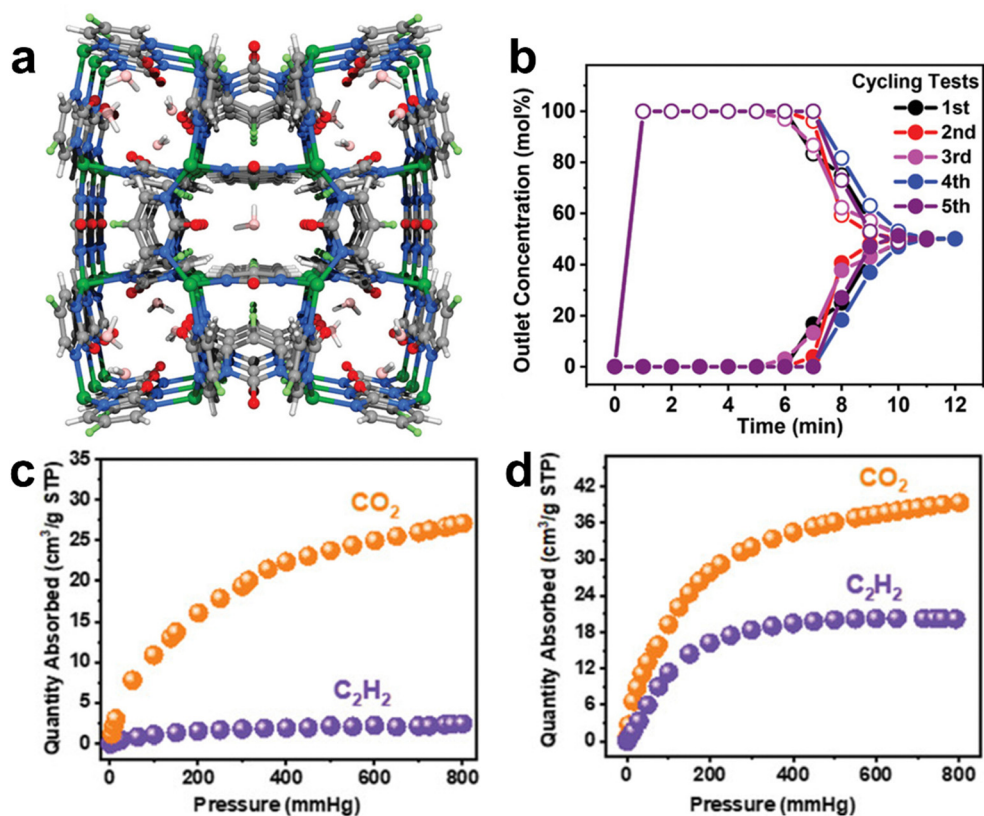


Fig. 11 (a) Schematic structure of Cu-F-pymo MOF with residual water molecules. (b) Breakthrough cycling tests of the equimolar CO<sub>2</sub>/C<sub>2</sub>H<sub>2</sub> mixture. (c) and (d) Separation performance toward CO<sub>2</sub> and C<sub>2</sub>H<sub>2</sub> in Cu-F-pymo under different activation conditions. Reprinted with permission from ref. 143 Copyright 2021 Wiley-VCH.

and show negligible C<sub>2</sub>H<sub>2</sub> uptake (0.1 mmol g<sup>-1</sup>) at 298 K and 1 bar. Breakthrough experiments revealed that highly pure acetylene (>99.9%) can be obtained directly from a 50/50 CO<sub>2</sub>/C<sub>2</sub>H<sub>2</sub> mixture by a single separation operation. Modeling studies demonstrated that CO<sub>2</sub> can be preferentially adsorbed in the 1D channels, while C<sub>2</sub>H<sub>2</sub> primarily occupies the spherical cavities. Therefore, the remaining water molecules in the spherical cavities blocked the preferential site, leading to the molecular sieving effect of Cu-F-pymo for CO<sub>2</sub>/C<sub>2</sub>H<sub>2</sub>.

Besides size-matching between gas molecules and the pore structure, reasonable charge distribution would also facilitate the selective recognition of CO<sub>2</sub> over C<sub>2</sub>H<sub>2</sub>. Chen *et al.* reported an ultramicroporous porous material Cd[Fe(CN)<sub>5</sub>NO] (Cd-NP) that exhibits stronger affinity for CO<sub>2</sub> in contrast to C<sub>2</sub>H<sub>2</sub>. Cd-NP contains quasi-discrete ellipsoidal cavities (6.1 × 4.5 × 4.5 Å<sup>3</sup>) connected by small apertures (3.2 Å), and its BET surface area is 305 m<sup>2</sup> g<sup>-1</sup> (Fig. 12).<sup>144</sup> Thanks to suitable pore sizes and electrostatic distribution on pore surfaces, Cd-NP shows a high CO<sub>2</sub> uptake of 58.0 cm<sup>3</sup> g<sup>-1</sup> (2.59 mmol g<sup>-1</sup>) but a lower C<sub>2</sub>H<sub>2</sub> uptake of 9.7 cm<sup>3</sup> g<sup>-1</sup> (0.43 mmol g<sup>-1</sup>) at 1 bar and 298 K, thus showing a high IAST selectivity (85) for an equimolar CO<sub>2</sub>/C<sub>2</sub>H<sub>2</sub> mixture. The *Q*<sub>st</sub> of CO<sub>2</sub> was calculated to be 27.7 kJ mol<sup>-1</sup>, which would facilitate regeneration of the material under mild conditions. The breakthrough process showed that Cd-NP was capable of producing a high purity C<sub>2</sub>H<sub>2</sub> (99.9%) directly from

50/50 CO<sub>2</sub>/C<sub>2</sub>H<sub>2</sub> with a productivity of 2.34 mol L<sup>-1</sup>. GCMC simulations and neutron powder diffraction experiments showed that the preferential adsorption of CO<sub>2</sub> in Cd-NP can be attributed to the confinement effect of the pore cavity and electrostatically complementary pore surface.

CO<sub>2</sub>/C<sub>2</sub>H<sub>2</sub> inverse separation can also be achieved using synergistic effects of thermodynamics and kinetics. Li *et al.* reported an ultramicroporous MOF, Y-bptc, to achieve one-step C<sub>2</sub>H<sub>2</sub> purification from a CO<sub>2</sub>/C<sub>2</sub>H<sub>2</sub> mixture. Y-bptc processes small windows (4.2 Å) interconnected with large cubic cages with **ftw** topology. Equilibrium and kinetic adsorption studies revealed that Y-bptc absorbs 55 cm<sup>3</sup> g<sup>-1</sup> (2.45 mmol g<sup>-1</sup>) CO<sub>2</sub> and a lower C<sub>2</sub>H<sub>2</sub> uptake at 298 K and 1 bar with an IAST selectivity of 4.1 for 50/50 CO<sub>2</sub>/C<sub>2</sub>H<sub>2</sub>.<sup>136</sup> Moreover, CO<sub>2</sub> diffuses faster than C<sub>2</sub>H<sub>2</sub> in Y-bptc, and the calculated kinetic separation coefficient reaches 114 at 298 K. Breakthrough experiments confirmed that CO<sub>2</sub> in a 1:1 CO<sub>2</sub>/C<sub>2</sub>H<sub>2</sub> mixture can be readily removed by Y-bptc, giving C<sub>2</sub>H<sub>2</sub> with a purity of >99% and productivity of 1.52 mmol g<sup>-1</sup> in a one-step separation process. GCMC simulations further revealed the high affinity of Y-bptc for CO<sub>2</sub> resulting from the formation of hydrogen-bonding interactions between μ<sub>3</sub>-OH<sup>-</sup> groups of the framework and CO<sub>2</sub> molecules.

In 2023, Wade *et al.* reported two isostructural MOFs [Zn<sub>5</sub>Cl<sub>4</sub>(bbta)<sub>3</sub>] (MUF-4, bbta<sup>2-</sup> = benzo-1,2,4,5-bistriazolate) and MUF-4-F, which exhibited completely opposite adsorption

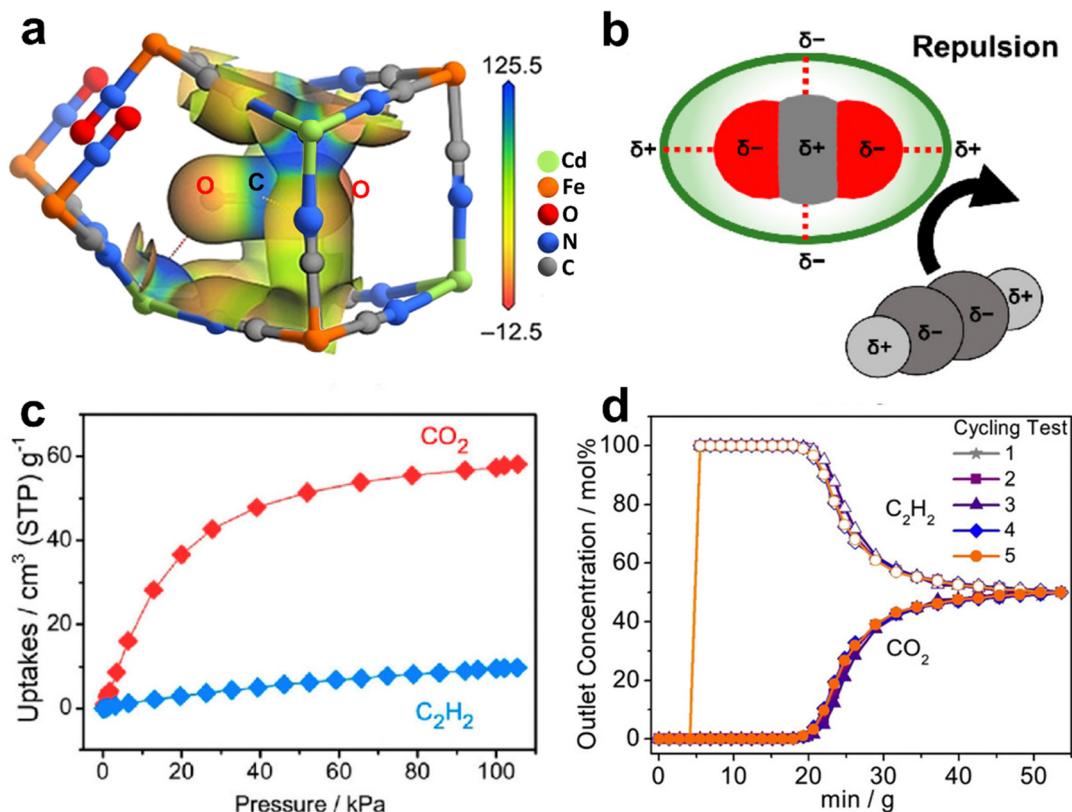


Fig. 12 (a) Electrostatic potential (ESP) of Cd-NP  $\supset$  CO<sub>2</sub> mapped onto the 0.15 e<sup>-</sup> Å<sup>-3</sup> electron density isosurface. (b) Electrostatically driven adsorption mechanism towards CO<sub>2</sub> and C<sub>2</sub>H<sub>2</sub> molecules. (c) CO<sub>2</sub> and C<sub>2</sub>H<sub>2</sub> sorption isotherms for Cd-NP at 298 K. (d) Cycling tests of the equimolar CO<sub>2</sub>/C<sub>2</sub>H<sub>2</sub> mixture in a column packed with Cd-NP at 298 K and 1 bar. Reproduced with permission from ref. 144. Copyright 2021 Wiley-VCH.

selectivity for CO<sub>2</sub>/C<sub>2</sub>H<sub>2</sub>. MUF-4-F can be derived by F<sup>-</sup> to Cl<sup>-</sup> ligand exchange of MUF-4.<sup>139</sup> Both MUF-4-F and MFU-4 possess alternating large pore and small pore cavities but have different connecting windows (~3.7 Å and ~2.2 Å, respectively). C<sub>2</sub>H<sub>2</sub> molecules can easily enter MFU-4-F. Equilibrium and kinetic adsorption studies revealed that MFU-4-F exhibits a higher C<sub>2</sub>H<sub>2</sub> (6.66 mmol g<sup>-1</sup>) uptake than CO<sub>2</sub> (3.24 mmol g<sup>-1</sup>) at 300 K and 1 bar and shows a fast adsorption rate for both gases. In contrast, MFU-4 exhibits high kinetic selectivity for uptake of CO<sub>2</sub> over C<sub>2</sub>H<sub>2</sub> up to 3360 at 300 K. Computational studies revealed that C<sub>2</sub>H<sub>2</sub> was blocked by the smaller windows created by the Zn-Cl groups in MUF-4. Breakthrough experiments demonstrated that high purity (>98%) C<sub>2</sub>H<sub>2</sub> can be obtained directly from a 50/50 CO<sub>2</sub>/C<sub>2</sub>H<sub>2</sub> mixture in MUF-4.

## 2.5. C<sub>3</sub>H<sub>6</sub> and C<sub>3</sub>H<sub>8</sub> separation

Propylene (C<sub>3</sub>H<sub>6</sub>) is also an essential industrial feedstock with large demand that is only lower than that of ethylene. The industrial production of C<sub>3</sub>H<sub>6</sub> inevitably contains a certain amount of propane (C<sub>3</sub>H<sub>8</sub>) impurity. However, they have very similar molecular sizes (C<sub>3</sub>H<sub>6</sub>: 3.8 × 4.0 × 6.5 Å<sup>3</sup>, and C<sub>3</sub>H<sub>8</sub>: 3.8 × 4.2 × 6.8 Å<sup>3</sup>), kinetic diameters (C<sub>3</sub>H<sub>6</sub>: 4.0 Å, and C<sub>3</sub>H<sub>8</sub>: 4.2 Å) and physical properties (boiling points of 189.3 and 194.7 K, respectively). Therefore, it is more challenging to tune the pore size for sieving separation of C<sub>3</sub>H<sub>6</sub>/C<sub>3</sub>H<sub>8</sub>, because they

have highly similar molecular sizes and kinetic diameters, whereas possible changes of the size and shapes of MOF apertures may occur in the adsorption process, as many MOFs are actually flexible. Fortunately, significant research progress about highly efficient separation of C<sub>3</sub>H<sub>6</sub>/C<sub>3</sub>H<sub>8</sub> has been recently realized by MOFs through rational structural design and modification of the pore size and pore surface.<sup>149-168</sup>

The incorporation of active sites in MOFs' pore surface improves not only kinetic selectivity but also thermodynamic selectivity for gas separation. In 2019, Zhang *et al.* reported a MAF, MAF-23-O, which can be easily synthesized by heating the flexible prototype [Zn<sub>2</sub>(btm)<sub>2</sub>] (MAF-23, H<sub>2</sub>btm = bis(5-methyl-1H-1,2,4-triazol-3-yl)methane) under oxygen gas flow (Fig. 13).<sup>149</sup> Single-crystal structure analyses showed that MAF-23-O is isostructural to MAF-23 and contains half the amount of the oxidized btm<sup>2-</sup> ligands, namely, btk<sup>2-</sup> (H<sub>2</sub>btk = bis(5-methyl-1,2,4-triazol-3-yl)methanone). This *in situ* ligand oxidative modification makes the framework more rigid and more hydrophilic. The IAST selectivity for C<sub>3</sub>H<sub>6</sub>/C<sub>3</sub>H<sub>8</sub> in MAF-23-O was calculated to be 8-9, which was higher than that of MAF-23 (3-4). Moreover, C<sub>3</sub>H<sub>6</sub> and C<sub>3</sub>H<sub>8</sub> exhibit similar diffusion rates in MAF-23, but show very different diffusion rates in MAF-23-O with a high kinetic selectivity of 71. Theoretical calculations demonstrated that the exposed oxygen atoms in the framework of MAF-23-O can form strong C-H...O/N interaction with C<sub>3</sub>H<sub>6</sub>, improving the thermodynamic selectivity of

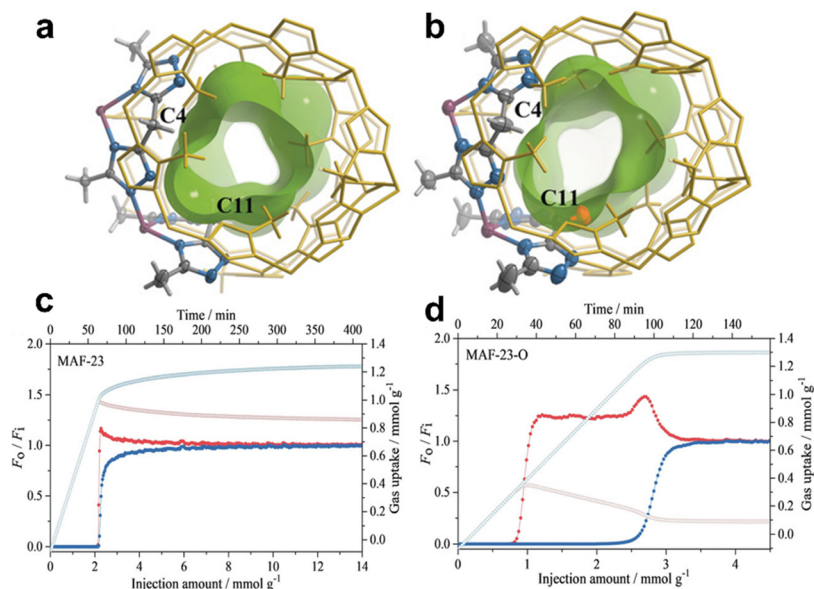


**Fig. 13** Crystal and pore structures of (a) MAF-23 and (b) MAF-23-O. Breakthrough curves (filled symbols) and adsorption kinetic curves (open symbols) for (c) MAF-23 and (d) MAF-23-O using an equimolar  $C_3H_6/C_3H_8$  (blue/red) mixture at 298 K and 1 bar. Reprinted with permission from ref. 149. Copyright 2019 Wiley-VCH.

MAF-23-O for  $C_3H_6$ . Additionally, the decreased flexibility of the framework slows down the diffusion of  $C_3H_6$ , thus improving the kinetic selectivity. Breakthrough experiments revealed that MAF-23-O exhibits efficient separation for an equimolar  $C_3H_6/C_3H_8$  mixture at 298 K and 1 bar with an adsorption selectivity of 15, which is 10 times that of MAF-23.

In 2016, Eddaoudi *et al.* reported a oxyfluoride-based MOF  $[Ni(pyr)_2(NbOF_5)] \cdot 2H_2O$  (NbOFFIVE-1-Ni, or KAUST-7, pyr = pyrazine) for selective adsorption of  $C_3H_6$  from  $C_3H_8$ .<sup>150</sup> KAUST-7 is isostructural to SIFSIX-3 and composed of Ni(II)-pyrazine square-grid layers and  $(NbOF_5)^{2-}$  pillars with **pcu** topology, exhibiting 1D channels with an aperture size of 3.0 Å and a periodic array of fluoride anions on the pore surface. Single-component sorption experiments revealed that KAUST-7 can adsorb  $\sim 60 \text{ mg g}^{-1}$  ( $1.43 \text{ mmol g}^{-1}$ )  $C_3H_6$  but negligible  $C_3H_8$  uptake at 298 K and 1 bar. Breakthrough experiments demonstrated that  $C_3H_8$  of 97% purity can be obtained from  $C_3H_6/C_3H_8$  50/50 mixed-gas by a packed column bed of KAUST-7, with a separation productivity of  $0.6 \text{ mol g}^{-1}$ . KAUST-7 also can adsorb  $C_3H_8$  by pore-opening sorption behavior at 273 K.

In 2023, Chen *et al.* reported another SIFSIX MOF  $[Ni(WO_2F_4)(pyz)_2]$  (UTSA-400) featuring 1D channels that can exclude  $C_3H_8$  molecules and adsorb  $C_3H_6$  molecules with a high binding affinity (Fig. 14).<sup>151</sup> UTSA-400 shows an isostructural framework with SIFSIX-3 and NbOFFIVE-1-Ni, but with highly tilted pyrazine linkers owing to larger  $WO_2F_4^{2-}$  in contrast to  $SiF_6^{2-}$  and  $NbOF_5^{2-}$ . The pore cavities in UTSA-400 are  $6.7 \times 5.5 \times 3.7 \text{ \AA}^3$  with exposed oxide/fluoride pairs on the pore surface (BET surface area:  $226 \text{ m}^2 \text{ g}^{-1}$ ) that can serve as the binding sites for propylene molecules. Single-component sorption results of UTSA-400 indicated a much higher  $C_3H_6$  capacity ( $92.1 \text{ cm}^3 \text{ cm}^{-3}$ ,  $2.62 \text{ mmol g}^{-1}$ ) than NbOFFIVE-1-Ni ( $54.3 \text{ cm}^3 \text{ cm}^{-3}$ ,  $1.34 \text{ mmol g}^{-1}$ ) by 63%, at 1 bar and 298 K,

which is also higher than those of Y-abtc ( $64.6 \text{ cm}^3 \text{ cm}^{-3}$ ,  $1.98 \text{ mmol g}^{-1}$ ) and Co-gallate ( $66.6 \text{ cm}^3 \text{ cm}^{-3}$ ,  $1.79 \text{ mmol g}^{-1}$ ). Under the same conditions, UTSA-400 showed negligible  $C_3H_8$  uptake because of inaccessible inward diffusion of propane molecules. The  $Q_{st}$  of UTSA-400 for  $C_3H_6$  is  $60.5 \text{ kJ mol}^{-1}$ , being comparable to those of MOFs with OMSs ( $44\text{--}57 \text{ kJ mol}^{-1}$ ).<sup>30,45</sup> Breakthrough separation experiment demonstrated that polymer-grade (99.7%) propylene can be obtained from an equimolar  $C_3H_6/C_3H_8$  mixture with a productivity of  $56.7 \text{ L L}^{-1}$ . Besides size exclusion, the separation performance of UTSA-400 can also be attributed to strong C–H  $\cdots$  O/F interactions, as confirmed by *in situ* infrared spectroscopy and DFT-D calculations.

In 2018, Li *et al.* studied four microporous MOFs, namely, Zr-bptc, Zr-abtc, Y-bptc, and Y-abtc, which were obtained by the combination of two analogous metal clusters ( $Zr_6$  and  $Y_6$  clusters) and two different ligands (abtc = 3,3',5,5'-azobenzene-tetracarboxylates, and bptc = 3,3',5,5'-biphenyltetracarboxylates).<sup>152</sup> Among these materials, Y-abtc has cage-like pores connected through small windows, exhibiting **ftw** topology and optimal pore size (4.72 Å) that enables it to adsorb small  $C_3H_6$  molecules (4.48 Å) with fast kinetics but completely exclude larger  $C_3H_8$  molecules (5.1 Å). Single-component sorption experiments revealed that Zr-bptc exhibits similar adsorption capacities for  $C_3H_6$  and  $C_3H_8$ , whereas its isostructural Y-bptc excludes both gases, attributable to the presence of equilibrium cations (dimethylammonium) in the Y-bptc affecting its pore size. In contrast, Y-abtc with the optimal pore size shows a high adsorption capacity for  $C_3H_6$  ( $\sim 2 \text{ mmol g}^{-1}$ ) and a negligible  $C_3H_8$  uptake at 298 K. Column breakthrough experiments indicated that polymer-grade  $C_3H_6$  (99.5%) can be obtained from 5/95  $C_3H_6/C_3H_8$  mixtures by Y-abtc. Recently, the same group reported a new Y-based MOF,  $Y_6(OH)_8(eddi)_3(DMA)_2$  (HIAM-301,  $H_4eddi = 5,5'$ -(ethene-1,2-diyl)diisophthalic acid, and DMA = dimethylammonium), also

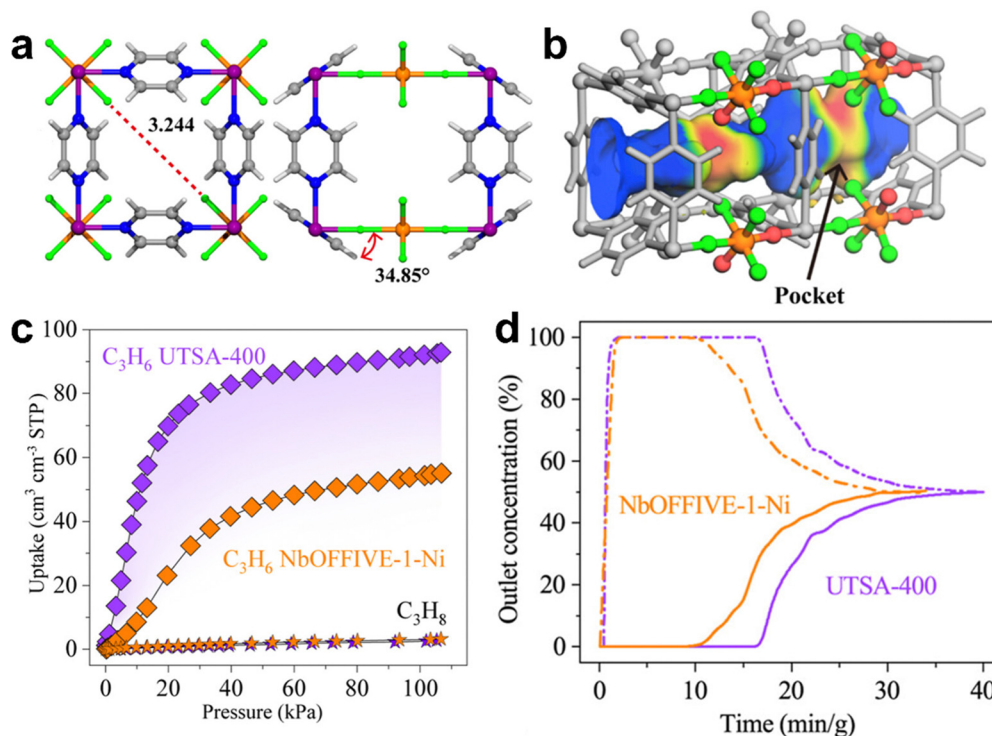


**Fig. 14** (a) Crystal structure of UTSA-400. (b) Connolly surface of UTSA-400 mapped with electrostatic potential with a probe of 1.2 Å. (c) Single-component adsorption isotherms of  $C_3H_6$  and  $C_3H_8$  for UTSA-400 and NbOFFIVE-1-Ni at 298 K. (d) Breakthrough curves for NbOFFIVE-1-Ni and UTSA-400 for an equimolar binary mixture of  $C_3H_6$  (solid line)/ $C_3H_8$  (dashed line) at 298 K and 1 bar. Reprinted with permission from ref. 151. Copyright 2023 American Chemical Society.

exhibiting the molecular sieving separation of  $C_3H_6/C_3H_8$  mixtures. HIAM-301 is composed of 12-connected  $Y_6(OH)_8(COO)_{12}$  clusters bridged by 4-connected eddi<sup>4-</sup> linkers to form a 3D framework with **ftw** topology and a pore size of 4.6 Å.<sup>153</sup> It is isostructural to Y-abtc and possesses distorted cubic cages (size:  $10 \times 10 \text{ \AA}^2$ ), which provides better control over guest accessibility. Single-component adsorption isotherms revealed that HIAM-301 can adsorb  $3.16 \text{ mmol g}^{-1}$   $C_3H_6$  and exhibit minor  $C_3H_8$  adsorption ( $<0.3 \text{ mmol g}^{-1}$ ) at 298 K and 1 bar, resulting in a high IAST selectivity ( $>150$ ) for equimolar  $C_3H_6/C_3H_8$  under the same condition. The practical performance for separation of 5/95  $C_3H_6/C_3H_8$  was confirmed by dynamic breakthrough experiments with a high productivity of  $46.4 \text{ cm}^3 \text{ g}^{-1}$  ( $>99.5\%$  purity).

In 2020, Chen *et al.* reported an ultramicroporous Co-gallate MOF [ $Co(C_7O_5H_4)$ ] (Co-gallate) with 3D channels, which exhibits efficient  $C_3H_6/C_3H_8$  separation by molecular sieving effect.<sup>154</sup> Co-gallate shows elliptical windows (size:  $4.2 \times 5.1 \text{ \AA}^2$ ), which are precisely between the sizes of  $C_3H_8$  and  $C_3H_6$  (Fig. 15). Single-component adsorption isotherms showed that Co-gallate has a high adsorption capacity of  $C_3H_6$  ( $66.6 \text{ cm}^3 \text{ cm}^{-3}$ ,  $1.79 \text{ mmol g}^{-1}$ ), whereas the adsorption of  $C_3H_8$  ( $5.2 \text{ cm}^3 \text{ cm}^{-3}$ ,  $0.14 \text{ mmol g}^{-1}$ ) is minor at 298 K. The IAST selectivity of Co-gallate for a 50/50  $C_3H_6/C_3H_8$  mixture was calculated up to 330 at 1 bar and 298 K. Fixed-bed breakthrough experiments further confirmed its molecular sieving separation performance for 50/50  $C_3H_6/C_3H_8$ , with a  $C_3H_6$  productivity of  $36.4 \text{ cm}^3 \text{ cm}^{-3}$ ,  $0.98 \text{ mmol g}^{-1}$  (97.7%+ purity).

In 2021, Li *et al.* reported a MOF (JNU-3a) featuring 1D channels (size  $\sim 4.5 \times 5.3 \text{ \AA}^2$ ) attached with small pockets arranged on both sides for  $C_3H_6/C_3H_8$  separation, where 1D channels could facilitate fast adsorption-desorption kinetics (Fig. 16).<sup>155</sup> In addition, the small pockets were connected with the 1D channel through small apertures ( $\sim 3.7 \text{ \AA}$ ) that can undergo gate-opening for  $C_3H_6$  and  $C_3H_8$  at different partial pressures. JNU-3a exhibits a stepwise adsorption isotherm and shows temperature-dependent gate-opening for  $C_3H_6$  and  $C_3H_8$ , where  $C_3H_8$  exhibits a higher gate-opening pressure than  $C_3H_6$ . Therefore, the high selectivity of JNU-3a for  $C_3H_6/C_3H_8$  can be obtained at optimal temperature (303 K). JNU-3a can adsorb  $58.6 \text{ cm}^3 \text{ g}^{-1}$  ( $2.62 \text{ mmol g}^{-1}$ )  $C_3H_6$  at 303 K, and the  $C_3H_6$  packing density inside JNU-3a was calculated to be  $404 \text{ g L}^{-1}$ . The dynamic feature of pore aperture was further revealed by single-crystal X-ray diffraction and theoretical calculation studies. Breakthrough experiment revealed that high-purity  $C_3H_6$  ( $\geq 99.5\%$ ) can be obtained from a 50/50  $C_3H_6/C_3H_8$  mixture by JNU-3a. After applying helium purge to those adsorbed gases,  $C_3H_6$  was collected with a maximum productivity of  $53.5 \text{ L kg}^{-1}$ . The unique pore structure reported in this work would inspire future design of novel MOFs for application in adsorptive separation.

In 2023, Bai *et al.* reported a supertetrahedral-cluster ( $Cu_{10}O_{13}$ )-based MOF (NTU-85) which possesses square-shaped 1D channels that host lattice water molecules.<sup>156</sup> The partial lattice water molecules can be precisely removed to form a

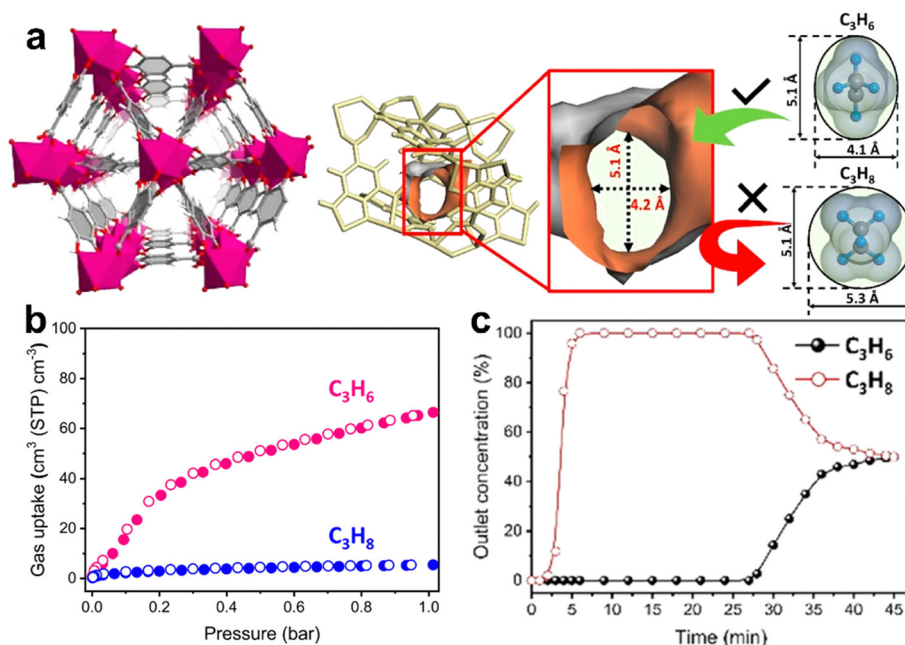


Fig. 15 (a) Structure of the Co-gallate MOF and rationale for C<sub>3</sub>H<sub>6</sub>/C<sub>3</sub>H<sub>8</sub> separation. (b) Gas sorption isotherms of propylene and propane at 298 K for Co-gallate. (c) The breakthrough experiments were carried out in a packed column. Reprinted with permission from ref. 154. Copyright 2020 American Chemical Society.

MOF (NTU-85-WNT) of pore surface decorated with water nanotubes ( $\sim 4.5$  Å). Single-component sorption results of NTU-85-WNT indicated a rapid C<sub>3</sub>H<sub>6</sub> uptake ( $20.9 \text{ mL mL}^{-1}$ ,  $0.45 \text{ mmol g}^{-1}$ ), while the adsorption of C<sub>3</sub>H<sub>8</sub> ( $0.13 \text{ mL mL}^{-1}$ ,  $0.003 \text{ mmol g}^{-1}$ ) at 298 K can be neglected. The IAST selectivity of NTU-85-WNT for an equimolar C<sub>3</sub>H<sub>6</sub>/C<sub>3</sub>H<sub>8</sub> mixture reaches up to 1570. Fixed-bed breakthrough experiments further confirmed its molecular sieving performance for an equimolar C<sub>3</sub>H<sub>6</sub>/C<sub>3</sub>H<sub>8</sub> mixture, with a C<sub>3</sub>H<sub>6</sub> productivity of  $1.6 \text{ mL mL}^{-1}$  (98.8%+ purity). It is worth noting that high purity C<sub>3</sub>H<sub>8</sub> (>99.5%) can be obtained in one adsorption–desorption cycle due to the efficient sieving performance.

An optimal pore size combined with high-density binding sites can efficiently separate C<sub>3</sub>H<sub>6</sub>/C<sub>3</sub>H<sub>8</sub>, allowing for high-density stacking of C<sub>3</sub>H<sub>8</sub> and maximizing its adsorption capacity. Recently, Chen *et al.* reported a robust Hofmann-type MOF, [Co(py<sub>2</sub>-NH<sub>2</sub>)Ni(CN)<sub>4</sub>] (ZJU-75a, py<sub>2</sub>-NH<sub>2</sub> = 2-aminopyrazine), with high-density binding sites, showing excellent separation performance for C<sub>3</sub>H<sub>6</sub>/C<sub>3</sub>H<sub>8</sub>.<sup>157</sup> ZJU-75a exhibits an isostructural framework with [Co(py<sub>2</sub>)Ni(CN)<sub>4</sub>] (ZJU-74a, py<sub>2</sub> = pyrazine), decorated with amino groups. ZJU-75a exhibits an appropriate pore size ( $4.1 \times 4.4 \text{ Å}^2$ ) and OMSs of high density ( $8.89 \text{ mmol cm}^{-3}$ ). Single-component sorption isotherms showed that ZJU-75a and ZJU-74a exhibit comparable C<sub>3</sub>H<sub>6</sub> uptakes of  $104.3 \text{ cm}^{-3} \text{ cm}^3$  ( $3.31 \text{ mmol g}^{-1}$ ) and  $111.4 \text{ cm}^{-3} \text{ cm}^3$  ( $3.68 \text{ mmol g}^{-1}$ ) at 1 bar and 296 K, respectively, whereas the C<sub>3</sub>H<sub>8</sub> adsorption capacity of ZJU-75a ( $73.5 \text{ cm}^{-3} \text{ cm}^3$ ,  $2.33 \text{ mmol g}^{-1}$ ) is obviously smaller than that of ZJU-74a ( $103.6 \text{ cm}^{-3} \text{ cm}^3$ ,  $3.42 \text{ mmol g}^{-1}$ ). Thus, the IAST selectivity of ZJU-75a for C<sub>3</sub>H<sub>6</sub>/C<sub>3</sub>H<sub>8</sub> was calculated to be 54.2 at 296 K and 1 bar, much higher than that of ZJU-74a (4.3). The breakthrough studies indicate that ZJU-75a can yield C<sub>3</sub>H<sub>6</sub>

of high-purity (99.5%+) with a productivity of  $18.7 \text{ L kg}^{-1}$  and separation factor of 14.7. Structural and computational studies indicated that high-density OMSs and nitrogen atoms (from [Ni(CN)<sub>4</sub>]<sub>2</sub> units and -NH<sub>2</sub> groups) in ZJU-75a contribute jointly to the strong adsorption of C<sub>3</sub>H<sub>6</sub>, thus resulting in a high C<sub>3</sub>H<sub>6</sub> storage density ( $0.818 \text{ g mL}^{-1}$ ).

C<sub>3</sub>H<sub>8</sub>-selective adsorptive separation would be a relatively simple and energy-efficient way to get pure propylene. However, the differences of the molecular size ( $\sim 0.5$  Å) and polarizability (C<sub>3</sub>H<sub>6</sub>:  $62.6 \times 10^{-25}$ , and C<sub>3</sub>H<sub>8</sub>:  $62.9\text{--}63.7 \times 10^{-25} \text{ cm}^3$ ) between C<sub>3</sub>H<sub>6</sub> and C<sub>3</sub>H<sub>8</sub> are smaller than those between C<sub>2</sub>H<sub>4</sub> and C<sub>2</sub>H<sub>6</sub>. So far, only a few C<sub>3</sub>H<sub>8</sub>-selective MOFs have been reported.<sup>169–180</sup>

In 2022, Xing *et al.* reported an ultramicroporous pillared layered MOF [Co(IPA)(DPG)]<sub>n</sub> (PCP-IPA, IPA = isophthalic acid, and DPG = *meso*- $\alpha,\beta$ -di(4-pyridyl)glycol) featuring 1D pores (size  $\sim 4.7 \times 5.6 \text{ Å}^2$ ) and periodic parallel-aligned isophthalic acid units on the pore surface, exhibiting an excellent selectivity for C<sub>2</sub>H<sub>6</sub> and C<sub>3</sub>H<sub>8</sub>.<sup>169</sup> Although C<sub>2</sub>H<sub>6</sub> and C<sub>3</sub>H<sub>8</sub> have different molecular sizes, the suitable pore size of PCP-IPA facilitates their directional adsorption and maximizes the interaction between PCP-IPA and C<sub>3</sub>H<sub>8</sub>/C<sub>2</sub>H<sub>6</sub>. Therefore, PCP-IPA exhibits not only a C<sub>3</sub>H<sub>8</sub>/C<sub>3</sub>H<sub>6</sub> (50/50) IAST selectivity of 2.48 but also a relatively high adsorption selectivity (2.80) for C<sub>2</sub>H<sub>6</sub>/C<sub>2</sub>H<sub>4</sub> (50/50) at 1.0 bar and 298 K. Both C<sub>3</sub>H<sub>8</sub> and C<sub>2</sub>H<sub>4</sub> can be directly obtained with high purity (99.99%) through a fixed-bed column from C<sub>3</sub>H<sub>8</sub>/C<sub>3</sub>H<sub>6</sub> (50/50) and C<sub>2</sub>H<sub>4</sub>/C<sub>2</sub>H<sub>6</sub> (50/50) mixtures, respectively, affording a high C<sub>3</sub>H<sub>6</sub> productivity ( $15.23 \text{ L kg}^{-1}$ ) and excellent C<sub>2</sub>H<sub>4</sub> productivity ( $26.2 \text{ L kg}^{-1}$ ). Modeling simulation studies revealed that tighter and more multiple vdW interactions (C–H $\cdots$ O/C) can be formed between paraffins and PCP-IPA compared to olefins.

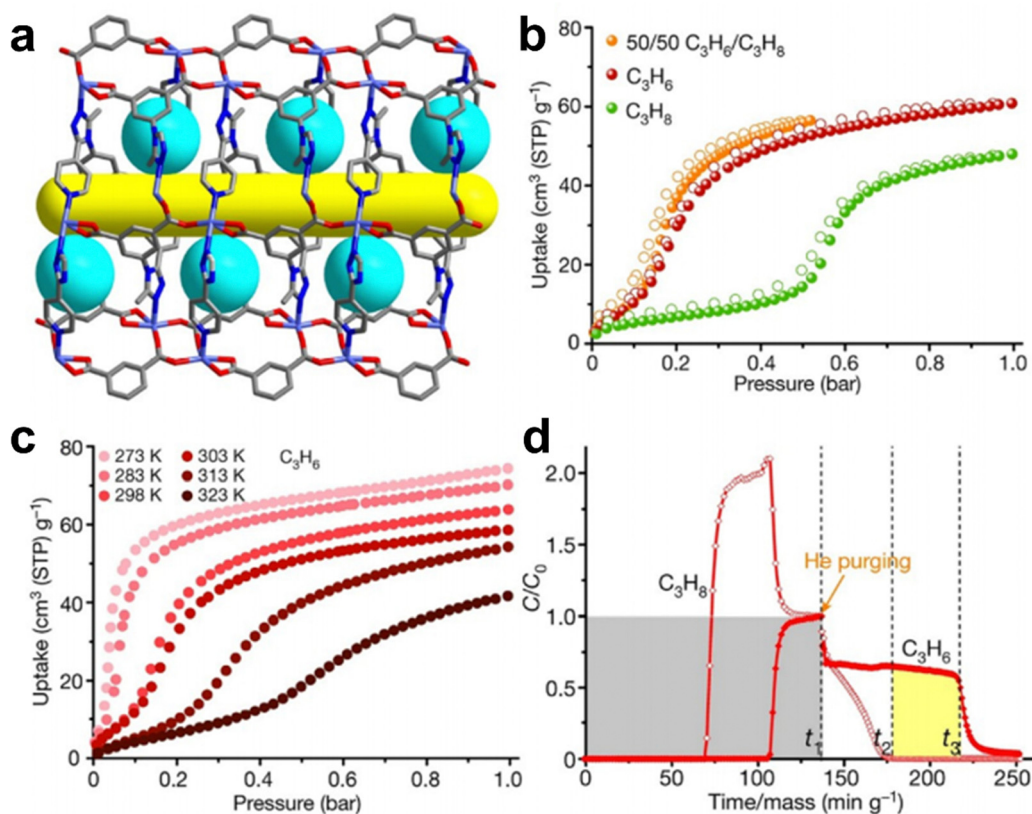


**Fig. 16** (a) Pore structure of JNU-3 viewed along the *b* axis showing the molecular pockets (turquoise) and 1D channels (yellow); (b) pure  $C_3H_8$  (green), pure  $C_3H_6$  (red), and an equimolar  $C_3H_6/C_3H_8$  mixture (orange) adsorption/desorption isotherms of JNU-3a at 303 K; (c)  $C_3H_6$  adsorption isotherms of JNU-3a at different temperatures; (d) breakthrough curves (starting at  $t = 0$ ) of an equimolar  $C_3H_6/C_3H_8$  mixture ( $1.0 \text{ mL min}^{-1}$ ) on JNU-3a, followed by desorption curves (starting at  $t = t_1$ ) under helium gas ( $10.0 \text{ mL min}^{-1}$ ) sweeping at 303 K.  $C_3H_8$ , open diamonds;  $C_3H_6$ , solid diamonds.  $C$  and  $C_0$  are the concentrations of each gas at the outlet and inlet, respectively. Grey area, mixed gas input; yellow area,  $C_3H_6$  gas output;  $t_1$ , the beginning of desorption;  $t_2$ , starting point of collecting  $C_3H_6$ ;  $t_3$ , the end point of collecting  $C_3H_6$ . Reprinted with permission from ref. 155. Copyright 2021 Nature Publishing Group.

Very recently, Li *et al.* reported two isostructural MOFs (FDMOF-1 and FDMOF-2) functionalized with different amounts of fluorinated functional groups ( $-CF_3$ ), showing strong affinity for  $C_3H_8$  over  $C_3H_6$  (Fig. 17).<sup>170</sup> Compared with the prototype MOF  $Zn_2(BDC)_2(DABCO)$  (Zn-DMOF, BDC = 1,4-benzenedicarboxylate), the introduction of different amounts of  $-CF_3$  groups into a MOF not only increases its stability but also adjusts the pore size/shape. Therefore, FDMOF-2 with the maximal amount of  $-CF_3$  groups shows the smallest aperture ( $5.1 \text{ \AA}$ ) and exhibits the optimal  $C_3H_8$  affinity. Single-component sorption isotherms showed that FDMOF-2 displays a higher  $C_3H_8$  uptake of  $140 \text{ cm}^3 \text{ cm}^{-3}$  ( $5.04 \text{ mmol g}^{-1}$ ) but a lower  $C_3H_6$  uptake of  $115 \text{ cm}^3 \text{ cm}^{-3}$  ( $4.14 \text{ mmol g}^{-1}$ ), resulting in the IAST selectivity for 50/50  $C_3H_8/C_3H_6$  up to 2.18 at 298 K and 1 bar. Breakthrough experiments revealed that high purity ( $>99.99\%$ )  $C_3H_6$  can be directly produced from 50/50  $C_3H_8/C_3H_6$  mixtures, affording  $0.501 \text{ mol L}^{-1}$  production of  $C_3H_6$ . It is worth pointing out that the excellent separation performance of FDMOF-2 for  $C_3H_8/C_3H_6$  can be maintained under 70% relative humidity conditions. Single-crystal X-ray diffraction and theoretical calculation studies confirmed that the strong affinity of UTSA-400 for  $C_3H_8$  can be attributed to strong non-classical C-H $\cdots\pi$ /F hydrogen-bonding

interactions, resulting in a stronger binding affinity for  $C_3H_8$  vs.  $C_3H_6$  with an initial  $Q_{st}$  value difference of  $-3.7 \text{ kJ mol}^{-1}$ .

## 2.6. $C_3H_4/C_3H_6$ separation

The removal of traces of propyne ( $C_3H_4$  of  $\sim 1\%$ ) from propylene is essential to obtain high purity propylene ( $C_3H_6$ ). However, it is very difficult to separate trace amounts of  $C_3H_4$  from  $C_3H_6$ , because their chemical/physical properties and molecular sizes ( $C_3H_4$ :  $6.2 \times 3.8 \times 3.8 \text{ \AA}^3$ ;  $C_3H_6$ :  $6.5 \times 4.0 \times 4.2 \text{ \AA}^3$ ) are highly similar. Nevertheless, some MOFs have been reported to show great potential for the separation of  $C_3H_4/C_3H_6$ .<sup>181–189</sup>

In 2017, Chen *et al.* reported a flexible-robust MOF  $[Cu(\text{bpy})_2(\text{OTf})_2]$  (ELM-12, bpy = 4,4'-bipyridine, and  $\text{OTf}^-$  = trifluoromethanesulfonate) which exhibits excellent performance for removing trace  $C_3H_4$  from a 1/99  $C_3H_4/C_3H_6$  mixture. ELM-12 composed of 2D square-grid sheets with dynamic dangling  $\text{OTf}^-$  groups exhibit two kinds of cavities of different shapes and sizes ( $6.1 \times 4.3 \times 4.3 \text{ \AA}^3$  and  $6.8 \times 4.0 \times 4.2 \text{ \AA}^3$ ), which were comparable with the size and shape of  $C_3H_4$  ( $6.2 \times 3.8 \times 3.8 \text{ \AA}^3$ ) (Fig. 18).<sup>181</sup> Single-component adsorption isotherms revealed that ELM-12 shows a sharp increasing adsorption for  $C_3H_6$  with an uptake of  $1.83 \text{ mmol g}^{-1}$  at 298 K and 1 bar, as well as a large  $Q_{st}$

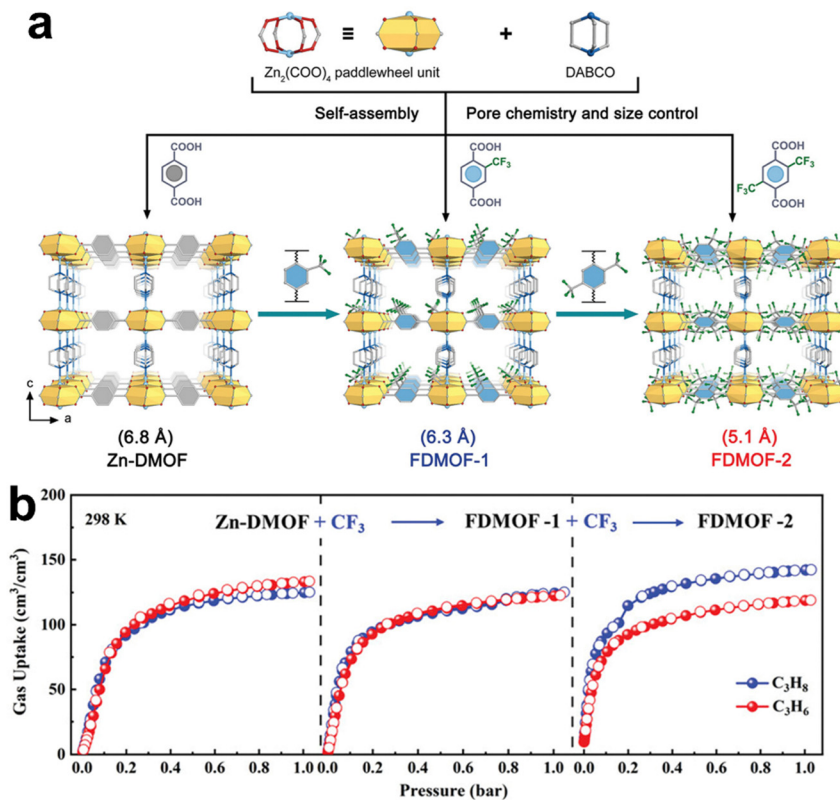


Fig. 17 (a) Crystal structures of Zn-DMOF, FDMOF-1, and FDMOF-2. (b) Single-component gas adsorption isotherms of the samples at 298 K. Reprinted with permission from ref. 170. Copyright 2023 Wiley-VCH.

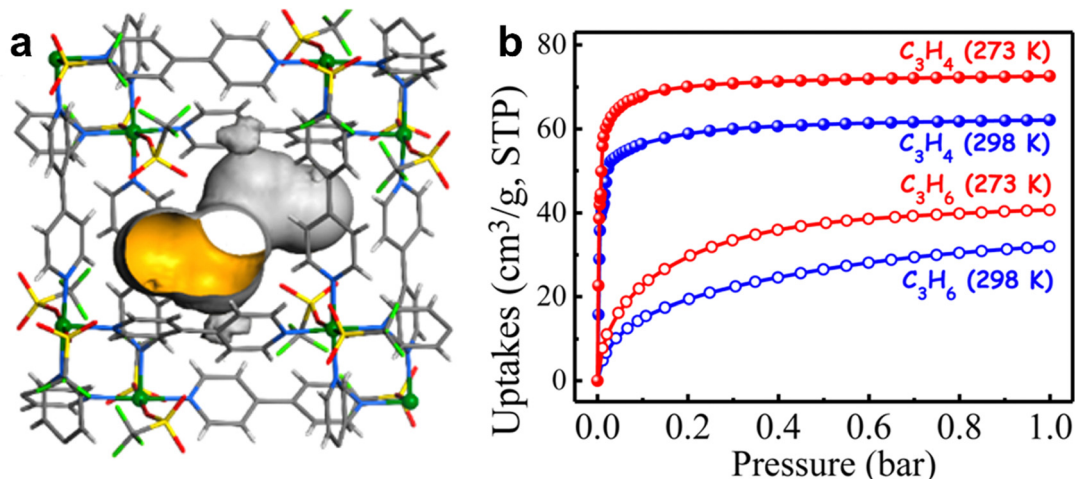


Fig. 18 (a) Crystal structure of ELM-12. (b)  $C_3H_4$  and  $C_3H_6$  adsorption isotherms of ELM-12. Reprinted with permission from ref. 181. Copyright 2017 American Chemical Society.

of 60.6  $kJ mol^{-1}$  for  $C_3H_6$ , indicating its strong interaction with the  $C_3H_6$  molecule. In contrast, both the uptake capacity (0.67  $mmol g^{-1}$  at 0.1 bar and 298 K) and  $Q_{st}$  (15.8  $kJ mol^{-1}$ ) of ELM-12 for  $C_3H_8$  are significantly lower. The multiple interactions, such as weak or non-classical C-D...O hydrogen bonds, between ELM-12 and  $C_3D_4$  molecules were further confirmed by high-resolution neutron powder diffraction studies. Breakthrough experiments demonstrated that high purity

(99.9998%) of  $C_3H_6$  can be obtained from a 1/99  $C_3H_4/C_3H_6$  mixture.

In 2018, Chen *et al.* studied a series of MOFs with different types of structures, functionalities, and pore sizes (Fig. 19).<sup>182</sup> Besides for highly selective  $C_2H_2/C_2H_4$  separation,<sup>70,71</sup> SIFSIX-type MOFs such as SIFX-1-Cu, SIFSIX-2-Cu-i, SIFSIX-3-Ni, and UTSA-200 also exhibit strong binding affinities for  $C_3H_4$  compared to  $C_3H_6$  and show high  $C_3H_4$  adsorption capacities at very

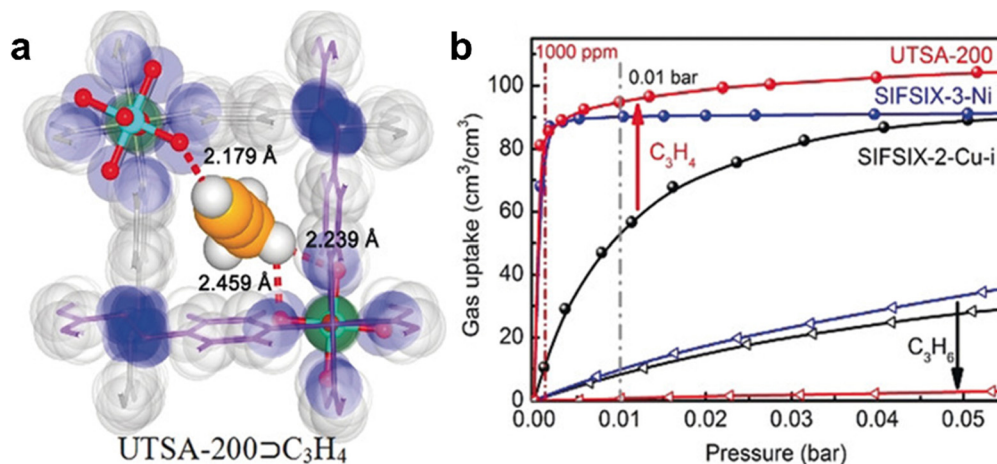


Fig. 19 (a) DFT-D optimized structure and binding sites of  $\text{UTSA-200} \supset \text{C}_3\text{H}_4$ . (b)  $\text{C}_3\text{H}_4$  and  $\text{C}_3\text{H}_6$  adsorption isotherms of UTSA-200 at 298 K. Reprinted with permission from ref. 182. Copyright 2018 Wiley-VCH.

low pressure. The former three SIFSIX-MOFs show slightly larger pore sizes than both  $\text{C}_3\text{H}_4$  and  $\text{C}_3\text{H}_6$ , which lead to moderate  $\text{C}_3\text{H}_4/\text{C}_3\text{H}_6$  selectivity. The activated UTSA-200 with the optimal pore size (3.4 Å) and strong binding sites has the best separation performance for  $\text{C}_3\text{H}_4/\text{C}_3\text{H}_6$ . Single-component adsorption isotherms revealed that UTSA-200 exhibits the highest  $\text{C}_3\text{H}_4$  uptake capacity of  $95 \text{ cm}^3 \text{ cm}^{-3}$  ( $2.99 \text{ mmol g}^{-1}$ ) at 0.01 bar and 298 K, while adsorbs negligible  $\text{C}_3\text{H}_6$  ( $0.33 \text{ mmol g}^{-1}$ , at 298 K and 0.4 bar), resulting in an extremely high IAST selectivity of 20 000 for 1/99  $\text{C}_3\text{H}_4/\text{C}_3\text{H}_6$  at 298 K and 1 bar. Breakthrough experiments demonstrated that high purity (99.9999%)  $\text{C}_3\text{H}_6$  can be yielded from 1:99 and 0.1:99.9  $\text{C}_3\text{H}_4/\text{C}_3\text{H}_6$  mixtures with a productivity of  $62.9 \text{ mmol g}^{-1}$  and  $143.8 \text{ mmol g}^{-1}$ , respectively. Neutron powder diffraction studies and DFT-D calculations revealed that  $\text{C}_3\text{H}_4$  molecules can open the pores of UTSA-200 and form strong C–H...F interactions with the framework.

In 2022, Xing *et al.* reported a flexible MOF GeFSIX-14-Cu-i (ZU-33, GeFSIX = hexafluorogermanate, and 14 = 4,4'-azopyridine), which exhibits guest/temperature-dependent structural dynamics and shows strong binding affinity towards acetylene and propadiene.<sup>188</sup> ZU-33 featuring a 2-fold interpenetrated structure is composed of Cu(II)-4,4'-azobipyridine 2D layers and  $\text{GeF}_6^{2-}$  pillars, and its pore size (3.08–5.04 Å) was dynamically adjustable by the rotational motion of  $\text{GeF}_6^{2-}$  pillars and the organic ligands. Single-component gas adsorption experiments revealed that ZU-33 shows a steep uptake for alkynes (acetylene and propyne) and propadiene at low pressure (0.01 bar) and 303 K, while there is a threshold pressure for olefin adsorption and a size exclusion effect for alkanes. In addition, for  $\text{C}_2\text{H}_4$  that is smaller than propyne and propadiene regarding the kinetic diameters, ZU-33 nearly inhibits  $\text{C}_2\text{H}_4$  molecules to diffuse into its pores, suggesting the inverse size sieving below 0.5 bar at 303 K. Molecular simulations and single-crystal X-ray diffraction revealed that the interactions between the alkyne molecules (propyne and propadiene) and ZU-33 are more intense, thus requiring less input energy to overcome the energy barrier for

the structural deformation. Breakthrough tests on a ZU-33 packed column verified that acetylene and propadiene can be directly removed from simulated cracking gases.

## 2.7. $\text{C}_4$ hydrocarbon separation

$\text{C}_4$  olefins including 1,3-butadiene (1,3- $\text{C}_4\text{H}_6$ ), 1-butene ( $n\text{-C}_4\text{H}_8$ ) and isobutene ( $i\text{-C}_4\text{H}_8$ ) are important raw materials for the production of synthetic rubbers and chemicals. However,  $\text{C}_4$  olefin separation represents one of the great challenges in hydrocarbon purification owing to the similar structures and physical properties.<sup>190,191</sup>

Xing *et al.* reported several interpenetrated anion-pillared ultra-microporous MOFs, such as GeFSIX-2-Cu-i (ZU-32), NbFSIX-2-Cu-i (ZU-52) and GeFSIX-14-Cu-i (ZU-33), and realized highly efficient separation of  $\text{C}_4$  olefins through molecular recognition.<sup>192</sup> This series of materials show ultrafine-tuning of the pore size/shape (4.20–4.83 Å) by replacing pillared inorganic anions with different bulks and different lengths of organic ligands. Among them, NbFSIX-2-Cu-i with a pore aperture size of 4.31 Å (F...F distance) exhibits high  $\text{C}_4\text{H}_6$  ( $2.64 \text{ mmol g}^{-1}$ ) and  $n\text{-C}_4\text{H}_8$  ( $2.26 \text{ mmol g}^{-1}$ ) uptake but negligible  $i\text{-C}_4\text{H}_8$  uptake ( $0.48 \text{ mmol g}^{-1}$ ), showing uptake selectivities of about 5.00 and 5.74 for  $n\text{-C}_4\text{H}_8/i\text{-C}_4\text{H}_8$  and  $\text{C}_4\text{H}_6/i\text{-C}_4\text{H}_8$ , respectively. In contrast, GeFSIX-14-Cu-i shows a smaller pore size of 4.20 Å (F...F distance), resulting in negligible adsorption of  $n\text{-C}_4\text{H}_8$  ( $0.57 \text{ mmol g}^{-1}$ ) and  $i\text{-C}_4\text{H}_8$  ( $0.42 \text{ mmol g}^{-1}$ ), but still retaining large uptake for  $\text{C}_4\text{H}_6$  ( $2.67 \text{ mmol g}^{-1}$ ), accompanying a gate-opening adsorption behavior for  $\text{C}_4\text{H}_6$ . Breakthrough experiments demonstrated that these materials can efficiently separate  $\text{C}_4\text{H}_6$  from  $\text{C}_4\text{H}_6/n\text{-C}_4\text{H}_8/i\text{-C}_4\text{H}_8/\text{He}$  (50/15/30/5) mixtures, as well as efficiently separate  $\text{C}_4\text{H}_6/n\text{-C}_4\text{H}_8$  (50/50) and  $n\text{-C}_4\text{H}_8/i\text{-C}_4\text{H}_8$  (50/50) mixtures.

Because of its high degree of unsaturation and strong coordination ability, 1,3- $\text{C}_4\text{H}_6$  is commonly adsorbed preferentially over other  $\text{C}_4$  hydrocarbons by MOFs with functional sites. It is thus energy-intensive and might induce undesired polymerization as the purification involves capture of 1,3- $\text{C}_4\text{H}_6$  and

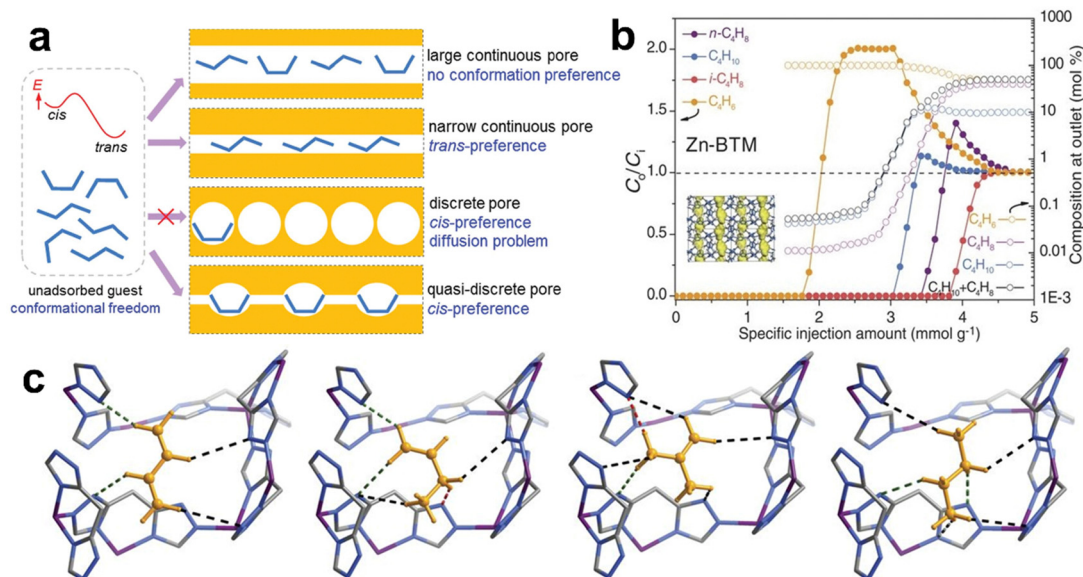


Fig. 20 (a) Schematic diagrams of controlling the guest conformation through the quasi-discrete pore in MAF-23. (b) Breakthrough curves of MAF-23 for a 5 : 2 : 2 : 1 C<sub>4</sub>H<sub>6</sub>/n-C<sub>4</sub>H<sub>8</sub>/i-C<sub>4</sub>H<sub>8</sub>/C<sub>4</sub>H<sub>10</sub> mixture. (c) Crystal structures of host-guest complexes of C<sub>4</sub>H<sub>6</sub>, n-C<sub>4</sub>H<sub>8</sub>, i-C<sub>4</sub>H<sub>8</sub>, and C<sub>4</sub>H<sub>10</sub>. Reprinted with permission from ref. 193. Copyright 2017 the American Association for the Advancement of Science.

its subsequent release through heating in general. Zhang *et al.* noticed that the collaborative interactions between the host framework and guest flexibility can significantly change the conformation of certain C<sub>4</sub> hydrocarbons and thus exhibit abnormal adsorption and reversed selectivity (Fig. 20).<sup>193</sup> In particular, a hydrophilic pore of a MAF with free N atoms, namely, [Zn<sub>2</sub>(btm)]<sub>2</sub> (MAF-23), with 1D quasi-discrete pores (aperture size 3.6 Å, and cage size *ca.* 6 Å) was employed for separation of four hydrocarbons, n-C<sub>4</sub>H<sub>8</sub>, i-C<sub>4</sub>H<sub>8</sub>, C<sub>4</sub>H<sub>10</sub> and 1,3-C<sub>4</sub>H<sub>6</sub>. As revealed by experimental and DFT calculations, n-C<sub>4</sub>H<sub>8</sub>, the most similar one to 1,3-C<sub>4</sub>H<sub>6</sub> among these gas molecules, adopts a metastable *cis* conformation to form stronger non-classical C-H...N interactions, and hence has a significantly stronger binding affinity, whereas 1,3-C<sub>4</sub>H<sub>6</sub> adopts the stable *trans* conformation and has the weakest binding affinity because of the unfitting configuration for forming stronger non-classical hydrogen-bonding interactions. In other words, MAF-23 with a unique pore structure and surface serves as a guest conformation-controlling adsorbent to achieve preferential adsorption of n-C<sub>4</sub>H<sub>8</sub>, i-C<sub>4</sub>H<sub>8</sub> and C<sub>4</sub>H<sub>10</sub> over 1,3-C<sub>4</sub>H<sub>6</sub>. Therefore, 1,3-C<sub>4</sub>H<sub>6</sub> can be first eluted during the breakthrough operation under ambient conditions, and directly purified for the desired purity (≥99.5%) to meet the industrial requirement in one single separation operation.

The separation of C<sub>4</sub> geometric isomers is also a challenging separation process, among which the separation of *trans/cis*-2-butene is of prime importance to increase the value of C<sub>4</sub> olefins. Ren *et al.* reported that M-gallate (M = Ni, Mg, and Co), featuring oval-shaped pores, are ideally suitable for shape-selective separation of *trans/cis*-2-butene through their difference in the minimum molecular cross-section sizes, in addition to a highly efficient separation of 1,3-butadiene, 1-butene, and *i*-butene.<sup>194</sup> Mg-gallate displays a narrow pore window size of 3.6 × 4.6 Å<sup>2</sup>, capturing the smaller *trans*-2-butene (3.5 × 4.6 Å<sup>2</sup>)

while excluding the slightly larger *cis*-2-butene (3.6 × 4.9 Å<sup>2</sup>), affording a high *trans/cis*-2-butene uptake selectivity of 3.19 at 298 K and 1.0 bar in single-component adsorption isotherms. DFT-D study showed that Mg-gallate interacts with *trans*-2-butene and 1,3-butadiene through short distances of intermolecular C...H-O interactions (C...H distances 2.57–2.83 and 2.45–2.79 Å, respectively).

The separation of isomeric C<sub>4</sub> paraffins is also an important task in the petrochemical industry. Zhong *et al.* regulated the pore aperture of the cage-like Zn-bzc by stepwise installation of methyl groups on its narrow aperture to achieve both molecular-sieving separation and a high n-C<sub>4</sub>H<sub>10</sub> uptake.<sup>195</sup> The resulting Zn-bzc-2CH<sub>3</sub> is not only a new benchmark adsorbent featuring molecular sieving for n-C<sub>4</sub>H<sub>10</sub>/iso-C<sub>4</sub>H<sub>10</sub> separation and a high n-C<sub>4</sub>H<sub>10</sub> adsorption capacity (2.42 mmol g<sup>-1</sup>), but also hydrophobic to eliminate the negative effect of water vapor on gas separation under humid conditions. Breakthrough tests proved that high-purity i-C<sub>4</sub>H<sub>10</sub> (99.99%) can be collected. The minimum energy path of n-C<sub>4</sub>H<sub>10</sub> and i-C<sub>4</sub>H<sub>10</sub> from cage to cage passing through the narrow aperture was determined for Zn-bzc-*n*CH<sub>3</sub> (*n* = 0, 1, 2), and the results suggested easy transports of both n-C<sub>4</sub>H<sub>10</sub> and i-C<sub>4</sub>H<sub>10</sub> for the larger apertures of the parent Zn-bzc MOF and Zn-bzc-CH<sub>3</sub> due to the low energy barrier together with a small barrier difference, while kinetic forbiddance with a dramatical increase of the diffusion energy barrier from 23.8 to 131.6 kJ mol<sup>-1</sup> for n-C<sub>4</sub>H<sub>10</sub> to migrate through Zn-bzc-2CH<sub>3</sub>.

## 2.8. Linear/branched alkane separation

The branched C<sub>5</sub>–C<sub>6</sub> paraffins are major components in high-octane gasoline, which have relatively higher Research Octane Number (RON) values than their normal counterparts. To boost octane ratings in gasoline, the separation of linear alkanes

from their branched isomers is very important in the petroleum industry, which is traditionally done by energy-intensive distillation processes.

Eddaoudi *et al.* reported two new 12-connected rare-earth metal ( $Y^{3+}$  and  $Tb^{3+}$ ) fumarate based fcu-MOFs with both octahedral and tetrahedral cages that were solely interconnected with triangular windows of aperture size *ca.* 4.7 Å, and discovered that both of them can act as a adsorbate-size cut-off for the total sieving of  $C_4$  and  $C_5$  branched paraffins.<sup>196</sup>

In addition, Li *et al.* prepared two Zr-MOF compounds, Zr-bptc and Zr-abtc, which are highly stable with optimal pore structures for the separation of  $C_6$  alkane isomers (Fig. 21).<sup>197</sup> For instance, Zr-abtc featuring an scu-type structure with 1D channels ( $d = 7$  Å) accommodates all  $C_6$  alkane isomers (*n*-hexane, 3-methylpentane and 2,3-dimethylbutane), but favors *n*-hexane because of its stronger interactions with the pore surface, resulting in a mono/dibranched separation factor ( $\sim 1.3$ ) in the breakthrough test.

In 2020, Li *et al.* reported a new flexible MOF, calcium chloranilate (HIAM-203), which specially possesses chloro-decorated 1D channels.<sup>198</sup> HIAM-203 exhibits structural flexibility upon adsorption of  $C_6$  alkanes with different branching, as well as similar temperature-dependent adsorption behavior toward alkane isomers. It can take up a plentiful amount of *n*-hexane and 3-methylpentane at 30 °C, but completely excludes 2,2-dimethylbutane, while at 150 °C 3-methylpentane is also excluded. This phenomenon may be rationalized by the significant difference in

binding affinity near the pore aperture of HIAM-203. As the pore size of HIAM-203 (5.6 Å) is between the kinetic diameters of 3-methylpentane (5.5 Å) and 2,2-dimethylbutane (6.2 Å), it thus inhibits the diffusion of 2,2-dimethylbutane.

In 2023, Bao *et al.* employed the Hofmann-type MOFs,  $[M(pz)Ni(CN)_4]$  ( $M = Co$  and  $Ni$ ) to demonstrate similar temperature-swing molecular exclusion for separation of hexane isomers.<sup>199</sup> CopzNi displays excellent separation efficiency for linear/mono-branched and mono-branched/di-branched alkanes with the highest adsorption capacity to date. CopzNi exhibits lower-energy regeneration, scalability, recyclability and high stability, representing a promising candidate for relevant separation processes.

There are also needs for purification of valuable  $C_5$ - $C_7$  olefins. Isoprene, which accounts for 15–25% of  $C_5$  fractions including important olefins like 1-pentene and *trans*-2-pentene, is widely used in the production of synthetic rubber, pharmaceutical and pesticide intermediates.<sup>200</sup> The regeneration and desorption efficiency should also be taken into account for separation.<sup>201</sup> Cui *et al.* found that anion-pillared hybrid porous materials, namely, ZU-62 (also termed NbOFFIVE-2-Cu-i) and TIFSIX-2-Cu-i, exhibit a good separation performance for  $C_5$  olefin mixtures (*trans*-2-pentene, 1-pentene and isoprene).<sup>202</sup> Owing to a contraction of pore aperture originating from the rotation of 4,4'-dipyridylacetylene ligand, ZU-62 excludes the relatively large molecule of isoprene in the low pressure range (0–6 kPa), while

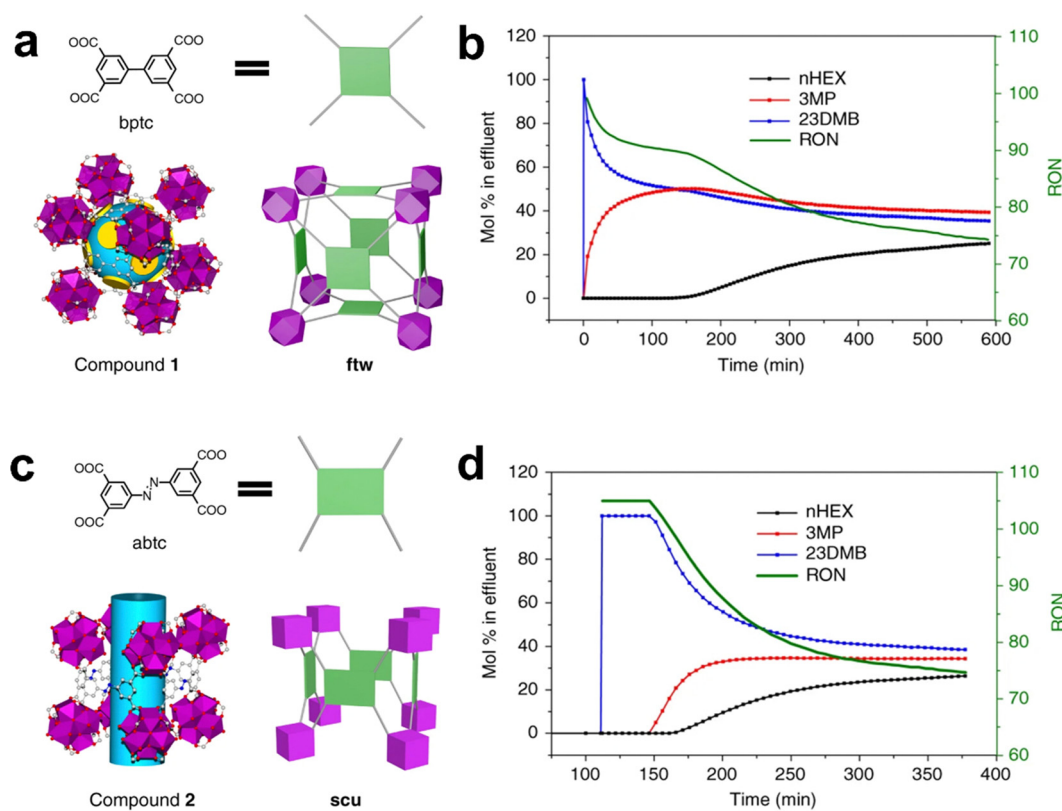


Fig. 21 (a) and (c) Organic ligands, crystal structures, and topologies of Zr-bptc and Zr-abtc. (b) and (d) Breakthrough curves of an equimolar ternary mixture of  $C_6$  alkane isomers at 150 °C for Zr-bptc (top) and Zr-abtc (bottom). The green curve represents the real-time RON of the eluted products. Reprinted with permission from ref. 197. Copyright 2018 Nature Publishing Group.

TIFSIX-2-Cu-i is able to distinguish the three C<sub>5</sub> olefins with a high uptake of *trans*-2-pentene (3.1 mmol·g<sup>-1</sup>), superior to that of zeolite 5A (2.0 mmol·g<sup>-1</sup>). DFT-D calculations confirmed that the selective adsorption was achieved by a favorable electrostatic environment as well as suitable pore confinement. Also, the regeneration tests showed that C<sub>5</sub> olefins can be easily desorbed from ZU-62 and TIFSIX-2-Cu-i at 298 K.

## 2.9. Aromatic isomer separation

The separation of C<sub>8</sub> aromatic compounds (xylene isomers, ethylbenzene and styrene) is also one of the important separations.<sup>1</sup> Tremendous efforts have been devoted to developing MOF adsorbents for relevant separations. Most of these adsorbents contain aromatic organic ligands, in which the phenyl or heterocycle rings allow strong  $\pi$ - $\pi$  stacking interactions with C<sub>8</sub> aromatic molecules to facilitate the adsorption.<sup>203,204</sup>

MOFs featuring structural flexibility like breathing or gate-opening have been applied for separation of aromatic isomers.<sup>18,37,205</sup> Li *et al.* reported that a stacked 1D manganese-based MOF [Mn(dhbq)(H<sub>2</sub>O)<sub>2</sub>] (Mn-dhbq, H<sub>2</sub>dhbq = 2,5-dihydroxy-1,4-benzoquinone) exhibits temperature-dependent discriminative adsorption of xylene isomers owing to reversible framework swelling.<sup>206</sup> At 363 K, *p*X can be fully intercepted from the *p*X/*m*X/*o*X ternary mixture by a column of Mn-dhbq, whereas the effluent of the *m*X/*o*X mixture can be further separated by another column of Mn-dhbq at a lower temperature (303 K) where mainly *o*X finally flows out. The purity of *p*X is over 97% collected during the desorption cycle when using 1,4-diethylbenzene as an eluent at 433 K for 1 hour after liquid-phase adsorption of a quaternary mixture (*p*X/*m*X/*o*X/EB, 22/22/50/6) at 393 K. DFT calculations indicated that the temperature-dependent flexibility between 1D coordination chains (different degrees of swelling at different temperatures) endows such selective adsorption of xylene isomers through  $\pi$ - $\pi$  stacking interactions with the aromatic ligand.

Xing *et al.* reported a flexible anion pillared MOF [Ni(bpy)<sub>2</sub>(NbOF<sub>5</sub>)] (ZU-61) with *pcu* topology and a pore size of 7.8 Å exhibiting efficient separation performance for xylene isomer.<sup>207</sup> Single-component adsorption revealed that ZU-61 shows a higher low-pressure uptake for *m*X and *o*X than *p*X at

0.01 bar and 333 K, as well as a high capacity for *m*X (3.4 mmol g<sup>-1</sup>) and *o*X (3.2 mmol g<sup>-1</sup>). Breakthrough experiments for a 1:1:1 *p*X/*m*X/*o*X mixture confirmed that high purity (>99.9%) *p*X can elute from the column first, and then followed by *m*X and *o*X. The excellent performance for xylene isomer separation can be attributed to the rotational NbOF<sub>5</sub><sup>2-</sup> anions, which allows adaptive host-guest interaction (C-H...F interactions) depending on the shape of the xylene isomer, as confirmed by DFT calculations and crystallographic studies. These results showed that ZU-61 exhibits great potential for the purification of *p*X.

Given that all xylene isomers contain phenyl rings for  $\pi$ - $\pi$  stacking interactions, another approach to enhance the separation selectivity would be utilizing the difference of their alkyl groups while inhibiting the interactions with phenyl rings. Yang *et al.* constructed a pillar-layered MOF Cu(bpdc)(ted)<sub>0.5</sub> (ZUL-C3) by using poly-cycloalkane-type ligands to show a non-aromatic pore environment for xylene separation.<sup>208</sup> The pore space of the MOF magnifies the difference of host-guest interactions with xylene isomers and ethylbenzene owing to their different distribution of methyl (ethyl) groups. Liquid-phase batch experiment indicated that this MOF can separate xylene isomers and ethylbenzene from each other, showing separation potential for *o*X/*p*X and *o*X/*m*X separation.

A flexible MOF, [Cu<sub>2</sub>(fbdim)]-*p*-xylene (MAF-41-*p*X), showing a 3D hinged-fence-like framework and 1D channels (4.2 × 9.8 × 10.1 Å<sup>3</sup> cavities and 3.9 × 6.7 Å<sup>2</sup> apertures), was demonstrated by Zhang *et al.* to exhibit unprecedented inversed molecular sieving (so called intermediate-sized molecular sieving) for the purification of styrene (Fig. 22).<sup>209</sup> The framework structure can transform to a nonporous one upon removal of template molecules. The activated MAF-41 can adsorb styrene (ST) to restore the as-synthesized structure while totally excluding ethylbenzene (EB), toluene (Tol), and benzene (Bz). Styrene with a purity of 99.9%+ can be obtained from the multicomponent mixture after one single adsorption-desorption cycle because the pores are individually opened and simultaneously occupied by the target guest. The aperiodic pore opening is believed to avoid co-adsorption of guest molecules smaller than the opened pores. Kinetic sorption studies revealed that the EB/Tol/Bz

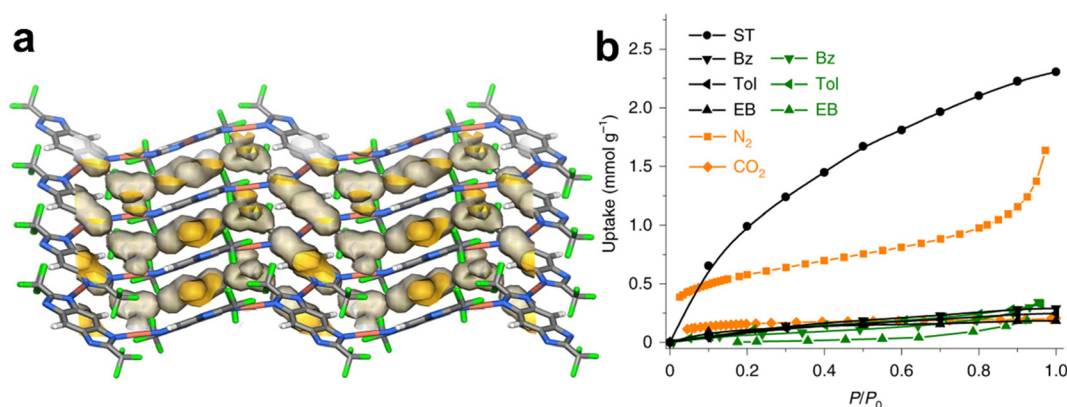


Fig. 22 (a) Crystal structure of guest-free MAF-41. (b) Adsorption isotherms of activated MAF-41 for ST (styrene, 298 K), EB (ethylbenzene, 298 K), Tol (toluene, 298 K), Bz (benzene, 298 K), N<sub>2</sub> (77 K), and CO<sub>2</sub> (195 K). Reprinted with permission from ref. 209. Copyright 2019 Nature Publishing Group.

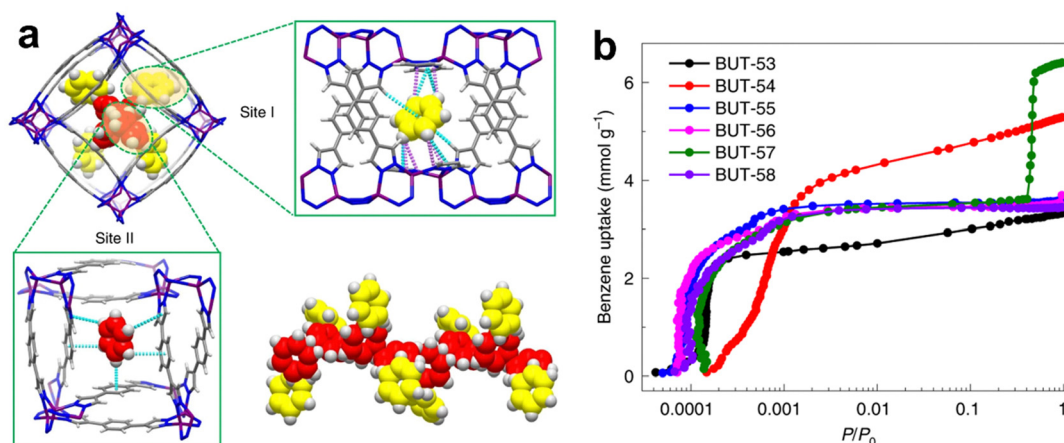


Fig. 23 (a) Structures of  $C_6H_6@BUT-55$  and benzene–benzene interactions. (b) Logarithmic-scale plots of  $P/P_0$  to view the benzene adsorption of BUT-53 to BUT-58 at low partial pressure. Reprinted with permission from ref. 210. Copyright 2022 Nature Publishing Group.

adsorptions stayed quite low all the time, while the ST uptake of MAF-41 significantly increased for both the single-component and mixtures, which confirms no EB/Tol/Bz co-adsorption or replacement of ST in MAF-41. Although Cu(I) complexes and Cu(I)-based MOFs may have poor stability in air and/or water, guest-free MAF-41 did not collapse not only at temperatures up to 500 °C, but also in boiling water for at least one week, and even remained stable in a solution of pH 3–14 at room temperature for at least 3 days.

In 2022, Li *et al.* reported a family of double-walled metal-dipyrazolate frameworks (BUT-53 to -58) composed of divalent metal ions and dipyrazolate ligands with different symmetries, lengths, and functionalities for trace benzene removal (Fig. 23).<sup>210</sup> In this study, multiple merits, *e.g.*, high stability, tunable pore, high adsorption capacity and selectivity, were integrated into these hydrophobic MOFs, which all exhibited high benzene uptakes (2.47–3.28 mmol g<sup>-1</sup>) at room temperature and ultra-low pressures (<10 Pa). BUT-55 is the best-performing adsorbent for the capture of trace benzene among them. It shows an extremely long breakthrough time of ~8000 h g<sup>-1</sup> for a benzene-containing (10 ppm, 10 mL min<sup>-1</sup>) gas mixture under both dry and humid (relative humidity = 50%) conditions. When the

relative humidity was 80%, the breakthrough time decreased to ~6000 h g<sup>-1</sup>, which is still much higher than that of other previously reported materials. After adsorption of benzene, BUT-55 can be regenerated under mild heating. As revealed by both the single-crystal structure of benzene-loaded BUT-55 and DFT calculations, multiple non-classical hydrogen-bonding C–H···X (X = N, O, π) interactions are the key to its strong affinity and high sensitivity toward benzene. The high benzene binding energy of BUT-55 contributes to its high adsorption selectivity of benzene over water or other volatile organic compounds (VOCs), such as cyclohexane and ethanol. It should also be pointed out that the BUT-55 sample is able to work continuously around one year under the breakthrough experiment conditions. In other words, a certain amount of BUT-55 can be used to capture trace airborne benzene for a long time due to its high benzene adsorption capacity under ultra-low pressures and high adsorption selectivity. The performance of these MOFs demonstrates high potential in the removal of benzene from ambient air.

Very recently, Mo *et al.* reported a flexible MOF, [Sr<sub>2</sub>(BIN-DI)(H<sub>2</sub>O)<sub>2</sub>] (WYU-62, H<sub>4</sub>BINDI = N,N'-bis(5-isophthalic acid)-naphthalenediimide) with electron-deficient NDI cores, which shows fast adsorption of trace benzene vapor at low pressure,

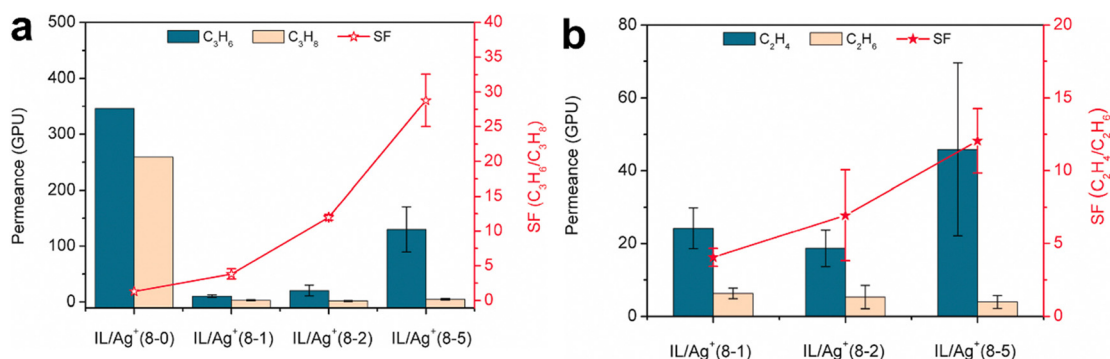


Fig. 24 (a)  $C_3H_6/C_3H_8$  separation performance of  $Zn_2(bim)_4$  membranes modified by diversified composites, IL/Ag<sup>+</sup>(8-0), IL/Ag<sup>+</sup>(8-1), IL/Ag<sup>+</sup>(8-2) and IL/Ag<sup>+</sup>(8-5). (b)  $C_2H_4/C_2H_6$  separation performance of  $Zn_2(bim)_4$  membranes modified by diversified composites, IL/Ag<sup>+</sup>(8-1), IL/Ag<sup>+</sup>(8-2) and IL/Ag<sup>+</sup>(8-5). Reprinted with permission from ref. 217. Copyright 2021 Elsevier.

accompanying a fluorescence-enhanced sensing (limit of detection =  $0.133 \text{ mg L}^{-1}$ ).<sup>211</sup> WYU-62 could be easily obtained by immersing the as-synthesized MOF [Sr<sub>2</sub>(BNDI)(DMF)(H<sub>2</sub>O)] (MYU-61) in water, during which discrete 0D pores of MYU-61 have transformed to 1D channels (aperture size =  $5.1 \times 9.1 \text{ \AA}^2$ ). Aromatic hydrocarbon vapor adsorption isotherms revealed that WYU-62a can show high benzene uptake at very low pressure ( $P/P_0 < 0.01$ ). DFT calculations and crystallographic studies indicated that electron-rich benzene was tightly wrapped between the two electron-deficient NDI moieties with strong  $\pi$ - $\pi$  and C-H... $\pi$  interactions. Therefore, it has excellent benzene adsorption capacity, whereas the accompanying host-guest charge transfer enables visual detection of trace benzene vapor.

### 3. MOF-based membranes for separating gaseous hydrocarbons

Though a variety of MOFs have been extensively studied for light-hydrocarbon purification in recent two decades, only a few have been fabricated into MOF-based mixed matrix membranes (MMMs), which may integrate the advantages of the separation performance of MOFs and processability of polymers for olefin/paraffin separation.<sup>212</sup> For example, MAF-4 (or ZIF-8) and Zr-fum-fcu-MOF (or MOF-801) have been incorporated with membranes for C<sub>3</sub>H<sub>6</sub>/C<sub>3</sub>H<sub>8</sub> separation.<sup>213,214</sup>

Modification of MOF membranes with the composite ionic liquid/Ag<sup>+</sup> (IL/Ag<sup>+</sup>) can efficiently improve their olefin/paraffin separation properties. Yang *et al.* synthesized layered Zn<sub>2</sub>(bim)<sub>4</sub> membranes<sup>215</sup> using the *in situ* interfacial assembly (ISIA)<sup>216</sup> method and further modified them with varied IL/Ag<sup>+</sup> composites.<sup>217</sup> Adsorption isotherms for Zn<sub>2</sub>(bim)<sub>4</sub> powder and its IL/Ag<sup>+</sup> modified sample showed that the adsorption capacity for olefin can significantly improve after modification with IL/Ag<sup>+</sup> but the adsorption for paraffin shows negligible changes, which is attributed to the strong  $\pi$ -complexation of olefins with Ag<sup>+</sup>. Further study revealed that the pristine Zn<sub>2</sub>(bim)<sub>4</sub> membrane showed a C<sub>3</sub>H<sub>6</sub>/C<sub>3</sub>H<sub>8</sub> separation factor of 1.14 with a C<sub>3</sub>H<sub>6</sub> permeance of 106 GPU (SF<sub>C<sub>2</sub>H<sub>4</sub>/C<sub>2</sub>H<sub>6</sub></sub>: 1.42, and P<sub>C<sub>2</sub>H<sub>4</sub></sub>: 311) (Fig. 24). In contrast, the modified membranes exhibited a significant improvement in olefin/paraffin separation with the optimized C<sub>3</sub>H<sub>6</sub>/C<sub>3</sub>H<sub>8</sub> separation factor of  $28.8 \pm 3.8$  with the C<sub>3</sub>H<sub>6</sub> permeance of  $129.8 \pm 40.4$  GPU (SF<sub>C<sub>2</sub>H<sub>4</sub>/C<sub>2</sub>H<sub>6</sub></sub>:  $12.0 \pm 2.2$ , and P<sub>C<sub>2</sub>H<sub>4</sub></sub>:  $45.6 \pm 23.7$  GPU). The preferential binding affinity of Ag<sup>+</sup> in IL for olefins facilitates the delivery of olefins in the modified Zn<sub>2</sub>(bim)<sub>4</sub> membranes. On the other hand, Ag<sup>+</sup> filling in the space of laminated modified Zn<sub>2</sub>(bim)<sub>4</sub> membranes further blocks paraffin penetration and thus improves the olefin/paraffin selectivity. In addition to the composite modification membrane strategy, intrinsic structural regulation of MOF membranes is also crucial. Recently, a series of Zn<sub>2</sub>(bim)<sub>4</sub> membranes functionalized with different amounts of amino groups, namely, Nx-Zn<sub>2</sub>(bim)<sub>4</sub> (x represents the molar ratio of raw 5-aminobenzimidazole, bim) were also investigated for separation.<sup>218</sup> Among them, the N10-Zn<sub>2</sub>(bim)<sub>4</sub> membrane exhibits the highest H<sub>2</sub>/CO<sub>2</sub> separation performance with a

separation factor of 1158 and a H<sub>2</sub> permeance of 1417 GPU. Moreover, its ideal selectivities for H<sub>2</sub>/CO<sub>2</sub>, H<sub>2</sub>/CH<sub>4</sub> and H<sub>2</sub>/C<sub>3</sub>H<sub>8</sub> were 829, 99, and 33, respectively, showing a distinct size exclusion effect for relatively large molecules.

Long *et al.* fabricated a series of membranes with M<sub>2</sub>(dobdc) (M = Co, Ni, Mg, and Mn) as fillers and 6FDA-DAM as the primary polymer by reducing the filler size to the sub-100 nm level to specially improve the filler-polymer compatibility and dispersion.<sup>219</sup> Among them, Ni<sub>2</sub>(dobdc) showed the best C<sub>2</sub>H<sub>4</sub>/C<sub>2</sub>H<sub>6</sub> separation performance without reduction in selectivity even under high-pressure owing to the presence of strong and multiple nanocrystal-polymer interactions, which suppresses plasticization by reducing polymer chain mobility.

Polycrystalline MOF membranes are less explored but also important. Liu *et al.*<sup>220</sup> have recently prepared a polycrystalline Co-gallate membrane with a reported freezing contra-diffusion protocol<sup>221</sup> that can enable more accurate control over the reaction kinetics between metal ions and ligands to effectively tune the MOF nucleation and growth in the bulk solution. Maintaining the frozen state of the metal precursor inside the macroporous  $\alpha$ -Al<sub>2</sub>O<sub>3</sub> substrate resulted in the formation of the preferred *c*-oriented and well-intergrown Co-gallate membrane with not only abundant open metal sites (at the increased missing-linker defects), but also reduced the thickness of the membrane. The multiscale structure endows the Co-gallate membrane with an outstanding C<sub>2</sub>H<sub>4</sub>/C<sub>2</sub>H<sub>6</sub> separation performance superior to those of state-of-the-art membranes including polycrystalline MOF membranes, MOF-based MMMs, and polymeric membranes. The optimized C<sub>2</sub>H<sub>4</sub>/C<sub>2</sub>H<sub>6</sub> selectivity is 8.3 with a C<sub>2</sub>H<sub>6</sub> permeance of 72.6 GPU. The resultant membrane also shows a negative correlation with the operation temperature and high long-term stability.

### 4. Conclusion and outlook

MOF materials have made significant progress in the separation of gaseous hydrocarbons in the past few years, which was achieved by rational control over their pore chemistry/size, affording an alternative separation technology for relevant applications. The high crystallinity of MOFs facilitates systematic and deep investigation on the exact adsorbent-adsorbate interactions in the type of porous materials for high separation performance, as demonstrated by their crystallographic studies on the host-guest interactions. Controlling of the pore structure of MOF materials at high-accuracy level is applicable due to the high modularity and diverse functionality of MOFs, which facilitates highly efficient separation of methane, olefin/paraffin, alkyne/olefin, alkane isomers and aromatics. As outlined in this review, the collaborative control of the pore size and pore surface has been explored for the potential of MOFs for hydrocarbon separation. MOFs with high separation selectivities and large gas uptakes have been documented. The development of this realm has gradually turned to evaluate the potential of MOFs in practical separation processes, which required continuous research endeavors.

There are many important issues remaining unaddressed before further industrial and commercial usage of MOFs. Shaping/pelleting of MOFs would be the first step in actual processes given engineering considerations, but that would lead to loss of adsorption capacity; thus, further study on mechanical stabilities of MOFs might be necessary. Simultaneously, the diffusion kinetics of MOF pellets should be comprehensively investigated. There are also concerns on current research for evaluations of their separation performances through swing adsorption or membrane separation processes, as these evaluations mainly focus on evaluating candidate materials under simulated conditions rather than the actual applications. In relevant simulated evaluations, the presence of contaminants such as water has gradually got involved. In contrast, the actual gas streams would be more complicated, while the separation condition can be even harsher (under elevated pressures/temperatures), which require the adsorbents to show good stability and durability, including good water resistance and impurity tolerance. The long-term durability and regeneration of MOFs during separation processes have been rarely involved in current research. Moreover, systematic evaluation of materials production, including capital and operating costs, should be performed prior to large-scale deployments of MOF-based adsorptive separation technology. Solvent-free and continuous synthesis methods have been demonstrated to be applicable for MOFs, which show great potential for large-scale production of MOF materials. In addition, new technical issues such as thermal management during the adsorption process would come out when sorption is scaled up. For membrane-based separation, there are also several challenges although it is capable of direct production of pure gas and can be simply operated under mild conditions. Several mixed-matrix MOF-based membranes have been developed, which show large permeance differences for hydrocarbon separation. However, the processability, defect, compatibility, and scaling up in membrane fabrication as well as the permeability-selectivity trade-off are still quite challenging. In terms of membrane separation, molecular sieving of hydrocarbons is still highly desirable. As the structure numbers of MOFs keep growing, there are also emerging technologies like machine learning under artificial intelligence for the computational design and discovery of novel MOF materials, while automated chemistry for high-throughput screening is also possible by combination with robotics.

As promising adsorbent materials for hydrocarbon separation, MOFs with high separation performance can be synthesized by combination of rational control of their pore size and pore surface. Continuous collaborative efforts among scientists, engineers and industrial partners will promote the application of MOF adsorbents to scientifically and technologically important industrial hydrocarbon separation, which would reap great benefits for society.

## Conflicts of interest

There are no conflicts to declare.

## Acknowledgements

The authors acknowledge supports from the National Natural Science Foundation of China (22090061, 22101307), the Hundred Talents Program of Sun Yat-Sen University and the Fundamental Research Funds for the Central Universities (Sun Yat-Sen University, 22qntd2301).

## Notes and references

- 1 D. S. Sholl and R. P. Lively, Seven chemical separations to change the world, *Nature*, 2016, **532**, 435–437.
- 2 S. Chu, Y. Cui and N. Liu, The path towards sustainable energy, *Nat. Mater.*, 2017, **16**, 16–22.
- 3 H. Furukawa, K. E. Cordova, M. O’Keeffe and O. M. Yaghi, The Chemistry and Applications of Metal-Organic Frameworks, *Science*, 2013, **341**, 1230444.
- 4 S. Kitagawa, R. Kitaura and S. I. Noro, Functional Porous Coordination Polymers, *Angew. Chem., Int. Ed.*, 2004, **43**, 2334–2375.
- 5 B. Chen, S. Xiang and G. Qian, Metal-Organic Frameworks with Functional Pores for Recognition of Small Molecules, *Acc. Chem. Res.*, 2010, **43**, 1115–1124.
- 6 Y. Cui, B. Li, H. He, W. Zhou, B. Chen and G. Qian, Metal-Organic Frameworks as Platforms for Functional Materials, *Acc. Chem. Res.*, 2016, **49**, 483–493.
- 7 I. M. Hönicke, I. Senkowska, V. Bon, I. A. Baburin, N. Bönisch, S. Raschke, J. D. Evans and S. Kaskel, Balancing Mechanical Stability and Ultrahigh Porosity in Crystalline Framework Materials, *Angew. Chem., Int. Ed.*, 2018, **57**, 13780–13783.
- 8 Z.-S. Wang, M. Li, Y.-L. Peng, Z. Zhang, W. Chen and X.-C. Huang, An Ultrastable Metal Azolate Framework with Binding Pockets for Optimal Carbon Dioxide Capture, *Angew. Chem., Int. Ed.*, 2019, **58**, 16071–16076.
- 9 R.-B. Lin, S. Xiang, B. Li, Y. Cui, G. Qian, W. Zhou and B. Chen, Our journey of developing multifunctional metal-organic frameworks, *Coord. Chem. Rev.*, 2019, **384**, 21–36.
- 10 R.-B. Lin, S. Xiang, H. Xing, W. Zhou and B. Chen, Exploration of porous metal-organic frameworks for gas separation and purification, *Coord. Chem. Rev.*, 2019, **378**, 87–103.
- 11 K. Adil, Y. Belmabkhout, R. S. Pillai, A. Cadiou, P. M. Bhatt, A. H. Assen, G. Maurin, M. Eddaoudi and K. Adil, Gas/vapour separation using ultra-microporous metal-organic frameworks: insights into the structure/separation relationship, *Chem. Soc. Rev.*, 2017, **46**, 3402–3430.
- 12 J.-R. Li, R. J. Kuppler, H.-C. Zhou and J.-R. Li, Selective gas adsorption and separation in metal-organic frameworks, *Chem. Soc. Rev.*, 2009, **38**, 1477–1504.
- 13 R.-B. Lin, S. Xiang, W. Zhou and B. Chen, Microporous Metal-Organic Framework Materials for Gas Separation, *Chem*, 2020, **6**, 337–363.
- 14 R.-B. Lin, Z. Zhang and B. Chen, Achieving High Performance Metal-Organic Framework Materials through Pore Engineering, *Acc. Chem. Res.*, 2021, **54**, 3362–3376.

- 15 H. Wang and J. Li, Microporous Metal-Organic Frameworks for Adsorptive Separation of C<sub>5</sub>-C<sub>6</sub> Alkane Isomers, *Acc. Chem. Res.*, 2019, **52**, 1968–1978.
- 16 H. Wang, Y. Liu and J. Li, Designer Metal-Organic Frameworks for Size-Exclusion-Based Hydrocarbon Separations: Progress and Challenges, *Adv. Mater.*, 2020, **32**, 2002603.
- 17 F. Xie, L. Yu, H. Wang and J. Li, Metal-Organic Frameworks for C<sub>6</sub> Alkane Separation, *Angew. Chem., Int. Ed.*, 2023, **62**, e202300722.
- 18 D.-D. Zhou and J.-P. Zhang, On the Role of Flexibility for Adsorptive Separation, *Acc. Chem. Res.*, 2022, **55**, 2966–2977.
- 19 J.-P. Zhang, Y.-B. Zhang, J.-B. Lin and X.-M. Chen, Metal Azolate Frameworks: From Crystal Engineering to Functional Materials, *Chem. Rev.*, 2011, **112**, 1001–1033.
- 20 Y. Wang and D. Zhao, Beyond Equilibrium: Metal-Organic Frameworks for Molecular Sieving and Kinetic Gas Separation, *Cryst. Growth Des.*, 2017, **17**, 2291–2308.
- 21 J.-P. Zhang, H.-L. Zhou, D.-D. Zhou, P.-Q. Liao and X.-M. Chen, Controlling flexibility of metal-organic frameworks, *Natl. Sci. Rev.*, 2018, **5**, 907–919.
- 22 I. Karakurt, G. Aydin and K. Aydiner, Mine ventilation air methane as a sustainable energy source, *Renewable Sustainable Energy Rev.*, 2011, **15**, 1042–1049.
- 23 Z. Niu, X. Cui, T. Pham, P. C. Lan, H. Xing, K. A. Forrest, L. Wojtas, B. Space and S. Ma, A Metal-Organic Framework Based Methane Nano-trap for the Capture of Coal-Mine Methane, *Angew. Chem., Int. Ed.*, 2019, **58**, 10138–10141.
- 24 S.-M. Wang, M. Shivanna and Q.-Y. Yang, Nickel-Based Metal-Organic Frameworks for Coal-Bed Methane Purification with Record CH<sub>4</sub>/N<sub>2</sub> Selectivity, *Angew. Chem., Int. Ed.*, 2022, **61**, e202201017.
- 25 T. Li, X. Jia, H. Chen, Z. Chang, L. Li, Y. Wang and J. Li, Tuning the Pore Environment of MOFs toward Efficient CH<sub>4</sub>/N<sub>2</sub> Separation under Humid Conditions, *ACS Appl. Mater. Interfaces*, 2022, **14**, 15830–15839.
- 26 M. Chang, Y. Zhao, D. Liu, J. Yang, J. Li and C. Zhong, Methane-trapping metal-organic frameworks with an aliphatic ligand for efficient CH<sub>4</sub>/N<sub>2</sub> separation, *Sustainable Energy Fuels*, 2019, **4**, 138–142.
- 27 X.-W. Zhang, D.-D. Zhou and J.-P. Zhang, Tuning the gating energy barrier of metal-organic framework for molecular sieving, *Chem*, 2021, **7**, 1006–1019.
- 28 Q. Min Wang, D. Shen, M. Bülow, M. Ling Lau, S. Deng, F. R. Fitch, N. O. Lemcoff and J. Semanscin, Metallo-organic molecular sieve for gas separation and purification, *Microporous Mesoporous Mater.*, 2002, **55**, 217–230.
- 29 Z. Bao, S. Alnemrat, L. Yu, I. Vasiliev, Q. Ren, X. Lu and S. Deng, Adsorption of Ethane, Ethylene, Propane, and Propylene on a Magnesium-Based Metal-Organic Framework, *Langmuir*, 2011, **27**, 13554–13562.
- 30 E. D. Bloch, W. L. Queen, R. Krishna, J. M. Zadrozny, C. M. Brown and J. R. Long, Hydrocarbon Separations in a Metal-Organic Framework with Open Iron(II) Coordination Sites, *Science*, 2012, **335**, 1606–1610.
- 31 S. J. Geier, J. A. Mason, E. D. Bloch, W. L. Queen, M. R. Hudson, C. M. Brown and J. R. Long, Selective adsorption of ethylene over ethane and propylene over propane in the metal-organic frameworks M<sub>2</sub>(dobdc) (M = Mg, Mn, Fe, Co, Ni, Zn), *Chem. Sci.*, 2013, **4**, 2054.
- 32 G. Chang, M. Huang, Y. Su, H. Xing, B. Su, Z. Zhang, Q. Yang, Y. Yang, Q. Ren, Z. Bao and B. Chen, Immobilization of Ag(I) into a metal-organic framework with –SO<sub>3</sub>H sites for highly selective olefin–paraffin separation at room temperature, *Chem. Commun.*, 2015, **51**, 2859–2862.
- 33 J. E. Bachman, M. T. Kapelewski, D. A. Reed, M. I. Gonzalez and J. R. Long, M<sub>2</sub>(m-dobdc) (M = Mn, Fe, Co, Ni) Metal-Organic Frameworks as Highly Selective, High-Capacity Adsorbents for Olefin/Paraffin Separations, *J. Am. Chem. Soc.*, 2017, **139**, 15363–15370.
- 34 S. Sen, N. Hosono, J.-J. Zheng, S. Kusaka, R. Matsuda, S. Sakaki and S. Kitagawa, Cooperative Bond Scission in a Soft Porous Crystal Enables Discriminatory Gate Opening for Ethylene over Ethane, *J. Am. Chem. Soc.*, 2017, **139**, 18313–18321.
- 35 R.-B. Lin, L. Li, H.-L. Zhou, H. Wu, C. He, S. Li, R. Krishna, J. Li, W. Zhou and B. Chen, Molecular sieving of ethylene from ethane using a rigid metal-organic framework, *Nat. Mater.*, 2018, **17**, 1128–1133.
- 36 Z. Bao, J. Wang, Z. Zhang, H. Xing, Q. Yang, Y. Yang, H. Wu, R. Krishna, W. Zhou, B. Chen and Q. Ren, Molecular Sieving of Ethane from Ethylene through the Molecular Cross-Section Size Differentiation in Gallate-based Metal-Organic Frameworks, *Angew. Chem., Int. Ed.*, 2018, **57**, 16020–16025.
- 37 C. Gu, N. Hosono, J.-J. Zheng, Y. Sato, S. Kusaka, S. Sakaki and S. Kitagawa, Design and control of gas diffusion process in a nanoporous soft crystal, *Science*, 2019, **363**, 387–391.
- 38 M. H. Mohamed, Y. Yang, L. Li, S. Zhang, J. P. Ruffley, A. G. Jarvi, S. Saxena, G. Veser, J. K. Johnson and N. L. Rosi, Designing Open Metal Sites in Metal-Organic Frameworks for Paraffin/Olefin Separations, *J. Am. Chem. Soc.*, 2019, **141**, 13003–13007.
- 39 Q. Ding, Z. Zhang, C. Yu, P. Zhang, J. Wang, X. Cui, C.-H. He, S. Deng and H. Xing, Exploiting equilibrium-kinetic synergetic effect for separation of ethylene and ethane in a microporous metal-organic framework, *Sci. Adv.*, 2020, **6**, eaaz4322.
- 40 C. Yu, Z. Guo, L. Yang, J. Cui, S. Chen, Y. Bo, X. Suo, Q. Gong, S. Zhang, X. Cui, S. He and H. Xing, A Robust Metal-Organic Framework with Scalable Synthesis and Optimal Adsorption and Desorption for Energy-Efficient Ethylene Purification, *Angew. Chem., Int. Ed.*, 2023, **62**, e202218027.
- 41 L. Zhang, L. Li, E. Hu, L. Yang, K. Shao, L. Yao, K. Jiang, Y. Cui, Y. Yang, B. Li, B. Chen and G. Qian, Boosting Ethylene/Ethane Separation within Copper(I)-Chelated Metal-Organic Frameworks through Tailor-Made Aperture and Specific  $\pi$ -Complexation, *Adv. Sci.*, 2020, **7**, 1901918.
- 42 P. J. Bereciartua, Á. Cantín, A. Corma, J. L. Jordá, M. Palomino, F. Rey, S. Valencia, E. W. Corcoran, P. Kortunov, P. I. Ravikovitch, A. Burton, C. Yoon,

- Y. Wang, C. Paur, J. Guzman, A. R. Bishop and G. L. Casty, Control of zeolite framework flexibility and pore topology for separation of ethane and ethylene, *Science*, 2017, **358**, 1068–1071.
- 43 B. Li, Y. Zhang, R. Krishna, K. Yao, Y. Han, Z. Wu, D. Ma, Z. Shi, T. Pham, B. Space, J. Liu, P. K. Thallapally, J. Liu, M. Chrzanowski and S. Ma, Introduction of  $\pi$ -Complexation into Porous Aromatic Framework for Highly Selective Adsorption of Ethylene over Ethane, *J. Am. Chem. Soc.*, 2014, **136**, 8654–8660.
- 44 Y. Yang, L. Li, R.-B. Lin, Y. Ye, Z. Yao, L. Yang, F. Xiang, S. Chen, Z. Zhang, S. Xiang and B. Chen, Ethylene/ethane separation in a stable hydrogen-bonded organic framework through a gating mechanism, *Nat. Chem.*, 2021, **13**, 933–939.
- 45 J. W. Yoon, Y.-K. Seo, Y. K. Hwang, J.-S. Chang, H. Leclerc, S. Wuttke, P. Bazin, A. Vimont, M. Daturi, E. Bloch, P. L. Llewellyn, C. Serre, P. Horcajada, J.-M. Grenèche, A. E. Rodrigues and G. Férey, Controlled Reducibility of a Metal-Organic Framework with Coordinatively Unsaturated Sites for Preferential Gas Sorption, *Angew. Chem., Int. Ed.*, 2010, **49**, 5949–5952.
- 46 C.-X. Chen, Z.-W. Wei, T. Pham, P. C. Lan, L. Zhang, K. A. Forrest, S. Chen, A. M. Al-Enizi, A. Nafady, C.-Y. Su and S. Ma, Nanospace Engineering of Metal-Organic Frameworks through Dynamic Spacer Installation of Multifunctionalities for Efficient Separation of Ethane from Ethane/Ethylene Mixtures, *Angew. Chem., Int. Ed.*, 2021, **60**, 9680–9685.
- 47 J. Pires, M. L. Pinto and V. K. Saini, Ethane Selective IRMOF-8 and Its Significance in Ethane–Ethylene Separation by Adsorption, *ACS Appl. Mater. Interfaces*, 2014, **6**, 12093–12099.
- 48 H. Yang, Y. Wang, R. Krishna, X. Jia, Y. Wang, A. N. Hong, C. Dang, H. E. Castillo, X. Bu and P. Feng, Pore-Space-Partition-Enabled Exceptional Ethane Uptake and Ethane-Selective Ethane–Ethylene Separation, *J. Am. Chem. Soc.*, 2020, **142**, 2222–2227.
- 49 Z. Y. Di, C. P. Liu, J. D. Pang, S. X. Zou, Z. Y. Ji, F. L. Hu, C. Chen, D. Q. Yuan, M. C. Hong and M. Y. Wu, A Metal-Organic Framework with Nonpolar Pore Surfaces for the One-Step Acquisition of  $C_2H_4$  from a  $C_2H_4$  and  $C_2H_6$  Mixture, *Angew. Chem., Int. Ed.*, 2022, **61**, e202210343.
- 50 S. Geng, E. Lin, X. Li, W. Liu, T. Wang, Z. Wang, D. Sensharma, S. Darwish, Y. H. Andaloussi, T. Pham, P. Cheng, M. J. Zaworotko, Y. Chen and Z. Zhang, Scalable Room-Temperature Synthesis of Highly Robust Ethane-Selective Metal-Organic Frameworks for Efficient Ethylene Purification, *J. Am. Chem. Soc.*, 2021, **143**, 8654–8660.
- 51 M. Kang, S. Yoon, S. Ga, D. W. Kang, S. Han, J. H. Choe, H. Kim, D. W. Kim, Y. G. Chung and C. S. Hong, High-Throughput Discovery of  $Ni(IN)_2$  for Ethane/Ethylene Separation, *Adv. Sci.*, 2021, **8**, 2004940.
- 52 Y.-P. Li, Y.-N. Zhao, S.-N. Li, D.-Q. Yuan, Y.-C. Jiang, X. Bu, M.-C. Hu and Q.-G. Zhai, Ultrahigh-Uptake Capacity-Enabled Gas Separation and Fruit Preservation by a New Single-Walled Nickel-Organic Framework, *Adv. Sci.*, 2021, **8**, 2003141.
- 53 W. Liu, S. Geng, N. Li, S. Wang, S. Jia, F. Jin, T. Wang, K. A. Forrest, T. Pham, P. Cheng, Y. Chen, J.-G. Ma and Z. Zhang, Highly Robust Microporous Metal-Organic Frameworks for Efficient Ethylene Purification under Dry and Humid Conditions, *Angew. Chem., Int. Ed.*, 2023, **62**, e202217662.
- 54 A. A. Lysova, D. G. Samsonenko, K. A. Kovalenko, A. S. Nizovtsev, D. N. Dybtsev and V. P. Fedin, A Series of Mesoporous Metal-Organic Frameworks with Tunable Windows Sizes and Exceptionally High Ethane over Ethylene Adsorption Selectivity, *Angew. Chem., Int. Ed.*, 2020, **59**, 20561–20567.
- 55 J. Pei, J.-X. Wang, K. Shao, Y. Yang, Y. Cui, H. Wu, W. Zhou, B. Li and G. Qian, Engineering microporous ethane-trapping metal-organic frameworks for boosting ethane/ethylene separation, *J. Mater. Chem. A*, 2020, **8**, 3613–3620.
- 56 O. T. Qazvini, R. Babarao, Z.-L. Shi, Y.-B. Zhang and S. G. Telfer, A Robust Ethane-Trapping Metal-Organic Framework with a High Capacity for Ethylene Purification, *J. Am. Chem. Soc.*, 2019, **141**, 5014–5020.
- 57 Y. Ye, Y. Xie, Y. Shi, L. Gong, J. Phipps, A. M. Al-Enizi, A. Nafady, B. Chen and S. Ma, A Microporous Metal-Organic Framework with Unique Aromatic Pore Surfaces for High Performance  $C_2H_6/C_2H_4$  Separation, *Angew. Chem., Int. Ed.*, 2023, **62**, e202302564.
- 58 C. Gücüyener, J. van den Bergh, J. Gascon and F. Kapteijn, Ethane/Ethene Separation Turned on Its Head: Selective Ethane Adsorption on the Metal-Organic Framework ZIF-7 through a Gate-Opening Mechanism, *J. Am. Chem. Soc.*, 2010, **132**, 17704–17706.
- 59 P.-Q. Liao, W.-X. Zhang, J.-P. Zhang and X.-M. Chen, Efficient purification of ethene by an ethane-trapping metal-organic framework, *Nat. Commun.*, 2015, **6**, 8697.
- 60 R.-B. Lin, H. Wu, L. Li, X.-L. Tang, Z. Li, J. Gao, H. Cui, W. Zhou and B. Chen, Boosting Ethane/Ethylene Separation within Isoreticular Ultramicroporous Metal-Organic Frameworks, *J. Am. Chem. Soc.*, 2018, **140**, 12940–12946.
- 61 L. Li, R.-B. Lin, R. Krishna, H. Li, S. Xiang, H. Wu, J. Li, W. Zhou and B. Chen, Ethane/ethylene separation in a metal-organic framework with iron-peroxo sites, *Science*, 2018, **362**, 443–446.
- 62 S. Jiang, J. Li, M. Feng, R. Chen, L. Guo, Q. Xu, L. Chen, F. Shen, Z. Zhang, Y. Yang, Q. Ren, Q. Yang and Z. Bao, Hydrophobic paraffin-selective pillared-layer MOFs for olefin purification, *J. Mater. Chem. A*, 2022, **10**, 24127–24136.
- 63 G. D. Wang, R. Krishna, Y. Z. Li, W. J. Shi, L. Hou, Y. Y. Wang and Z. H. Zhu, Boosting Ethane/Ethylene Separation by MOFs through the Amino-Functionalization of Pores, *Angew. Chem., Int. Ed.*, 2022, **61**, e202213015.
- 64 L. Yang, L. Yan, W. Niu, Y. Feng, Q. Fu, S. Zhang, Y. Zhang, L. Li, X. Gu, P. Dai, D. Liu, Q. Zheng and X. Zhao, Adsorption in Reversed Order of  $C_2$  Hydrocarbons on an Ultramicroporous Fluorinated Metal-Organic Framework, *Angew. Chem., Int. Ed.*, 2022, **61**, e202204046.
- 65 M. H. Yu, H. Fang, H. L. Huang, M. Zhao, Z. Y. Su, H. X. Nie, Z. Chang and T. L. Hu, Tuning the Trade-Off

- between Ethane/Ethylene Selectivity and Adsorption Capacity within Isorecticular Microporous Metal-Organic Frameworks by Linker Fine-Fluorination, *Small*, 2023, **19**, 2300821.
- 66 H. Zeng, X.-J. Xie, M. Xie, Y.-L. Huang, D. Luo, T. Wang, Y. Zhao, W. Lu and D. Li, Cage-Interconnected Metal-Organic Framework with Tailored Apertures for Efficient C<sub>2</sub>H<sub>6</sub>/C<sub>2</sub>H<sub>4</sub> Separation under Humid Conditions, *J. Am. Chem. Soc.*, 2019, **141**, 20390–20396.
- 67 S.-C. Xiang, Z. Zhang, C.-G. Zhao, K. Hong, X. Zhao, D.-R. Ding, M.-H. Xie, C.-D. Wu, M. C. Das, R. Gill, K. M. Thomas and B. Chen, Rationally tuned micropores within enantiopure metal-organic frameworks for highly selective separation of acetylene and ethylene, *Nat. Commun.*, 2011, **2**, 204.
- 68 T.-L. Hu, H. Wang, B. Li, R. Krishna, H. Wu, W. Zhou, Y. Zhao, Y. Han, X. Wang, W. Zhu, Z. Yao, S. Xiang and B. Chen, Microporous metal-organic framework with dual functionalities for highly efficient removal of acetylene from ethylene/acetylene mixtures, *Nat. Commun.*, 2015, **6**, 7328.
- 69 S. Yang, A. J. Ramirez-Cuesta, R. Newby, V. Garcia-Sakai, P. Manuel, S. K. Callear, S. I. Campbell, C. C. Tang and M. Schröder, Supramolecular binding and separation of hydrocarbons within a functionalized porous metal-organic framework, *Nat. Chem.*, 2015, **7**, 121–129.
- 70 X. Cui, K. Chen, H. Xing, Q. Yang, R. Krishna, Z. Bao, H. Wu, W. Zhou, X. Dong, Y. Han, B. Li, Q. Ren, M. J. Zaworotko and B. Chen, Pore chemistry and size control in hybrid porous materials for acetylene capture from ethylene, *Science*, 2016, **353**, 141–144.
- 71 B. Li, X. Cui, D. O’Nolan, H.-M. Wen, M. Jiang, R. Krishna, H. Wu, R.-B. Lin, Y.-S. Chen, D. Yuan, H. Xing, W. Zhou, Q. Ren, G. Qian, M. J. Zaworotko and B. Chen, An Ideal Molecular Sieve for Acetylene Removal from Ethylene with Record Selectivity and Productivity, *Adv. Mater.*, 2017, **29**, 1704210.
- 72 R.-B. Lin, L. Li, H. Wu, H. Arman, B. Li, R.-G. Lin, W. Zhou and B. Chen, Optimized Separation of Acetylene from Carbon Dioxide and Ethylene in a Microporous Material, *J. Am. Chem. Soc.*, 2017, **139**, 8022–8028.
- 73 T. Ke, Q. Wang, J. Shen, J. Zhou, Z. Bao, Q. Yang and Q. Ren, Molecular Sieving of C<sub>2</sub>-C<sub>3</sub> Alkene from Alkyne with Tuned Threshold Pressure in Robust Layered Metal-Organic Frameworks, *Angew. Chem., Int. Ed.*, 2020, **59**, 12725–12730.
- 74 S. Mukherjee, S. Chen, A. A. Bezrukov, M. Mostrom, V. V. Terskikh, D. Franz, S.-Q. Wang, A. Kumar, M. Chen, B. Space, Y. Huang and M. J. Zaworotko, Ultramicropore Engineering by Dehydration to Enable Molecular Sieving of H<sub>2</sub> by Calcium Trimesate, *Angew. Chem., Int. Ed.*, 2020, **59**, 16188–16194.
- 75 J. Shen, X. He, T. Ke, R. Krishna, J. M. van Baten, R. Chen, Z. Bao, H. Xing, M. Dincă, Z. Zhang, Q. Yang and Q. Ren, Simultaneous interlayer and intralayer space control in two-dimensional metal-organic frameworks for acetylene/ethylene separation, *Nat. Commun.*, 2020, **11**, 6259.
- 76 J. Wang, Y. Zhang, P. Zhang, J. Hu, R.-B. Lin, Q. Deng, Z. Zeng, H. Xing, S. Deng and B. Chen, Optimizing Pore Space for Flexible-Robust Metal-Organic Framework to Boost Trace Acetylene Removal, *J. Am. Chem. Soc.*, 2020, **142**, 9744–9751.
- 77 Z. Zhang, S. B. Peh, Y. Wang, C. Kang, W. Fan and D. Zhao, Efficient Trapping of Trace Acetylene from Ethylene in an Ultramicroporous Metal-Organic Framework: Synergistic Effect of High-Density Open Metal and Electronegative Sites, *Angew. Chem., Int. Ed.*, 2020, **59**, 18927–18932.
- 78 J.-W. Wang, S.-C. Fan, H.-P. Li, X. Bu, Y.-Y. Xue and Q.-G. Zhai, De-Linker-Enabled Exceptional Volumetric Acetylene Storage Capacity and Benchmark C<sub>2</sub>H<sub>2</sub>/C<sub>2</sub>H<sub>4</sub> and C<sub>2</sub>H<sub>2</sub>/CO<sub>2</sub> Separations in Metal-Organic Frameworks, *Angew. Chem., Int. Ed.*, 2023, **62**, e202217839.
- 79 H.-G. Hao, Y.-F. Zhao, D.-M. Chen, J.-M. Yu, K. Tan, S. Ma, Y. Chabal, Z.-M. Zhang, J.-M. Dou, Z.-H. Xiao, G. Day, H.-C. Zhou and T.-B. Lu, Simultaneous Trapping of C<sub>2</sub>H<sub>2</sub> and C<sub>2</sub>H<sub>6</sub> from a Ternary Mixture of C<sub>2</sub>H<sub>2</sub>/C<sub>2</sub>H<sub>4</sub>/C<sub>2</sub>H<sub>6</sub> in a Robust Metal-Organic Framework for the Purification of C<sub>2</sub>H<sub>4</sub>, *Angew. Chem., Int. Ed.*, 2018, **57**, 16067–16071.
- 80 K.-J. Chen, D. G. Madden, S. Mukherjee, T. Pham, K. A. Forrest, A. Kumar, B. Space, J. Kong, Q.-Y. Zhang and M. J. Zaworotko, Synergistic sorbent separation for one-step ethylene purification from a four-component mixture, *Science*, 2019, **366**, 241–246.
- 81 Q. Dong, X. Zhang, S. Liu, R.-B. Lin, Y. Guo, Y. Ma, A. Yonezu, R. Krishna, G. Liu, J. Duan, R. Matsuda, W. Jin and B. Chen, Tuning Gate-Opening of a Flexible Metal-Organic Framework for Ternary Gas Sieving Separation, *Angew. Chem., Int. Ed.*, 2020, **59**, 22756–22762.
- 82 Z. Xu, X. Xiong, J. Xiong, R. Krishna, L. Li, Y. Fan, F. Luo and B. Chen, A robust Th-azole framework for highly efficient purification of C<sub>2</sub>H<sub>4</sub> from a C<sub>2</sub>H<sub>4</sub>/C<sub>2</sub>H<sub>2</sub>/C<sub>2</sub>H<sub>6</sub> mixture, *Nat. Commun.*, 2020, **11**, 3163.
- 83 J.-W. Cao, S. Mukherjee, T. Pham, Y. Wang, T. Wang, T. Zhang, X. Jiang, H.-J. Tang, K. A. Forrest, B. Space, M. J. Zaworotko and K.-J. Chen, One-step ethylene production from a four-component gas mixture by a single physisorbent, *Nat. Commun.*, 2021, **12**, 6507.
- 84 S. Mukherjee, N. Kumar, A. A. Bezrukov, K. Tan, T. Pham, K. A. Forrest, K. A. Oyekan, O. T. Qazvini, D. G. Madden, B. Space and M. J. Zaworotko, Amino-Functionalised Hybrid Ultramicroporous Materials that Enable Single-Step Ethylene Purification from a Ternary Mixture, *Angew. Chem., Int. Ed.*, 2021, **60**, 10902–10909.
- 85 Y. Wang, C. Hao, W. Fan, M. Fu, X. Wang, Z. Wang, L. Zhu, Y. Li, X. Lu, F. Dai, Z. Kang, R. Wang, W. Guo, S. Hu and D. Sun, One-step Ethylene Purification from an Acetylene/Ethylene/Ethane Ternary Mixture by Cyclopentadiene Cobalt-Functionalized Metal-Organic Frameworks, *Angew. Chem., Int. Ed.*, 2021, **60**, 11350–11358.
- 86 B. Zhu, J. W. Cao, S. Mukherjee, T. Pham, T. Zhang, T. Wang, X. Jiang, K. A. Forrest, M. J. Zaworotko and K. J. Chen, Pore Engineering for One-Step Ethylene Purification from a Three-Component Hydrocarbon Mixture, *J. Am. Chem. Soc.*, 2021, **143**, 1485–1492.

- 87 Q. Ding, Z. Zhang, Y. Liu, K. Chai, R. Krishna and S. Zhang, One-Step Ethylene Purification from Ternary Mixtures in a Metal-Organic Framework with Customized Pore Chemistry and Shape, *Angew. Chem., Int. Ed.*, 2022, **61**, e202208134.
- 88 X. W. Gu, J. X. Wang, E. Wu, H. Wu, W. Zhou, G. Qian, B. Chen and B. Li, Immobilization of Lewis Basic Sites into a Stable Ethane-Selective MOF Enabling One-Step Separation of Ethylene from a Ternary Mixture, *J. Am. Chem. Soc.*, 2022, **144**, 2614–2623.
- 89 G. D. Wang, Y. Z. Li, W. J. Shi, L. Hou, Y. Y. Wang and Z. Zhu, One-Step  $C_2H_4$  Purification from Ternary  $C_2H_6/C_2H_4/C_2H_2$  Mixtures by a Robust Metal-Organic Framework with Customized Pore Environment, *Angew. Chem., Int. Ed.*, 2022, **61**, e202205427.
- 90 Y. Wang, M. Fu, S. Zhou, H. Liu, X. Wang, W. Fan, Z. Liu, Z. Wang, D. Li, H. Hao, X. Lu, S. Hu and D. Sun, Guest-molecule-induced self-adaptive pore engineering facilitates purification of ethylene from ternary mixture, *Chem*, 2022, **8**, 3263–3274.
- 91 P. Zhang, Y. Zhong, Y. Zhang, Z. Zhu, Y. Liu, Y. Su, J. Chen, S. Chen, Z. Zeng, H. Xing, S. Deng and J. Wang, Synergistic binding sites in a hybrid ultramicroporous material for one-step ethylene purification from ternary  $C_2$  hydrocarbon mixtures, *Sci. Adv.*, 2022, **8**, eabn9231.
- 92 Y. Jiang, Y. Hu, B. Luan, L. Wang, R. Krishna, H. Ni, X. Hu and Y. Zhang, Benchmark single-step ethylene purification from ternary mixtures by a customized fluorinated anion-embedded MOF, *Nat. Commun.*, 2023, **14**, 401.
- 93 H. Sun, F. Chen, R. Chen, J. Li, L. Guo, Y. Liu, F. Shen, Q. Yang, Z. Zhang, Q. Ren and Z. Bao, Customizing Metal-Organic Frameworks by Lego-Brick Strategy for One-Step Purification of Ethylene from a Quaternary Gas Mixture, *Small*, 2023, **19**, e2208182.
- 94 L. Wang, H. Huang, X. Zhang, H. Zhao, F. Li and Y. Gu, Designed metal-organic frameworks with potential for multi-component hydrocarbon separation, *Coord. Chem. Rev.*, 2023, **484**, 215111.
- 95 J.-P. Zhang and X.-M. Chen, Optimized Acetylene/Carbon Dioxide Sorption in a Dynamic Porous Crystal, *J. Am. Chem. Soc.*, 2009, **131**, 5516–5521.
- 96 C.-T. He, Z.-M. Ye, Y.-T. Xu, D.-D. Zhou, H.-L. Zhou, D. Chen, J.-P. Zhang and X.-M. Chen, Hyperfine adjustment of flexible pore-surface pockets enables smart recognition of gas size and quadrupole moment, *Chem. Sci.*, 2017, **8**, 7560–7565.
- 97 X. Liu, P. Zhang, H. Xiong, Y. Zhang, K. Wu, J. Liu, R. Krishna, J. Chen, S. Chen, Z. Zeng, S. Deng and J. Wang, Engineering Pore Environments of Sulfate-pillared Metal-Organic Framework for Efficient  $C_2H_2/CO_2$  Separation with Record Selectivity, *Adv. Mater.*, 2023, **35**, 2210415.
- 98 X. Zhu, T. Ke, J. Zhou, Y. Song, Q. Xu, Z. Zhang, Z. Bao, Y. Yang, Q. Ren and Q. Yang, Vertex Strategy in Layered 2D MOFs: Simultaneous Improvement of Thermodynamics and Kinetics for Record  $C_2H_2/CO_2$  Separation Performance, *J. Am. Chem. Soc.*, 2023, **145**, 9254–9263.
- 99 R. Matsuda, R. Kitaura, S. Kitagawa, Y. Kubota, R. V. Belosludov, T. C. Kobayashi, H. Sakamoto, T. Chiba, M. Takata, Y. Kawazoe and Y. Mita, Highly controlled acetylene accommodation in a metal-organic microporous material, *Nature*, 2005, **436**, 238–241.
- 100 J. Gao, X. Qian, R.-B. Lin, R. Krishna, H. Wu, W. Zhou and B. Chen, Mixed Metal-Organic Framework with Multiple Binding Sites for Efficient  $C_2H_2/CO_2$  Separation, *Angew. Chem., Int. Ed.*, 2020, **59**, 4396–4400.
- 101 F. Luo, C. Yan, L. Dang, R. Krishna, W. Zhou, H. Wu, X. Dong, Y. Han, T.-L. Hu, M. O’Keeffe, L. Wang, M. Luo, R.-B. Lin and B. Chen, UTSA-74: A MOF-74 Isomer with Two Accessible Binding Sites per Metal Center for Highly Selective Gas Separation, *J. Am. Chem. Soc.*, 2016, **138**, 5678–5684.
- 102 Z. Niu, X. Cui, T. Pham, G. Verma, P. C. Lan, C. Shan, H. Xing, K. A. Forrest, S. Suepaul, B. Space, A. Nafady, A. M. Al-Enizi and S. Ma, A MOF-based Ultra-Strong Acetylene Nano-trap for Highly Efficient  $C_2H_2/CO_2$  Separation, *Angew. Chem., Int. Ed.*, 2021, **60**, 5283–5288.
- 103 J. Pei, K. Shao, J.-X. Wang, H.-M. Wen, Y. Yang, Y. Cui, R. Krishna, B. Li and G. Qian, A Chemically Stable Hofmann-Type Metal-Organic Framework with Sandwich-Like Binding Sites for Benchmark Acetylene Capture, *Adv. Mater.*, 2020, **32**, 1908275.
- 104 Y.-L. Peng, T. Pham, P. Li, T. Wang, Y. Chen, K.-J. Chen, K. A. Forrest, B. Space, P. Cheng, M. J. Zaworotko and Z. Zhang, Robust Ultramicroporous Metal-Organic Frameworks with Benchmark Affinity for Acetylene, *Angew. Chem., Int. Ed.*, 2018, **57**, 10971–10975.
- 105 K. Shao, H.-M. Wen, C.-C. Liang, X. Xiao, X.-W. Gu, B. Chen, G. Qian and B. Li, Engineering Supramolecular Binding Sites in a Chemically Stable Metal-Organic Framework for Simultaneous High  $C_2H_2$  Storage and Separation, *Angew. Chem., Int. Ed.*, 2022, **61**, e202211523.
- 106 H. Zeng, M. Xie, Y.-L. Huang, Y. Zhao, X.-J. Xie, J.-P. Bai, M.-Y. Wan, R. Krishna, W. Lu and D. Li, Induced Fit of  $C_2H_2$  in a Flexible MOF Through Cooperative Action of Open Metal Sites, *Angew. Chem., Int. Ed.*, 2019, **58**, 8515–8519.
- 107 L. Zhang, K. Jiang, L. Yang, L. Li, E. Hu, L. Yang, K. Shao, H. Xing, Y. Cui, Y. Yang, B. Li, B. Chen and G. Qian, Benchmark  $C_2H_2/CO_2$  Separation in an Ultra-Microporous Metal-Organic Framework via Copper(I)-Alkynyl Chemistry, *Angew. Chem., Int. Ed.*, 2021, **60**, 15995–16002.
- 108 H. Zeng, X.-J. Xie, Y. Wang, D. Luo, R.-J. Wei, W. Lu and D. Li, Spatial disposition of square-planar mononuclear nodes in metal-organic frameworks for  $C_2H_2/CO_2$  separation, *Chem. Sci.*, 2022, **13**, 12876–12882.
- 109 S. R. Caskey, A. G. Wong-Foy and A. J. Matzger, Dramatic Tuning of Carbon Dioxide Uptake via Metal Substitution in a Coordination Polymer with Cylindrical Pores, *J. Am. Chem. Soc.*, 2008, **130**, 10870–10871.
- 110 M. Fischer, F. Hoffmann and M. Fröba, New Microporous Materials for Acetylene Storage and  $C_2H_2/CO_2$  Separation: Insights from Molecular Simulations, *ChemPhysChem*, 2010, **11**, 2220–2229.

- 111 S. Xiang, W. Zhou, J. M. Gallegos, Y. Liu and B. Chen, Exceptionally high acetylene uptake in a microporous metal-organic framework with open metal sites, *J. Am. Chem. Soc.*, 2009, **131**, 12415–12419.
- 112 Y.-P. Li, Y. Wang, Y.-Y. Xue, H.-P. Li, Q.-G. Zhai, S.-N. Li, Y.-C. Jiang, M.-C. Hu and X. Bu, Ultramicroporous Building Units as a Path to Bi-microporous Metal-Organic Frameworks with High Acetylene Storage and Separation Performance, *Angew. Chem., Int. Ed.*, 2019, **58**, 13590–13595.
- 113 W. Fan, S. Yuan, W. Wang, L. Feng, X. Liu, X. Zhang, X. Wang, Z. Kang, F. Dai, D. Yuan, D. Sun and H.-C. Zhou, Optimizing Multivariate Metal-Organic Frameworks for Efficient C<sub>2</sub>H<sub>2</sub>/CO<sub>2</sub> Separation, *J. Am. Chem. Soc.*, 2020, **142**, 8728–8737.
- 114 L. Yang, L. Yan, Y. Wang, Z. Liu, J. He, Q. Fu, D. Liu, X. Gu, P. Dai, L. Li and X. Zhao, Adsorption Site Selective Occupation Strategy within a Metal-Organic Framework for Highly Efficient Sieving Acetylene from Carbon Dioxide, *Angew. Chem., Int. Ed.*, 2021, **60**, 4570–4574.
- 115 J. Pei, H.-M. Wen, X.-W. Gu, Q.-L. Qian, Y. Yang, Y. Cui, B. Li, B. Chen and G. Qian, Dense Packing of Acetylene in a Stable and Low-Cost Metal-Organic Framework for Efficient C<sub>2</sub>H<sub>2</sub>/CO<sub>2</sub> Separation, *Angew. Chem., Int. Ed.*, 2021, **60**, 25068–25074.
- 116 X. Zhang, R.-B. Lin, H. Wu, Y. Huang, Y. Ye, J. Duan, W. Zhou, J.-R. Li and B. Chen, Maximizing acetylene packing density for highly efficient C<sub>2</sub>H<sub>2</sub>/CO<sub>2</sub> separation through immobilization of amine sites within a prototype MOF, *Chem. Eng. J.*, 2022, **431**, 134184.
- 117 Z. Di, C. Liu, J. Pang, C. Chen, F. Hu, D. Yuan, M. Wu and M. Hong, Cage-Like Porous Materials with Simultaneous High C<sub>2</sub>H<sub>2</sub> Storage and Excellent C<sub>2</sub>H<sub>2</sub>/CO<sub>2</sub> Separation Performance, *Angew. Chem., Int. Ed.*, 2021, **60**, 10828–10832.
- 118 W. Gong, H. Cui, Y. Xie, Y. Li, X. Tang, Y. Liu, Y. Cui and B. Chen, Efficient C<sub>2</sub>H<sub>2</sub>/CO<sub>2</sub> Separation in Ultramicroporous Metal-Organic Frameworks with Record C<sub>2</sub>H<sub>2</sub> Storage Density, *J. Am. Chem. Soc.*, 2021, **143**, 14869–14876.
- 119 J. Lee, C. Y. Chuah, J. Kim, Y. Kim, N. Ko, Y. Seo, K. Kim, T. H. Bae and E. Lee, Separation of Acetylene from Carbon Dioxide and Ethylene by a Water-Stable Microporous Metal-Organic Framework with Aligned Imidazolium Groups inside the Channels, *Angew. Chem., Int. Ed.*, 2018, **57**, 7869–7873.
- 120 L. Liu, Z. Yao, Y. Ye, Y. Yang, Q. Lin, Z. Zhang, M. O’Keeffe and S. Xiang, Integrating the Pillared-Layer Strategy and Pore-Space Partition Method to Construct Multicomponent MOFs for C<sub>2</sub>H<sub>2</sub>/CO<sub>2</sub> Separation, *J. Am. Chem. Soc.*, 2020, **142**, 9258–9266.
- 121 L. Wang, W. Sun, Y. Zhang, N. Xu, R. Krishna, J. Hu, Y. Jiang, Y. He and H. Xing, Interpenetration Symmetry Control Within Ultramicroporous Robust Boron Cluster Hybrid MOFs for Benchmark Purification of Acetylene from Carbon Dioxide, *Angew. Chem., Int. Ed.*, 2021, **60**, 22865–22870.
- 122 Y. Ye, Z. Ma, R.-B. Lin, R. Krishna, W. Zhou, Q. Lin, Z. Zhang, S. Xiang and B. Chen, Pore Space Partition within a Metal-Organic Framework for Highly Efficient C<sub>2</sub>H<sub>2</sub>/CO<sub>2</sub> Separation, *J. Am. Chem. Soc.*, 2019, **141**, 4130–4136.
- 123 Y. Ye, S. Xian, H. Cui, K. Tan, L. Gong, B. Liang, T. Pham, H. Pandey, R. Krishna, P. C. Lan, K. A. Forrest, B. Space, T. Thonhauser, J. Li and S. Ma, Metal-Organic Framework Based Hydrogen-Bonding Nanotrap for Efficient Acetylene Storage and Separation, *J. Am. Chem. Soc.*, 2022, **144**, 1681–1689.
- 124 Q.-G. Zhai, X. Bu, X. Zhao, D.-S. Li and P. Feng, Pore Space Partition in Metal-Organic Frameworks, *Acc. Chem. Res.*, 2017, **50**, 407–417.
- 125 J. Wang, Y. Zhang, Y. Su, X. Liu, P. Zhang, R.-B. Lin, S. Chen, Q. Deng, Z. Zeng, S. Deng and B. Chen, Fine pore engineering in a series of isoreticular metal-organic frameworks for efficient C<sub>2</sub>H<sub>2</sub>/CO<sub>2</sub> separation, *Nat. Commun.*, 2022, **13**, 200.
- 126 M. Shivanna, K.-i Otake, B.-Q. Song, L. M. van Wyk, Q.-Y. Yang, N. Kumar, W. K. Feldmann, T. Pham, S. Suepaul, B. Space, L. J. Barbour, S. Kitagawa and M. J. Zaworotko, Benchmark Acetylene Binding Affinity and Separation through Induced Fit in a Flexible Hybrid Ultramicroporous Material, *Angew. Chem., Int. Ed.*, 2021, **60**, 20383–20390.
- 127 J. Tian, Q. Chen, F. Jiang, D. Yuan and M. Hong, Optimizing Acetylene Sorption through Induced-fit Transformations in a Chemically Stable Microporous Framework, *Angew. Chem., Int. Ed.*, 2023, **62**, e202215253.
- 128 D. Sensharma, D. J. O’Hearn, A. Koochaki, A. A. Bezrukov, N. Kumar, B. H. Wilson, M. Vandichel and M. J. Zaworotko, The First Sulfate-Pillared Hybrid Ultramicroporous Material, SOFOUR-1-Zn, and Its Acetylene Capture Properties, *Angew. Chem., Int. Ed.*, 2022, **61**, e202116145.
- 129 L.-Z. Cai, Z.-Z. Yao, S.-J. Lin, M.-S. Wang and G.-C. Guo, Photoinduced Electron-Transfer (PIET) Strategy for Selective Adsorption of CO<sub>2</sub> over C<sub>2</sub>H<sub>2</sub> in a MOF, *Angew. Chem., Int. Ed.*, 2021, **60**, 18223–18230.
- 130 K.-J. Chen, H. S. Scott, D. G. Madden, T. Pham, A. Kumar, A. Bajpai, M. Lusi, K. A. Forrest, B. Space, J. J. Perry and M. J. Zaworotko, Benchmark C<sub>2</sub>H<sub>2</sub>/CO<sub>2</sub> and CO<sub>2</sub>/C<sub>2</sub>H<sub>2</sub> Separation by Two Closely Related Hybrid Ultramicroporous Materials, *Chem*, 2016, **1**, 753–765.
- 131 D. S. Choi, D. W. Kim, D. W. Kang, M. Kang, Y. S. Chae and C. S. Hong, Highly selective CO<sub>2</sub> separation from a CO<sub>2</sub>/C<sub>2</sub>H<sub>2</sub> mixture using a diamine-appended metal-organic framework, *J. Mater. Chem. A*, 2021, **9**, 21424–21428.
- 132 J. Cui, Z. Qiu, L. Yang, Z. Zhang, X. Cui and H. Xing, Kinetic-Sieving of Carbon Dioxide from Acetylene through a Novel Sulfonic Ultramicroporous Material, *Angew. Chem., Int. Ed.*, 2022, **61**, e202208756.
- 133 M. L. Foo, R. Matsuda, Y. Hijikata, R. Krishna, H. Sato, S. Horike, A. Hori, J. Duan, Y. Sato, Y. Kubota, M. Takata and S. Kitagawa, An Adsorbate Discriminatory Gate Effect in a Flexible Porous Coordination Polymer for Selective Adsorption of CO<sub>2</sub> over C<sub>2</sub>H<sub>2</sub>, *J. Am. Chem. Soc.*, 2016, **138**, 3022–3030.
- 134 Y. Gu, J.-J. Zheng, K.-I. Otake, M. Shivanna, S. Sakaki, H. Yoshino, M. Ohba, S. Kawaguchi, Y. Wang, F. Li and

- S. Kitagawa, Host-Guest Interaction Modulation in Porous Coordination Polymers for Inverse Selective CO<sub>2</sub>/C<sub>2</sub>H<sub>2</sub> Separation, *Angew. Chem., Int. Ed.*, 2021, **60**, 11688–11694.
- 135 C. Hao, H. Ren, H. Zhu, Y. Chi, W. Zhao, X. Liu and W. Guo, CO<sub>2</sub>-favored metal-organic frameworks SU-101(M) (M = Bi, In, Ga, and Al) with inverse and high selectivity of CO<sub>2</sub> from C<sub>2</sub>H<sub>2</sub> and C<sub>2</sub>H<sub>4</sub>, *Sep. Purif. Technol.*, 2022, **290**, 120804.
- 136 C. He, P. Zhang, Y. Wang, Y. Zhang, T. Hu, L. Li and J. Li, Thermodynamic and kinetic synergetic separation of CO<sub>2</sub>/C<sub>2</sub>H<sub>2</sub> in an ultramicroporous metal-organic framework, *Sep. Purif. Technol.*, 2023, **304**, 122318.
- 137 L. Li, J. Wang, Z. Zhang, Q. Yang, Y. Yang, B. Su, Z. Bao and Q. Ren, Inverse Adsorption Separation of CO<sub>2</sub>/C<sub>2</sub>H<sub>2</sub> Mixture in Cyclodextrin-Based Metal-Organic Frameworks, *ACS Appl. Mater. Interfaces*, 2019, **11**, 2543–2550.
- 138 X.-Y. Li, Y. Song, C.-X. Zhang, C.-X. Zhao and C. He, Inverse CO<sub>2</sub>/C<sub>2</sub>H<sub>2</sub> separation in a pillared-layer framework featuring a chlorine-modified channel by quadrupole-moment sieving, *Sep. Purif. Technol.*, 2021, **279**, 119608.
- 139 Q. Liu, S. G. Cho, J. Hilliard, T.-Y. Wang, S.-C. Chien, L.-C. Lin, A. C. Co and C. R. Wade, Inverse CO<sub>2</sub>/C<sub>2</sub>H<sub>2</sub> Separation with MFU-4 and Selectivity Reversal via Postsynthetic Ligand Exchange, *Angew. Chem., Int. Ed.*, 2023, **62**, e202218854.
- 140 B. Ma, D. Li, Q. Zhu, Y. Li, W. Ueda and Z. Zhang, A Zeolitic Octahedral Metal Oxide with Ultra-Microporosity for Inverse CO<sub>2</sub>/C<sub>2</sub>H<sub>2</sub> Separation at High Temperature and Humidity, *Angew. Chem., Int. Ed.*, 2022, **61**, e202209121.
- 141 D. Ma, Z. Li, J. Zhu, Y. Zhou, L. Chen, X. Mai, M. Liufu, Y. Wu and Y. Li, Inverse and highly selective separation of CO<sub>2</sub>/C<sub>2</sub>H<sub>2</sub> on a thulium-organic framework, *J. Mater. Chem. A*, 2020, **8**, 11933–11937.
- 142 O. T. Qazvini, R. Babarao and S. G. Telfer, Selective capture of carbon dioxide from hydrocarbons using a metal-organic framework, *Nat. Commun.*, 2021, **12**, 197.
- 143 Y. Shi, Y. Xie, H. Cui, Y. Ye, H. Wu, W. Zhou, H. Arman, R.-B. Lin and B. Chen, Highly Selective Adsorption of Carbon Dioxide over Acetylene in an Ultramicroporous Metal-Organic Framework, *Adv. Mater.*, 2021, **33**, 2105880.
- 144 Y. Xie, H. Cui, H. Wu, R.-B. Lin, W. Zhou and B. Chen, Electrostatically Driven Selective Adsorption of Carbon Dioxide over Acetylene in an Ultramicroporous Material, *Angew. Chem., Int. Ed.*, 2021, **60**, 9604–9609.
- 145 J. Yang, M. Tong, G. Han, M. Chang, T. Yan, Y. Ying, Q. Yang and D. Liu, Solubility-Boosted Molecular Sieving-Based Separation for Purification of Acetylene in Core-Shell IL@MOF Composites, *Adv. Funct. Mater.*, 2023, **33**, 2213743.
- 146 J. Yu, J. Zhang, P. Zhang, Y. Wang, S.-N. Li and Q.-G. Zhai, Controllable inverse C<sub>2</sub>H<sub>2</sub>/CO<sub>2</sub> separation in ultra-stable Zn-organic frameworks for efficient removal of trace CO<sub>2</sub> from acetylene, *J. Mater. Chem. A*, 2022, **10**, 23630–23638.
- 147 Z. Zhang, S. B. Peh, R. Krishna, C. Kang, K. Chai, Y. Wang, D. Shi and D. Zhao, Optimal Pore Chemistry in an Ultramicroporous Metal-Organic Framework for Benchmark Inverse CO<sub>2</sub>/C<sub>2</sub>H<sub>2</sub> Separation, *Angew. Chem., Int. Ed.*, 2021, **60**, 17198–17204.
- 148 Z. Zhang, Z. Deng, H. A. Evans, D. Mullangi, C. Kang, S. B. Peh, Y. Wang, C. M. Brown, J. Wang, P. Canepa, A. K. Cheetham and D. Zhao, Exclusive Recognition of CO<sub>2</sub> from Hydrocarbons by Aluminum Formate with Hydrogen-Confining Pore Cavities, *J. Am. Chem. Soc.*, 2023, **145**, 11643–11649.
- 149 Y. Wang, N.-Y. Huang, X.-W. Zhang, H. He, R.-K. Huang, Z.-M. Ye, Y. Li, D.-D. Zhou, P.-Q. Liao, X.-M. Chen and J.-P. Zhang, Selective Aerobic Oxidation of a Metal-Organic Framework Boosts Thermodynamic and Kinetic Propylene/Propane Selectivity, *Angew. Chem., Int. Ed.*, 2019, **58**, 7692–7696.
- 150 A. Cadiau, K. Adil, P. M. Bhatt, Y. Belmabkhout and M. Eddaoudi, A metal-organic framework-based splitter for separating propylene from propane, *Science*, 2016, **353**, 137–140.
- 151 Y. Xie, Y. Shi, E. M. Cedeño Morales, A. El Karch, B. Wang, H. Arman, K. Tan and B. Chen, Optimal Binding Affinity for Sieving Separation of Propylene from Propane in an Oxyfluoride Anion-Based Metal-Organic Framework, *J. Am. Chem. Soc.*, 2023, **145**, 2386–2394.
- 152 H. Wang, X. Dong, V. Colombo, Q. Wang, Y. Liu, W. Liu, X.-L. Wang, X.-Y. Huang, D. M. Proserpio, A. Sironi, Y. Han and J. Li, Tailor-Made Microporous Metal-Organic Frameworks for the Full Separation of Propane from Propylene Through Selective Size Exclusion, *Adv. Mater.*, 2018, **30**, 1805088.
- 153 L. Yu, X. Han, H. Wang, S. Ullah, Q. Xia, W. Li, J. Li, I. da Silva, P. Manuel, S. Rudić, Y. Cheng, S. Yang, T. Thonhauser and J. Li, Pore Distortion in a Metal-Organic Framework for Regulated Separation of Propane and Propylene, *J. Am. Chem. Soc.*, 2021, **143**, 19300–19305.
- 154 B. Liang, X. Zhang, Y. Xie, R.-B. Lin, R. Krishna, H. Cui, Z. Li, Y. Shi, H. Wu, W. Zhou and B. Chen, An Ultramicroporous Metal-Organic Framework for High Sieving Separation of Propylene from Propane, *J. Am. Chem. Soc.*, 2020, **142**, 17795–17801.
- 155 H. Zeng, M. Xie, T. Wang, R.-J. Wei, X.-J. Xie, Y. Zhao, W. Lu and D. Li, Orthogonal-array dynamic molecular sieving of propylene/propane mixtures, *Nature*, 2021, **595**, 542–548.
- 156 Q. Dong, Y. Huang, J. Wan, Z. Lu, Z. Wang, C. Gu, J. Duan and J. Bai, Confining Water Nanotubes in a Cu<sub>10</sub>O<sub>13</sub>-Based Metal-Organic Framework for Propylene/Propane Separation with Record-High Selectivity, *J. Am. Chem. Soc.*, 2023, **145**, 8043–8051.
- 157 D. Liu, J. Pei, X. Zhang, X.-W. Gu, H.-M. Wen, B. Chen, G. Qian and B. Li, Scalable Green Synthesis of Robust Ultra-Microporous Hofmann Clathrate Material with Record C<sub>3</sub>H<sub>6</sub> Storage Density for Efficient C<sub>3</sub>H<sub>6</sub>/C<sub>3</sub>H<sub>8</sub> Separation, *Angew. Chem., Int. Ed.*, 2023, **62**, e202218590.
- 158 M.-H. Yu, B. Space, D. Franz, W. Zhou, C. He, L. Li, R. Krishna, Z. Chang, W. Li, T.-L. Hu and X.-H. Bu, Enhanced Gas Uptake in a Microporous Metal-Organic Framework via a Sorbate Induced-Fit Mechanism, *J. Am. Chem. Soc.*, 2019, **141**, 17703–17712.
- 159 X. Wang, R. Krishna, L. Li, B. Wang, T. He, Y.-Z. Zhang, J.-R. Li and J. Li, Guest-dependent pressure induced gate-opening effect enables effective separation of propene and

- propane in a flexible MOF, *Chem. Eng. J.*, 2018, **346**, 489–496.
- 160 S. Tu, L. Yu, Y. Wu, Y. Chen, H. Wu, L. Wang, B. Liu, X. Zhou, J. Xiao and Q. Xia, A new yttrium-based metal-organic framework for molecular sieving of propane from propylene with high propylene capacity, *AlChE J.*, 2022, **68**, e17551.
- 161 J. Peng, H. Wang, D. H. Olson, Z. Li and J. Li, Efficient kinetic separation of propene and propane using two microporous metal organic frameworks, *Chem. Commun.*, 2017, **53**, 9332–9335.
- 162 L. Li, R.-B. Lin, X. Wang, W. Zhou, L. Jia, J. Li and B. Chen, Kinetic separation of propylene over propane in a microporous metal-organic framework, *Chem. Eng. J.*, 2018, **354**, 977–982.
- 163 K. Li, D. H. Olson, J. Seidel, T. J. Emge, H. Gong, H. Zeng and J. Li, Zeolitic Imidazolate Frameworks for Kinetic Separation of Propane and Propene, *J. Am. Chem. Soc.*, 2009, **131**, 10368–10369.
- 164 C. Y. Lee, Y.-S. Bae, N. C. Jeong, O. K. Farha, A. A. Sarjeant, C. L. Stern, P. Nickias, R. Q. Snurr, J. T. Hupp and S. T. Nguyen, Kinetic Separation of Propene and Propane in Metal-Organic Frameworks: Controlling Diffusion Rates in Plate-Shaped Crystals via Tuning of Pore Apertures and Crystallite Aspect Ratios, *J. Am. Chem. Soc.*, 2011, **133**, 5228–5231.
- 165 N. Lamia, M. Jorge, M. A. Granato, F. A. Almeida Paz, H. Chevreau and A. E. Rodrigues, Adsorption of propane, propylene and isobutane on a metal-organic framework: Molecular simulation and experiment, *Chem. Eng. Sci.*, 2009, **64**, 3246–3259.
- 166 A. Knebel, B. Geppert, K. Volgmann, D. I. Kolokolov, A. G. Stepanov, J. Twiefel, P. Heitjans, D. Volkmer and J. Caro, Defibrillation of soft porous metal-organic frameworks with electric fields, *Science*, 2017, **358**, 347–351.
- 167 Q. Ding, Z. Zhang, C. Yu, P. Zhang, J. Wang, L. Kong, X. Cui, C.-H. He, S. Deng and H. Xing, Separation of propylene and propane with a microporous metal-organic framework via equilibrium-kinetic synergetic effect, *AlChE J.*, 2021, **67**, e17094.
- 168 Y. Chen, Z. Qiao, D. Lv, C. Duan, X. Sun, H. Wu, R. Shi, Q. Xia and Z. Li, Efficient adsorptive separation of C<sub>3</sub>H<sub>6</sub> over C<sub>3</sub>H<sub>8</sub> on flexible and thermoresponsive CPL-1, *Chem. Eng. J.*, 2017, **328**, 360–367.
- 169 P. Zhang, L. Yang, X. Liu, J. Wang, X. Suo, L. Chen, X. Cui and H. Xing, Ultramicroporous material based parallel and extended paraffin nano-trap for benchmark olefin purification, *Nat. Commun.*, 2022, **13**, 4928.
- 170 Y. Wang, T. Li, L. Li, R. B. Lin, X. Jia, Z. Chang, H. M. Wen, X. M. Chen and J. Li, Construction of Fluorinated Propane-Trap in Metal-Organic Frameworks for Record Polymer-Grade Propylene Production under High Humidity Conditions, *Adv. Mater.*, 2023, **35**, 2207955.
- 171 X. Li, J. Liu, K. Zhou, S. Ullah, H. Wang, J. Zou, T. Thonhauser and J. Li, Tuning Metal-Organic Framework (MOF) Topology by Regulating Ligand and Secondary Building Unit (SBU) Geometry: Structures Built on 8-Connected M<sub>6</sub> (M = Zr, Y) Clusters and a Flexible Tetracarboxylate for Propane-Selective Propane/Propylene Separation, *J. Am. Chem. Soc.*, 2022, **144**, 21702–21709.
- 172 S.-Q. Yang, F.-Z. Sun, R. Krishna, Q. Zhang, L. Zhou, Y.-H. Zhang and T.-L. Hu, Propane-Trapping Ultramicroporous Metal-Organic Framework in the Low-Pressure Area toward the Purification of Propylene, *ACS Appl. Mater. Interfaces*, 2021, **13**, 35990–35996.
- 173 A. N. Hong, H. Yang, T. Li, Y. Wang, Y. Wang, X. Jia, A. Zhou, E. Kusumoputro, J. Li, X. Bu and P. Feng, Pore-Space Partition and Optimization for Propane-Selective High-Performance Propane/Propylene Separation, *ACS Appl. Mater. Interfaces*, 2021, **13**, 52160–52166.
- 174 C. He, Y. Wang, Y. Chen, X. Wang, J. Yang, L. Li and J. Li, Modification of the pore environment in UiO-type metal-organic framework toward boosting the separation of propane/propylene, *Chem. Eng. J.*, 2021, **403**, 126428.
- 175 M. Chang, J. Ren, Y. Wei, J.-X. Wang, Q. Yang, D. Liu and J.-F. Chen, A robust metal-organic framework with guest molecules induced splint-like pore confinement to construct propane-trap for propylene purification, *Sep. Purif. Technol.*, 2021, **279**, 119656.
- 176 L. Yang, X. Cui, Q. Ding, Q. Wang, A. Jin, L. Ge and H. Xing, Polycatenated Molecular Cage-Based Propane Trap for Propylene Purification with Recorded Selectivity, *ACS Appl. Mater. Interfaces*, 2020, **12**, 2525–2530.
- 177 P. Iacomi, F. Formalik, J. Marreiros, J. Shang, J. Rogacka, A. Mohmeyer, P. Behrens, R. Ameloot, B. Kuchta and P. L. Llewellyn, Role of Structural Defects in the Adsorption and Separation of C<sub>3</sub> Hydrocarbons in Zr-Fumarate-MOF (MOF-801), *Chem. Mater.*, 2019, **31**, 8413–8423.
- 178 E. Andres-Garcia, L. Oar-Arteta, J. Gascon and F. Kapteijn, ZIF-67 as silver-bullet in adsorptive propane/propylene separation, *Chem. Eng. J.*, 2019, **360**, 10–14.
- 179 E. Andres-Garcia, J. López-Cabrelles, L. Oar-Arteta, B. Roldan-Martinez, M. Cano-Padilla, J. Gascon, G. Mínguez Espallargas and F. Kapteijn, Cation influence in adsorptive propane/propylene separation in ZIF-8 (SOD) topology, *Chem. Eng. J.*, 2019, **371**, 848–856.
- 180 U. Böhme, B. Barth, C. Paula, A. Kuhnt, W. Schwieger, A. Mundstock, J. Caro and M. Hartmann, Ethene/Ethane and Propene/Propane Separation via the Olefin and Paraffin Selective Metal-Organic Framework Adsorbents CPO-27 and ZIF-8, *Langmuir*, 2013, **29**, 8592–8600.
- 181 L. Li, R.-B. Lin, R. Krishna, X. Wang, B. Li, H. Wu, J. Li, W. Zhou and B. Chen, Flexible-Robust Metal-Organic Framework for Efficient Removal of Propyne from Propylene, *J. Am. Chem. Soc.*, 2017, **139**, 7733–7736.
- 182 L. Li, H.-M. Wen, C. He, R.-B. Lin, R. Krishna, H. Wu, W. Zhou, J. Li, B. Li and B. Chen, A Metal-Organic Framework with Suitable Pore Size and Specific Functional Sites for the Removal of Trace Propyne from Propylene, *Angew. Chem., Int. Ed.*, 2018, **57**, 15183–15188.
- 183 H.-M. Wen, L. Li, R.-B. Lin, B. Li, B. Hu, W. Zhou, J. Hu and B. Chen, Fine-tuning of nano-traps in a stable metal-organic framework for highly efficient removal of propyne from propylene, *J. Mater. Chem. A*, 2018, **6**, 6931–6937.

- 184 L. Yang, X. Cui, Q. Yang, S. Qian, H. Wu, Z. Bao, Z. Zhang, Q. Ren, W. Zhou, B. Chen and H. Xing, A Single-Molecule Propyne Trap: Highly Efficient Removal of Propyne from Propylene with Anion-Pillared Ultramicroporous Materials, *Adv. Mater.*, 2018, **30**, 1705374.
- 185 L. Yang, X. Cui, Z. Zhang, Q. Yang, Z. Bao, Q. Ren and H. Xing, An Asymmetric Anion-Pillared Metal-Organic Framework as a Multisite Adsorbent Enables Simultaneous Removal of Propyne and Propadiene from Propylene, *Angew. Chem., Int. Ed.*, 2018, **57**, 13145–13149.
- 186 Y.-L. Peng, C. He, T. Pham, T. Wang, P. Li, R. Krishna, K. A. Forrest, A. Hogan, S. Suepaul, B. Space, M. Fang, Y. Chen, M. J. Zaworotko, J. Li, L. Li, Z. Zhang, P. Cheng and B. Chen, Robust Microporous Metal-Organic Frameworks for Highly Efficient and Simultaneous Removal of Propyne and Propadiene from Propylene, *Angew. Chem., Int. Ed.*, 2019, **58**, 10209–10214.
- 187 Y. Jiang, J. Hu, L. Wang, W. Sun, N. Xu, R. Krishna, S. Duttwyler, X. Cui, H. Xing and Y. Zhang, Comprehensive Pore Tuning in an Ultrastable Fluorinated Anion Cross-Linked Cage-Like MOF for Simultaneous Benchmark Propyne Recovery and Propylene Purification, *Angew. Chem., Int. Ed.*, 2022, **61**, e202200947.
- 188 Q. Wang, J. Hu, L. Yang, Z. Zhang, T. Ke, X. Cui and H. Xing, One-step removal of alkynes and propadiene from cracking gases using a multi-functional molecular separator, *Nat. Commun.*, 2022, **13**, 2955.
- 189 M.-Y. Gao, A. A. Bezrukov, B.-Q. Song, M. He, S. J. Nikkhah, S.-Q. Wang, N. Kumar, S. Darwish, D. Sensharma, C. Deng, J. Li, L. Liu, R. Krishna, M. Vandichel, S. Yang and M. J. Zaworotko, Highly Productive C<sub>3</sub>H<sub>4</sub>/C<sub>3</sub>H<sub>6</sub> Trace Separation by a Packing Polymorph of a Layered Hybrid Ultramicroporous Material, *J. Am. Chem. Soc.*, 2023, **145**, 11837–11845.
- 190 H. I. Mahdi and O. Muraza, An exciting opportunity for zeolite adsorbent design in separation of C<sub>4</sub> olefins through adsorptive separation, *Sep. Purif. Technol.*, 2019, **221**, 126–151.
- 191 E. V. Makshina, M. Dusselier, W. Janssens, J. Degrève, P. A. Jacobs, B. F. Sels and E. V. Makshina, Review of old chemistry and new catalytic advances in the on-purpose synthesis of butadiene, *Chem. Soc. Rev.*, 2014, **43**, 7917–7953.
- 192 Z. Zhang, Q. Yang, X. Cui, L. Yang, Z. Bao, Q. Ren and H. Xing, Sorting of C<sub>4</sub> Olefins with Interpenetrated Hybrid Ultramicroporous Materials by Combining Molecular Recognition and Size-Sieving, *Angew. Chem., Int. Ed.*, 2017, **56**, 16282–16287.
- 193 P.-Q. Liao, N.-Y. Huang, W.-X. Zhang, J.-P. Zhang and X.-M. Chen, Controlling guest conformation for efficient purification of butadiene, *Science*, 2017, **356**, 1193–1196.
- 194 J. Chen, J. Wang, L. Guo, L. Li, Q. Yang, Z. Zhang, Y. Yang, Z. Bao and Q. Ren, Adsorptive Separation of Geometric Isomers of 2-Butene on Gallate-Based Metal-Organic Frameworks, *ACS Appl. Mater. Interfaces*, 2020, **12**, 9609–9616.
- 195 L. Wang, W. Xue, H. Zhu, X. Guo, H. Huang and C. Zhong, Stepwise Engineering the Pore Aperture of a Cage-like MOF for the Efficient Separation of Isomeric C<sub>4</sub> Paraffins under Humid Conditions, *Angew. Chem., Int. Ed.*, 2023, **62**, e202218596.
- 196 A. H. Assen, Y. Belmabkhout, K. Adil, P. M. Bhatt, D.-X. Xue, H. Jiang and M. Eddaoudi, Ultra-Tuning of the Rare-Earth fcu-MOF Aperture Size for Selective Molecular Exclusion of Branched Paraffins, *Angew. Chem., Int. Ed.*, 2015, **54**, 14353–14358.
- 197 H. Wang, X. Dong, J. Lin, S. J. Teat, S. Jensen, J. Cure, E. V. Alexandrov, Q. Xia, K. Tan, Q. Wang, D. H. Olson, D. M. Proserpio, Y. J. Chabal, T. Thonhauser, J. Sun, Y. Han and J. Li, Topologically guided tuning of Zr-MOF pore structures for highly selective separation of C<sub>6</sub> alkane isomers, *Nat. Commun.*, 2018, **9**, 1745.
- 198 Y. Lin, L. Yu, S. Ullah, X. Li, H. Wang, Q. Xia, T. Thonhauser and J. Li, Temperature-Programmed Separation of Hexane Isomers by a Porous Calcium Chloranilate Metal-Organic Framework, *Angew. Chem., Int. Ed.*, 2022, **134**, e202214060.
- 199 F. Zheng, L. Guo, R. Chen, F. Zhou, Z. Zhang, Q. Yang, Y. Yang, Q. Ren and Z. Bao, Temperature-swing molecular exclusion separation of hexane isomers in robust MOFs with double-accessible open metal sites, *Chem. Eng. J.*, 2023, **460**, 141743.
- 200 K. Jie, Y. Zhou, E. Li, R. Zhao, M. Liu and F. Huang, Linear Positional Isomer Sorting in Nonporous Adaptive Crystals of a Pillar[5]arene, *J. Am. Chem. Soc.*, 2018, **140**, 3190–3193.
- 201 T. Wang, J. Gu, Q. Cui and H. Wang, Study on Adsorption and Desorption Performances of Trace C<sub>4</sub>–C<sub>6</sub> Alkane Mixture on MIL-101(Cr) and WS-480, *Energy Fuels*, 2019, **33**, 7587–7594.
- 202 Y. Yu, L. Yang, B. Tan, J. Hu, Q. Wang, X. Cui and H. Xing, Remarkable separation of C<sub>5</sub> olefins in anion-pillared hybrid porous materials, *Nano Res.*, 2021, **14**, 541–545.
- 203 R. Lyndon, Y. Wang, I. M. Walton, Y. Ma, Y. Liu, Z. Yu, G. Zhu, S. Berens, Y. S. Chen, S. G. Wang, S. Vasenkov, D. S. Sholl, K. S. Walton, S. H. Pang and R. P. Lively, Unblocking a rigid purine MOF for kinetic separation of xylenes, *Chem. Commun.*, 2022, **58**, 12305–12308.
- 204 M. Shivanna, K.-I. Otake, J.-J. Zheng, S. Sakaki, S. Kitagawa and M. Shivanna, Control of local flexibility towards p-xylene sieving in Hofmann-type porous coordination polymers, *Chem. Commun.*, 2020, **56**, 9632–9635.
- 205 H. Wang, X. Dong, E. Velasco, D. H. Olson, Y. Han, J. Li and H. Wang, One-of-a-kind: a microporous metal-organic framework capable of adsorptive separation of linear, mono- and di-branched alkane isomers via temperature- and adsorbate-dependent molecular sieving, *Energy Environ. Sci.*, 2018, **11**, 1226–1231.
- 206 L. Li, L. Guo, D. H. Olson, S. Xian, Z. Zhang, Q. Yang, K. Wu, Y. Yang, Z. Bao, Q. Ren and J. Li, Discrimination of xylene isomers in a stacked coordination polymer, *Science*, 2022, **377**, 335–339.
- 207 X. Cui, Z. Niu, C. Shan, L. Yang, J. Hu, Q. Wang, P. C. Lan, Y. Li, L. Wojtas, S. Ma and H. Xing, Efficient separation of xylene isomers by a guest-responsive metal-organic framework with rotational anionic sites, *Nat. Commun.*, 2020, **11**, 5456.

- 208 J. Zhou, T. Ke, Y. Song, H. Cai, Z. A. Wang, L. Chen, Q. Xu, Z. Zhang, Z. Bao, Q. Ren and Q. Yang, Highly Efficient Separation of C<sub>8</sub> Aromatic Isomers by Rationally Designed Nonaromatic Metal-Organic Frameworks, *J. Am. Chem. Soc.*, 2022, **144**, 21417–21424.
- 209 D.-D. Zhou, P. Chen, C. Wang, S.-S. Wang, Y. Du, H. Yan, Z.-M. Ye, C.-T. He, R.-K. Huang, Z.-W. Mo, N.-Y. Huang and J.-P. Zhang, Intermediate-sized molecular sieving of styrene from larger and smaller analogues, *Nat. Mater.*, 2019, **18**, 994–998.
- 210 T. He, X.-J. Kong, Z.-X. Bian, Y.-Z. Zhang, G.-R. Si, L.-H. Xie, X.-Q. Wu, H. Huang, Z. Chang, X.-H. Bu, M. J. Zaworotko, Z.-R. Nie and J.-R. Li, Trace removal of benzene vapour using double-walled metal-dipyrazolate frameworks, *Nat. Mater.*, 2022, **21**, 689–695.
- 211 W.-B. Li, Y. Wu, X.-F. Zhong, X.-H. Chen, G. Liang, J.-W. Ye, Z.-W. Mo and X.-M. Chen, Fluorescence Enhancement of a Metal-Organic Framework for Ultra-Efficient Detection of Trace Benzene Vapor, *Angew. Chem., Int. Ed.*, 2023, **62**, e202303500.
- 212 R. Wei, X. Liu and Z. Lai, MOF or COF membranes for olefin/paraffin separation: Current status and future research directions, *Adv. Membr.*, 2022, **2**, 100035.
- 213 C. Zhang, Y. Dai, J. R. Johnson, O. Karvan and W. J. Koros, High performance ZIF-8/6FDA-DAM mixed matrix membrane for propylene/propane separations, *J. Membr. Sci.*, 2012, **389**, 34–42.
- 214 Y. Liu, Z. Chen, G. Liu, Y. Belmabkhout, K. Adil, M. Eddaoudi and W. Koros, Conformation-Controlled Molecular Sieving Effects for Membrane-Based Propylene/Propane Separation, *Adv. Mater.*, 2019, **31**, 1807513.
- 215 Y. Peng, Y. Li, Y. Ban, H. Jin, W. Jiao, X. Liu and W. Yang, Metal-organic framework nanosheets as building blocks for molecular sieving membranes, *Science*, 2014, **346**, 1356–1359.
- 216 K. Yang, Y. Ban, A. Guo, M. Zhao, Y. Zhou, N. Cao and W. Yang, *In situ* interfacial assembly of ultra-H<sub>2</sub>-permeable metal-organic framework membranes for H<sub>2</sub>/CO<sub>2</sub> separation, *J. Membr. Sci.*, 2020, **611**, 118419.
- 217 K. Yang, Y. Ban and W. Yang, Layered MOF membranes modified with ionic liquid/AgBF<sub>4</sub> composite for olefin/paraffin separation, *J. Membr. Sci.*, 2021, **639**, 119771.
- 218 H. Song, Y. Peng, C. Wang, L. Shu, C. Zhu, Y. Wang, H. He and W. Yang, Structure Regulation of MOF Nanosheet Membrane for Accurate H<sub>2</sub>/CO<sub>2</sub> Separation, *Angew. Chem., Int. Ed.*, 2023, **62**, e202218472.
- 219 J. E. Bachman, Z. P. Smith, T. Li, T. Xu and J. R. Long, Enhanced ethylene separation and plasticization resistance in polymer membranes incorporating metal-organic framework nanocrystals, *Nat. Mater.*, 2016, **15**, 845–849.
- 220 Y. Sun, T. Ji, Y. Gao, J. Yan, Y. He, G. Xu, F. Yan, Q. Bian and Y. Liu, Freezing Contra-diffusion: A New Protocol for Synthesizing Co-Gallate MOF Membranes toward Superior Ethylene/Ethane Separation Performance, *ACS Mater. Lett.*, 2023, **5**, 558–564.
- 221 L. Liu, Y. Song, T. Ji, Y. Sun, D. He, H. Hu and Y. Liu, Beyond Solution-Based Protocols: MOF Membrane Synthesis in Supercritical Environments for an Elegant Sustainability Performance Balance, *ACS Mater. Lett.*, 2020, **2**, 1142–1147.